2023

SYNTHESIS AND CHARACTERIZATION OF MIXED LIGAND COMPLEXES OF RUTHENIUM(II) CONTAINING 2,2'-BIPYRIDINE AND 3,3'-DIMETHYL-1,1'- METHYLENEBISIMIDAZOLIUM LIGANDS; A NEW SYNTHETIC APPROACH

Matthew Schneider

SYNTHESIS AND CHARACTERIZATION OF MIXED LIGAND COMPLEXES OF RUTHENIUM(II) CONTAINING 2,2’-BIPYRIDINE AND 3,3’-DIMETHYL-1,1’-METHYLENEBISIMIDAZOLIUM LIGANDS; A NEW SYNTHETIC APPROACH

A thesis submitted in partial fulfillment
of the requirements for the degree of

MASTER OF SCIENCE

to the faculty of the

DEPARTMENT OF CHEMISTRY

of

ST. JOHN’S COLLEGE OF LIBERAL ARTS AND SCIENCES

at

ST. JOHN'S UNIVERSITY
New York
by
Matthew Schneider

Date Submitted 7/12/2023 Date Approved 7/20/2023

_____	_____
Matthew Schneider	Dr. Elise Megehee

ABSTRACT

SYNTHESIS AND CHARACTERIZATION OF MIXED LIGAND COMPLEXES OF RUTHENIUM(II) CONTAINING 2,2'-BIPYRIDINE AND 3,3'-DIMETHYL-1,1'-METHYLENEBISIMIDAZOLIUM LIGANDS; A NEW SYNTHETIC APPROACH

Matthew Schneider

Research into solar cells has been prioritized given the global demand for better renewable energy technologies. This demand is a result of the long-term use of fossil fuels, which generates significant pollution in highly populated urban areas. One potential solar cell technology is the dye-sensitized solar cell (DSSC). This kind of solar technology utilizes organometallic dyes to expand the types of wavelengths solar cells can use to generate electricity.[12] Ruthenium(II) metal complexes of this type have been investigated heavily for this purpose.[13,14,36] The main reasoning behind this is the metal-to-ligand charge-transfer (MLCT) phenomenon that such complexes exhibit. MLCT has often been investigated for use in solar cells and sensory molecules.[1,2]

The objective of this thesis was to synthesize analogs of tris-bipyridine ruthenium(II) using the *N*-heterocyclic carbene (NHC) ligand 3,3'-dimethyl-1,1'-methylenebisimidazolium (dmmbi). The dmmbi ligand was chosen due to its capacity for π-backbonding with the ruthenium(II) metal center, which significantly alters the stability and electronic properties of the metal complex.[27,28] Four complexes in total were to be synthesized as represented by $[Ru(bpy)_x(dmmbi)_{3-x}](PF_6)_2$, where x ranges from 0 to 3. Three of these four complexes were synthesized successfully and characterized.

A new synthetic approach using sodium acetate (NaOAc) as the base was utilized.[25] The base is critical for deprotonating the free NHC molecule so that it can coordinate to the metal center. Following synthesis and purification, each complex was characterized. Characterizations included CHN elemental analysis, ^{1}H NMR, ^{13}C NMR, COSY NMR, IR spectroscopy, UV-Vis spectroscopy, and cyclic voltammetry. These characterizations were crucial for analyzing the electronic and optical properties of each complex.

ACKNOWLEDGEMENTS

First and foremost, I would like to thank Dr. Elise G. Megehee for her mentorship over these last two years. There is no other way that I would have wanted to begin my graduate studies, and I consider myself extraordinarily lucky to be able to work with her. Secondly, I would like to thank my committee members: Dr. Richard Rosso and Dr. Enju Wang. Their insight, advice, and expertise on a wide range of subjects proved to be invaluable and made my experience at St. John's University all the more enjoyable. I would also like to thank the entire chemistry department for creating an atmosphere that encourages students to seek assistance and to pursue excellence. My thanks also go to my fellow lab mates: Justine, Tiana, and Nicholas. Their help and support made working long hours in the lab possible and pleasant. Similarly, I would like to thank my fellow colleagues that participated in this academic journey with me: Rigoberto, Gonzalo, and Marcus. Finally, I have my family and friends to thank for their unending support.

TABLE OF CONTENTS

LIST OF TABLES

LIST OF FIGURES

INTRODUCTION

Fossil Fuels and Air Pollution

Fossil fuel consumption has remained a consistent issue throughout the 21st century. In 2018, the total world energy supply was up to 14,282 million tonnes of oil equivalent (Mtoe) compared to 6,098 Mtoe in 1973. Fossil fuels including oil, coal, and natural gas composed about 81.3% of that supply in 2018. Similarly, world total final consumption in 2018 was 9,938 Mtoe with fossil fuels being 67.0% of that total.[3] As a result of burning fossil fuels, greenhouse gases known to trap heat in the atmosphere, such as carbon dioxide (CO_2), have gradually been released,[4] and CO_2 emissions have increased significantly from 1973 to 2018 as shown in Figure 1. In 1973, CO_2 emissions are estimated to have been 15,459 million tonnes (Mt) whereas in 2018 the emission levels increased to 33,513 Mt. Oil was responsible for 34.1% of those emissions, while coal contributed to 44.0%.[3]

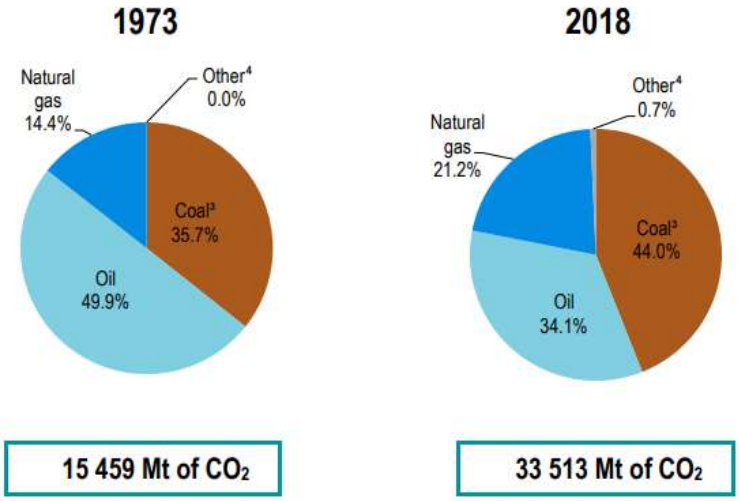

Figure 1. CO_2 emissions from fossil fuels.[3]

Aside from CO_2, nitrogen oxides and other volatile organic compounds released from the burning of fossil fuels have had significant environmental impacts. Nitrogen oxides contribute to the formation of smog and acid rain in the atmosphere, resulting in adverse effects on aquatic environments and human health.[5] Cars and trucks are major sources of nitrogen oxide pollution, which is why smog is generally seen to form in densely populated urban areas. Directly related to nitrogen oxide pollution is ozone. Ozone (O_3) is a gas that plays a crucial role in absorbing harmful ultraviolet radiation in the upper atmosphere, otherwise known as the stratosphere. While concentrations of ozone in the lower atmosphere, or troposphere, are less, photochemical reactions between volatile organic compounds and nitrogen oxides (Figure 2) have been known to increase ozone concentrations at this level.[6] Ozone also contributes to the formation of smog and can directly impact mortality when interacting with biomolecules in the respiratory tract. For example, in 2015 ozone pollution is estimated to have contributed to an additional 254,000 deaths and an overall decrease in lifespans worldwide.[7]

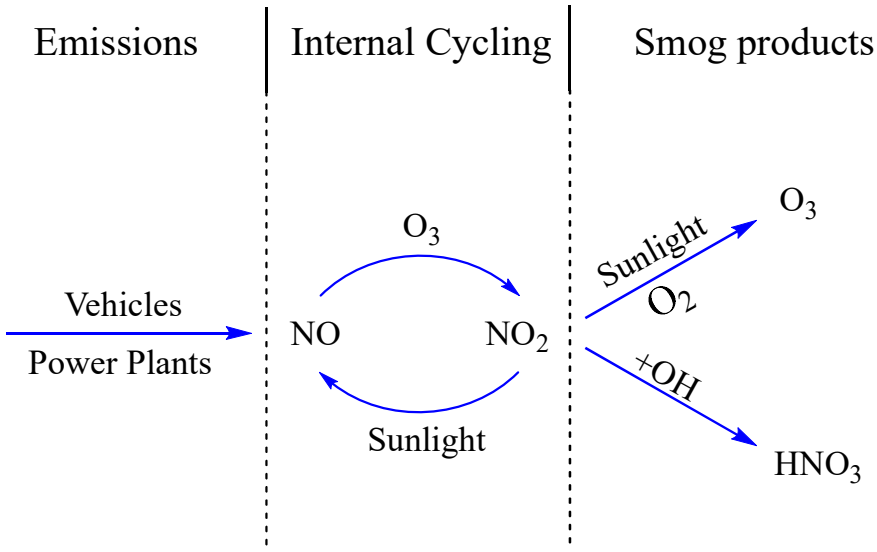

Figure 2. Formation of tropospheric ozone.[26]

Solar Cells

It is for previously stated reasons that a great interest in replacing fossil fuels has emerged. One promising technology is that of solar cells. Solar cells can convert solar energy into electrical energy without any side products such as carbon dioxide or nitrogen oxides. Such technologies decrease the potential harm caused by atmospheric pollutants by reducing the overall amounts in the atmosphere, especially near cities. The trend in using solar cell technology as an energy source has also increased over time, demonstrated by the world solar photovoltaic energy production jumping from 4 terawatt hours (TWh) in 2005 to 554 TWh in 2018.[3] The total generation of energy by solar also showed a growth rate of 20.5% worldwide in 2020.[8]

Although the general shift towards solar energy and other renewable energy sources is promising, solar cell efficiency remains an issue. This is due to what has been termed the 'detailed balance limit of efficiency' by Shockley and Queisser in 1960.[9] This term describes the upper limit of efficiency that can be reached by a p-n junction solar cell. This limit can theoretically be reached by direct bombardment of a solar cell with radiation, yet a planar solar cell experiencing more realistic instances of sunlight cannot reach it. The limit itself is dependent on a variety of factors, such as the energy gap of the solar cell, the intensity of sunlight, and the position of the sun.[9]

Two common types of solar cells are the silicon-based solar cell and the dye-sensitized solar cell (DSSC). The silicon-based solar cell, as the name implies, utilizes two layers of silicon semiconductors. One layer is classified as the p-type, while the other is the n-type. The p-type silicon layer is doped with electron-abundant atoms, and the n-type silicon layer is doped with electron-deficient atoms.[10] Electrons from the n-type layer fill

the vacancies caused by a lack of electrons in the p-type layer, creating a layer called the junction. This junction forms an electric field that prevents further electron transfers.[10] Electrons will be ejected from the silicon layer upon being irradiated by sunlight. These ejected electrons create vacancies in the junction, which in turn will be filled once again by more electrons from the n-type layer.[10] Figure 3 illustrates the mechanism of a silicon-based solar cell. This process can be utilized to generate electricity.[10] The single crystal silicon cell, dating back to 2004, has the highest efficiency of 27.6% among crystalline silicon cells. More recently in 2019, the multicrystalline silicon cell achieved an efficiency of 23.3%.[11]

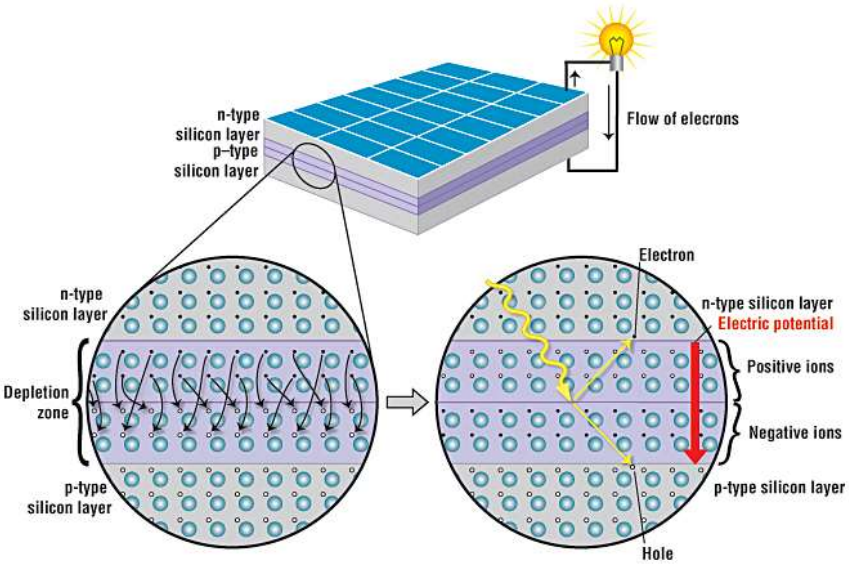

Figure 3. Design of a silicon-based solar cell.[10]

The DSSC, also referred to as the Gratzel cell, is a solar cell that is composed of a photoelectrode, semiconductor, sensitizer, electrolyte, and counter electrode.[12] The semiconductor is made up of an inorganic substance such as titanium dioxide (TiO_2). The sensitizer is adsorbed onto the surface of the semiconductor and varies with the type of dye

used. When sunlight reaches the sensitizer, electrons transition to an excited energy state. From there, the excited electrons transfer to the conduction band of the semiconductor. From the semiconductor, electrons travel through the photoelectrode to the counter electrode. Once there they reduce the redox mediator located within the electrolyte, which restores the sensitizer back to the ground state.[12] Upon contact with continuous sunlight, the completed circuit produces electricity. Figures 4 and 5 show the design and concept behind a DSSC.

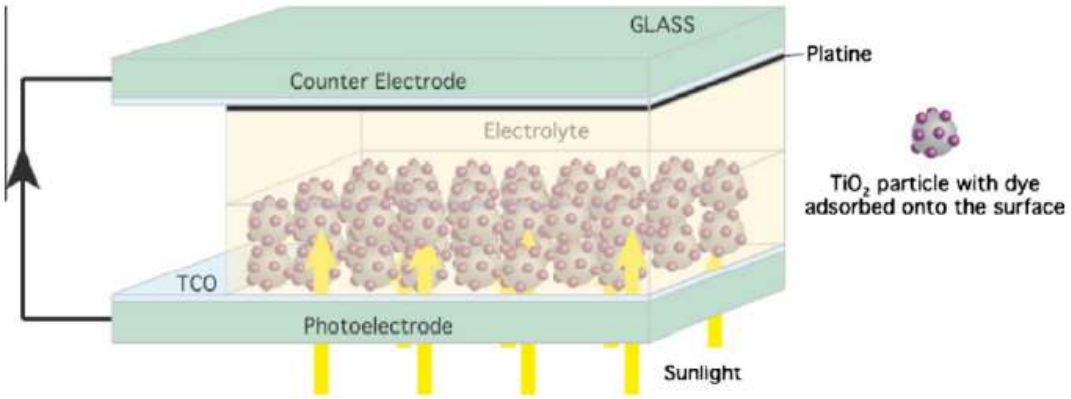

Figure 4. Simplified design of a Gratzel cell.[12]

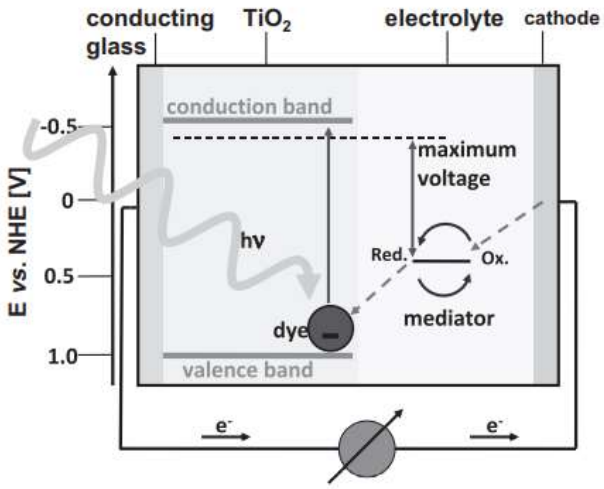

Figure 5. Conceptual representation of a Gratzel cell.[12]

The advantage that DSSC has over conventional n-type/p-type semiconductor solar cells is optimization. Conventional solar cells, such as the silicon-based ones discussed previously, require semiconducting materials that have both optimal light absorption and electron transport capabilities. The DSSC separates the two between the sensitizer and the semiconductor. Improvements on sunlight absorption can be focused on the sensitizer alone, while electron transport solely involves the semiconductor.[12] Compared to the crystalline solar cells, the highest efficiency of a DSSC was reported to be 13.0% in 2019.[11] Therefore, research on new materials for the DSSC prove to be highly valuable.

Metal-to-Ligand Charge Transfer

Sensitizers based on bidentate and tridentate ruthenium(II) complexes have been extensively researched to increase the efficiency of the DSSC.[13,14] Specifically, the tris(2,2'-bipyridine)ruthenium(II) complex $[Ru(bpy)_3]^{2+}$ has been shown to be a useful dye in this regard due to its properties in metal-to-ligand charge-transfer (MLCT).[15] In MLCT, an electron from the metal center of a complex migrates to the ligand (Figure 6). It is

observed between low oxidation state metals and ligands with low-lying π^* orbitals.[16] In organometallic ruthenium(II) complexes, absorbed photons transition electrons from the ground state to the excited state, resulting in $(Ru^{2+})^*$.[17] In a DSSC, as mentioned before, the electron would then be transferred to the conduction band of the semiconductor, oxidizing the ruthenium atom to Ru^{3+} in the process. After completing the circuit, the returning electrons could then reduce Ru^{3+} back to Ru^{2+} thus regenerating the sensitizer. However, a more efficient method is the catalytic reduction of Ru^{3+} to Ru^{2+} by iodide (I^-) ions within the electrolyte.[17]

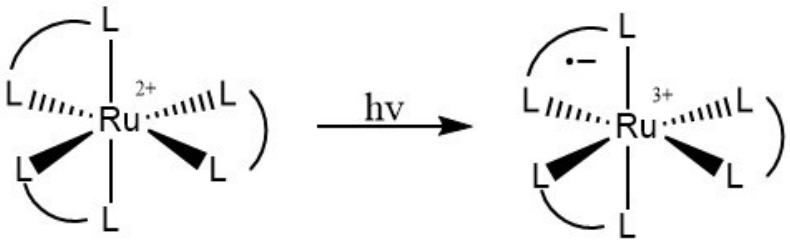

Figure 6. MLCT in a ruthenium(II) complex. (L = ligand)

Other Possible Applications

Aside from potential uses in solar energy, ruthenium(II) complexes can act as sensors for biomolecules such as DNA due to their strong luminescent properties. The ruthenium(II) complexes can bind to DNA molecules, and the interactions that take place between the two vary with the ligands present in the metal complex. For example, the photochemical properties and binding characteristics of organometallic ruthenium(II) complexes in the MLCT excited state to DNA have been investigated.[18] Ruthenium(II) polypyridyl complexes have also been researched as photosensitizers for photodynamic therapy, which is a form of anticancer treatment.[19]

N-Heterocyclic Carbene Ligands

The type of ligand plays an important role in MLCT. The ligands must have low-lying π^* orbitals, which is why diimines are commonly used.[16] When the metal ion is in a low oxidation state, the *d*-orbitals are able to interact with the ligand-based π^* orbitals due to a smaller energy gap. The two ligands of focus in this thesis are 2,2'-bipyridine (bpy) and 3,3'-dimethyl-1,1'-methylenebisimidazolium (dmmbi), as depicted in Figure 7. The dmmbi ligand is an *N*-heterocyclic carbene (NHC).

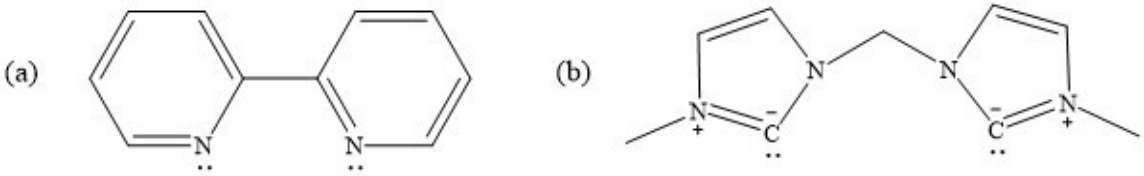

Figure 7. Structures of ligands. (a) bpy and (b) dmmbi.

Carbenes are molecules containing one or more carbon atoms that are divalent with valence shells encompassing six electrons (Figure 8a).[20] These molecules are of interest for the variety of ways in which they interact with a metal center, one chemical property being the ability to exhibit both electrophilic and nucleophilic properties.[20] The NHC is a cyclic diaminocarbene (Figure 8b) that can interact with transition metals to form Fischer-type complexes. Two forms that NHCs may take and then bind with metal centers are normal- and abnormal-substitutions (Figure 8c).[21]

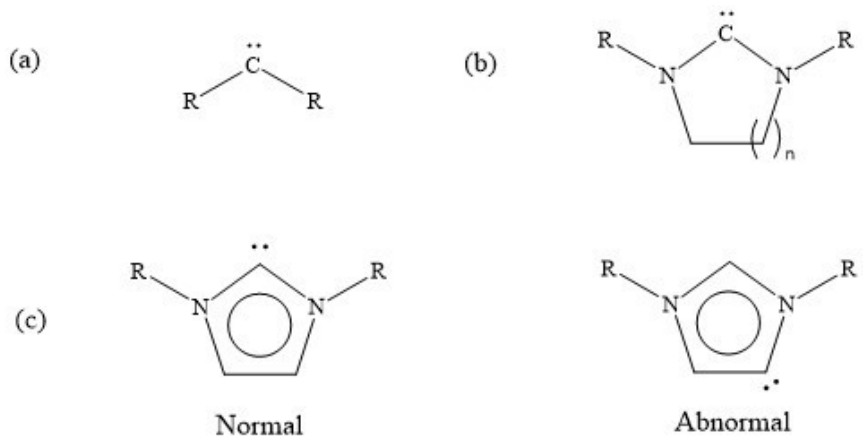

Figure 8. Carbene representations.[20,21] (a) Carbene structure. (b) NHC structure. (c) Normal and abnormal carbene substitutions.

Interactions between metal centers and normal-substitution NHCs can be achieved by deprotonating the carbene carbon using a base to form the free carbene, which can then coordinate to the metal center (Figure 9).[22] This kind of bonding is very stable as the carbon forms a strong bond to the metal center. In the case of ruthenium(II) complexes, NHCs can prove to be valuable ligands. The ability for NHC ligands to stabilize and activate the ruthenium(II) center while also exhibiting significant photochemical properties can help to enhance the complex.[23]

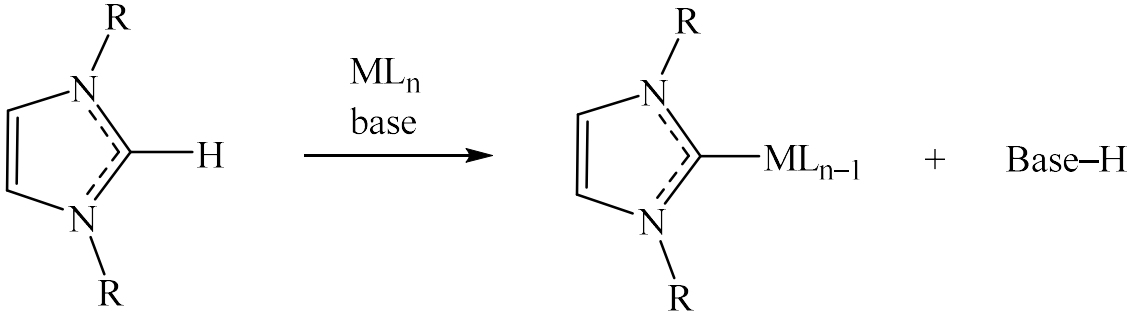

Figure 9. NHC deprotonation and interaction with metal center. (M = metal, L = ligand, base = alkoxide, acetate, triethylamine, etc.)[22]

π-Interactions

The stability of the NHC ligand can be attributed to two factors. The first is the π-donor interactions from the nitrogen atoms adjacent to the carbene carbon, which is further stabilized in our case by a ring structure with a double bond (Figure 10a).[27] The second is overlap between the *d*-orbital of the metal and the π-orbital of the carbene carbon (Figure 10b). This overlap results in two possible orbital interactions: π-backbonding and π-donation (Figure 10c and 10d). The π-backbonding interaction is more prevalent especially in late transition metals due to the more filled electron shells. It involves the overlap of the HOMO *d*-orbital of the metal with the π* orbital of the carbene carbon.[28] This further increases the stability of the metal-carbon bond by adding π-bonding characteristics to the predominantly σ-bond, and it gives rise to the qualities of interest with NHC ligands by affecting the electron distribution within the metal complex.

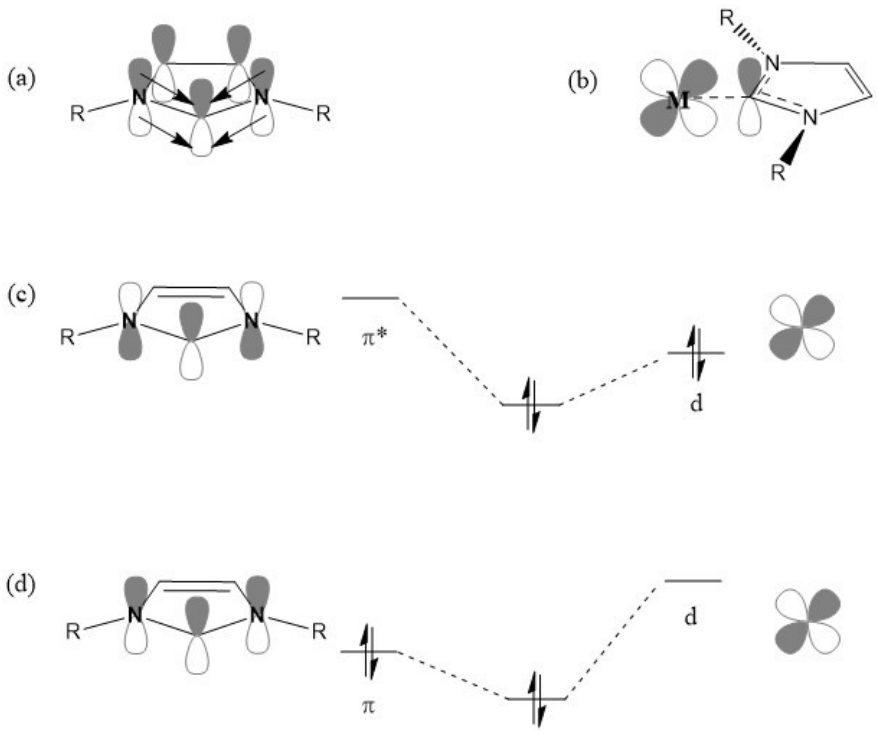

Figure 10. Stability of NHC molecules and orbital interactions. (a) Stability of the carbene carbon within an NHC ring structure containing a double bond. (b) Orbital overlap between the metal center and carbene carbon of an NHC ligand. (c) Simplified π-backbonding interaction. (d) Simplified π-donation interaction.[28]

Complexes

The proposed ruthenium(II) complexes to be synthesized are represented by $[Ru(bpy)_x(dmmbi)_{3-x}](PF_6)_2$, where x is an integer ranging from 0 to 3. Four complexes (Figure 11) with varying amounts of dmmbi were to be synthesized: tris(2,2'-bipyridine)ruthenium(II) hexafluorophosphate $[Ru(bpy)_3](PF_6)_2$, bis(2,2'-bipyridine)(3,3'-dimethyl-1,1'-methylenebisimidazolium)ruthenium(II) hexafluorophosphate $[Ru(bpy)_2(dmmbi)](PF_6)_2$, (2,2'-bipyridine)bis(3,3'-dimethyl-1,1'-methylenebisimidazolium)ruthenium(II) hexafluorophosphate $[Ru(bpy)(dmmbi)_2](PF_6)_2$, and tris(3,3'-dimethyl-1,1'-

methylenebisimidazolium)ruthenium(II) hexafluorophosphate [Ru(dmmbi)$_3$](PF$_6$). For this thesis, all four complexes would be characterized as well. Characterizations included CHN elemental analysis, ^{1}H nuclear magnetic resonance (NMR) spectroscopy, ^{13}C NMR spectroscopy, COSY NMR spectroscopy, infrared (IR) spectroscopy, ultraviolet-visible (UV-Vis) spectroscopy, and cyclic voltammetry (CV).

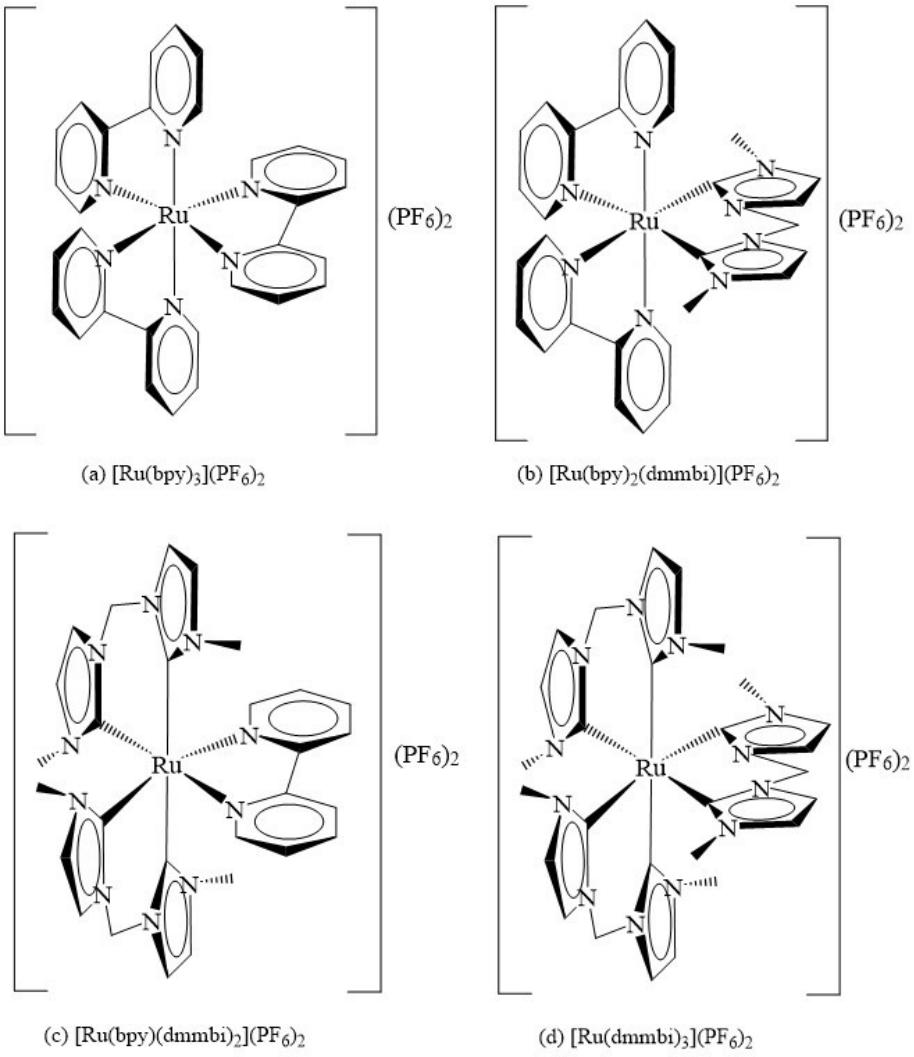

(a) [Ru(bpy)$_3$](PF$_6$)$_2$ (b) [Ru(bpy)$_2$(dmmbi)](PF$_6$)$_2$

(c) [Ru(bpy)(dmmbi)$_2$](PF$_6$)$_2$ (d) [Ru(dmmbi)$_3$](PF$_6$)$_2$

Figure 11. Proposed syntheses (a-d).

Previous work by Ryan Mahabir[24] demonstrated successful syntheses for $[Ru(bpy)_2(dmmbi)](PF_6)_2$ and $[Ru(dmmbi)_3](PF_6)_2$. Both reactions can be performed under reflux in 100 mL Schlenk flasks with an inert atmosphere and a 1:1 mixture of triethylamine : ethylene glycol. The specific reagents for the synthesis of $[Ru(bpy)_2(dmmbi)](PF_6)_2$ include a 1:1 mmol ratio of *cis*-bis(2,2'-bipyridine)dichlororuthenium(II) dihydrate $Ru(bpy)_2Cl_2 \cdot 2H_2O$ and 3,3'-dimethyl-1,1'-methylenebisimidazolium hexafluorophosphate $H_2(dmmbi)(PF_6)_2$. The specific reagents for the synthesis of $[Ru(dmmbi)_3](PF_6)_2$ include a 1:3 mmol ratio of ruthenium(III) chloride trihydrate $RuCl_3 \cdot 3H_2O$ and $H_2(dmmbi)(PF_6)_2$. For both reactions, careful consideration must be taken to ensure that a 1.1 excess amount of $H_2(dmmbi)(PF_6)_2$ is used to fully react all the ruthenium starting material.

Besiana Kurti and Jonathan Yuan in our private research group previously attempted syntheses for $[Ru(bpy)(dmmbi)_2](PF_6)_2$.[29] In a 150 mL high-pressure vessel, a 1:1 mmol mixture of $[Ru(dmmbi)_3](PF_6)_2$ and 2,2'-bipyridine were refluxed in a 1:1 mixture of triethylamine and ethylene glycol. This allowed for the removal of one dmmbi ligand and the replacement by one 2,2'-bipyridine ligand.

Each reaction described above can then be followed by the addition of aqueous potassium hexafluorophosphate (KPF_6) to the mixture while cooling in an ice bath. To ensure maximum precipitation, the products can be refrigerated overnight. The precipitates can then be extracted via vacuum filtration followed by washing three times each with 10 mL portions of both cold deionized water and cold diethyl ether. To test for purity, thin-layer chromatography (TLC) and NMR can be performed. If further purification is necessary, column chromatography using adsorption by an alumina stationary phase and a

mobile phase consisting of 1:1 acetonitrile:toluene can be utilized. Recrystallization using a minimal amount of dichloromethane and aqueous KPF_6 is also a viable option in some cases.

Another objective of this research was to develop a more efficient method for each synthesis. Each reaction previously employed the use of triethylamine. This proved tedious due to the tendency for triethylamine to evaporate out of solution while refluxing in the Schlenk flasks, which also tended to occur in high-pressure vessels. The purpose of the base is to deprotonate the ligand of interest so that it may bind to the metal center. One potential improvement was the use of sodium acetate (NaOAc) as the base. NaOAc has been investigated in past research for this purpose to form rhodium(III) di-NHC chelate complexes.[25] Normally, the reactions are refluxed between a temperature range of 160 – 170°C , which is well above the boiling point range of triethylamine. The use of NaOAc as a base would eliminate the potential for it to escape from solution, thus removing the need for more base to be added every couple of hours. The potential use of NaOAc in these reactions requires adjusting different conditions such as temperature, duration of reaction, amount of base, and type of reaction vessel (Schlenk flask, high-pressure vessel, etc.) to establish the highest yield and purity.

EXPERIMENTAL

Chemicals and Instrumentation

Ruthenium(III) trichloride trihydrate ($RuCl_3 \cdot 3H_2O$), 1-methylimidazole, and 2,2'-bipyridine were obtained from Beantown Chemical (BTC). Dibromomethane and ethylene glycol were obtained from Sigma Aldrich. Tetrahydrofuran (THF), N,N'-dimethylformamide (DMF), acetone, acetonitrile, toluene, and dichloromethane (DCM) were obtained from VWR. Potassium hexafluorophosphate (KPF_6), tetra-n-butylammonium hexafluorophosphate ($TBAPF_6$), lithium chloride (LiCl), and sodium acetate (NaOAc) were obtained from Alfa Aesar. Diethyl ether, potassium bromide (KBr), hydrochloric acid (HCl), alumina, sodium hydrosulfite ($Na_2S_2O_4$), and triethylamine were obtained from Fischer Chemical. Ethanol was obtained from Decon Labs. Magnesium sulfate ($MgSO_4$) was obtained from JT Baker. Dimethylsulfoxide-d_6 (DMSO-d_6) and acetonitrile-d_3 (CD_3CN) were obtained from Cambridge Isotope Laboratories. Alumina N thin-layer chromatography (TLC) plates were obtained from Sorbtech.

NMR spectra were recorded on a Bruker 400 MHz instrument. Samples were prepared in 0.5 – 0.75 mL of either CH_3CN-d_3 or DMSO-d_6. UV-Vis absorption spectra were recorded on an Agilent 8453 Diode Array UV-Vis spectrophotometer. Compounds were analyzed in dry acetonitrile solutions with concentrations ranging from 4.25×10^{-3} M to 3.47×10^{-7} M. Thirteen solutions were typically used, with more dilutions being performed if necessary. A scan range of 190 to 1100 nm was utilized. An integration time of 5.0 seconds and a total number of ten scans were used for each analysis. IR spectroscopy was performed using Perkin Elmer Spectrum One FT-IR Spectrometer. Samples were prepared as KBr pellets using a mini press from Wilks Scientific Corporation.

Approximately 1 mg of sample material was combined with 100 mg of KBr and ground to a fine powder before compressing to form the pellet. Transmission spectra (%T) were obtained using a range of 4000 – 600 cm^{-1}, a resolution of 4 cm^{-1}, and a total of one scan for each analysis. CV was performed using a BASi Epsilon potentiostat. Cyclic voltammograms were obtained in dry acetonitrile. The supporting electrolyte was 0.1 M $TBAPF_6$, the solid of which was first dried in an oven and then stored in a vacuum desiccator overnight. Analyte concentrations were approximately 1 mM. The cells consisted of three electrodes: a Pt working electrode, a Pt wire auxiliary electrode, and an Ag/AgCl reference electrode. The following parameters were used: a scan rate of 200 mV/s, a full-scale current of ±100 μA, and a 3-segment scan switching from 0 mV (initial) to –2.0 mV (1^{st} switch) to +2.0 mV (2^{nd} switch) to 0 mV (end). Nitrogen was used to degas the cells before measuring. CHN elemental analysis data was provided by Robertson Microlit Laboratories, Inc. located in Ledgewood, NJ. TLC was always performed using alumina N TLC plates in a 1:1 solution of acetonitrile:toluene.

Successful Syntheses

1. 3,3'-dimethyl-1,1'-methylenebisimidazolium hexafluorophosphate: $H_2(dmmbi)(PF_6)_2$

To a 100 mL pressure tube, 1-methylimidazole (9 mL, 0.113 mol) was added to dibromomethane (4 mL, 0.051 mol). This was followed by the addition of THF (45 mL). The contents of the tube were refluxed for 10 hours at 150°C. After 10 hours, the reaction was stopped, and the tube was allowed to cool overnight. The precipitate was isolated using vacuum filtration, and additional THF was used to further retrieve product from the pressure tube. It was then allowed to dry using vacuum suction.

The white crystals were dissolved in 25 mL of distilled water and added to a 500 mL Erlenmeyer flask. Approximately 160 mL of aqueous KPF_6 was added to the flask to precipitate the product. It was then stored in a refrigerator overnight to maximize precipitation. The precipitate was obtained via vacuum filtration and washed with 200 mL of cold distilled water. It was then dried using vacuum suction and stored in a vacuum desiccator. White crystals were obtained with a 24% yield. ^{1}H NMR (400 MHz, 298K, CD_3CN): δ (ppm) = 8.70 (s, 2H), 7.56 (s, 2H), 7.44 (s, 2H), 6.36 (s, 2H), 3.87 (s, 6H).

2. *cis*-Bis(2,2'-bipyridine)ruthenium(II)dichloride dihydrate: $[Ru(bpy)_2Cl_2 \cdot 2H_2O]$

To a 200 mL Schlenk flask, a mixture of $RuCl_3 \cdot 3H_2O$ (1.6448 g, 6.291 mmol), LiCl (1.8207, 42.951 mmol), and 2,2'-bipyridine (1.9484 g, 12.475 mmol) was added. This was followed by the addition of DMF (22 mL). The flask was degassed with argon while stirring for about 15 minutes. The flask was heated under reflux at ~160°C for 8 hours. It was then cooled in an ice bath for 5 minutes while stirring. This was followed by an addition of acetone (50 mL) to the flask, which was then refrigerated overnight. The precipitate was filtered via vacuum filtration and washed 3x with 10 mL portions of both

cold deionized water and cold diethyl ether. The precipitate was then allowed to dry using vacuum suction and stored in a vacuum desiccator. Dark brown crystals were obtained with a 68% yield. ^{1}H NMR (400 MHz, 298K, CD_3CN): δ (ppm) = 10.10 (d, 2H), 8.38 (d, 2H), 8.22, (d, 2H), 7.99 (t, 2H), 7.68 (t, 2H), 7.64 (d, 2H), 7.60 (t, 2H), 6.99 (t, 2H).

3. Tris(2,2'-bipyridine)ruthenium(II) hexafluorophosphate: $[Ru(bpy)_3](PF_6)_2$

The reaction was modified from the procedure reported by Stanley.[30] To a 100 mL Schlenk flask, 2,2'-bipyridine (60.6 mg, 0.388 mmol) was added to $Ru(bpy)_2Cl_2 \cdot 2H_2O$ (99.0 mg, 0.190 mmol). This was followed by the addition of a 3:1 ethanol : distilled water solution (24 mL). The reaction mixture was degassed with argon for 10 minutes and then refluxed at 80°C for 3 hours. After 3 hours, the reaction was stopped and allowed to cool. About 40 mL of aqueous KPF_6 was added to the flask, which was then stored in a refrigerator overnight to maximize precipitation of the product. Vacuum filtration was used to isolate the precipitate, followed by washing 3x with 10 mL portions of both cold distilled water and cold diethyl ether. It was then allowed to dry using vacuum suction.

The orange precipitate was dissolved in a minimal amount of acetonitrile, and any insoluble material was separated via vacuum filtration. Aqueous KPF_6 was added to the filtrate to precipitate out the product. It was then refrigerated overnight. Vacuum filtration was used to isolate the product, followed by washing 3x with 10 mL portions of cold distilled water and cold diethyl ether. It was then dried using vacuum suction and stored in a vacuum desiccator. Orang crystals were obtained with a 62% yield. ^{1}H NMR (400 MHz, 298K, CD_3CN): δ (ppm) = 8.52 (d, 6H), 8.06 (t, 6H), 7.75 (d, 6H), 7.41 (t, 6H).

4. Bis(2,2'-bipyridine)(3,3'-dimethyl-1,1'-methylenebisimidazolium)ruthenium(II) hexafluorophosphate: $[Ru(bpy)_2dmmbi](PF_6)_2$ (Trial 18)

To a 150 mL high pressure vessel, $H_2(dmmbi)(PF_6)_2$ (451.4 mg, 0.9642 mmol) was added in about 2-fold excess to $Ru(bpy)_2Cl_2 \cdot 2H_2O$ (250.5 mg, 0.4814 mmol). To the same vessel, a 16-fold excess of NaOAc (638.7 mg, 7.786 mmol) was added followed by ethylene glycol (100 mL). The reaction vessel was degassed under argon for 15 minutes and then heated at ~160°C for 16 hours. After 16 hours, 60 mL of aqueous KPF_6 was added. The vessel was then cooled in an ice bath while stirring for 15 minutes. It was then refrigerated overnight. The precipitate was filtered via vacuum filtration using a 30 mL glass frit, followed by washing 3x with 10 mL portions of cold deionized water and cold diethyl ether. It was then allowed to dry using vacuum suction. Red crystals were obtained.

Column chromatography was performed with alumina as the stationary phase and a mobile phase solution of 1:1 acetonitrile:toluene. Before use, the column was washed with 2% triethylamine in DCM and dried. The crude product was dissolved in a minimal amount of acetonitrile and added to the column. Only an orange band was present on the column. After the band reached the end of the column, the mobile phase was switched to 100% acetonitrile. A total of 5 fractions were collected. Fractions 1-5 were combined after being confirmed to be pure via TLC. The solvent was removed using a rotary evaporator, and the remaining red residue was dissolved in a minimal amount of acetonitrile. This was followed by the addition of 20 mL of aqueous KPF_6 and 20 mL of deionized water to recrystallize the product. It was then refrigerated overnight. The precipitate was isolated using vacuum filtration and washed 1x with 10 mL portions of cold deionized water and cold diethyl ether. It was then allowed to dry using vacuum suction and stored in a vacuum desiccator. Red crystals were obtained with a percent yield of 50%. ^1H NMR (400 MHz,

298K, CD_3CN): δ (ppm) = 8.93 (d, 2H), 8.36 (d, 2H), 8.27 (d, 2H), 8.07 (t, 2H), 7.86 (d/t, 4H), 7.68 (t, 2H), 7.37 (s, 2H), 7.27 (t, 2H), 6.98 (s, 2H), 6.64 (s, 2H), 3.57 (s, 6H).

5. Tris(3,3'-dimethyl-1,1'-methylenebisimidazolium)ruthenium(II) hexafluorophosphate: $[Ru(dmmbi)_3](PF_6)_2$ (Trial 5)

To a 150 mL high pressure vessel, $H_2(dmmbi)(PF_6)_2$ (2204.7 mg, 4.710 mmol) was added in 6-fold excess to $RuCl_3 \cdot 3H_2O$ (204.6 mg, 0.7825 mmol). To the same vessel, 80 mL of 1:1 triethylamine : ethylene glycol solution was added. The reaction vessel was degassed under argon for 15 minutes and then heated under reflux at 160°C for 96 hours. The next day, it was observed that the vessel cap had breached, and the triethylamine had evaporated out. The reaction was stopped and stored in a refrigerator for two days. It was then added to a 100 mL Schlenk flask followed by the addition of 40 mL more of triethylamine. After degassing with argon for 15 minutes, the solution was heated under an inert atmosphere under reflux at 160°C for 96 hours. Occasionally, 20 mL of triethylamine was added to the flask if the previous amount had slightly evaporated out. After 96 hours, 60 mL of aqueous KPF_6 was added to the flask and it was cooled in an ice bath while stirring for 15 minutes. It was then refrigerated for 2 days. Vacuum filtration was used to isolate the precipitate, followed by washing 3x with 10 mL portions of cold deionized water and cold diethyl ether. It was then allowed to dry using vacuum suction. Thin layer chromatography using 1:1 acetonitrile:toluene indicated the presence of only one tan-brown band.

Column chromatography was performed to remove any insoluble substances. Alumina was used as the stationary phase, and acetonitrile was used as the eluent. One tan-brown band was observed and collected in a single fraction. The solvent was then removed using a rotary evaporator. The remaining brown residue was dissolved in a minimal amount

of acetonitrile, followed by the addition of 60 mL of KPF_6 and 40 mL of cold deionized water. It was then refrigerated overnight. The precipitate was isolated using vacuum filtration, followed by washing 3x with 10 mL portions of cold diethyl ether. It was then dried using vacuum suction and stored in a vacuum desiccator. Tan-brown crystals were obtained with a 35% yield. ^1H NMR (400 MHz, 298K, CD_3CN): δ (ppm) = 7.06 (s, 6H), 6.87 (s, 6H), 6.29 (s, 6H), 3.65 (s, 18H).

Attempted Syntheses

*For most of these reactions, the ^{1}H NMR was impure except where noted.

Synthesis of [Ru(bpy)$_2$dmmbi](PF$_6$)$_2$: Trial 1

To a 100 mL Schlenk flask, H_2(dmmbi)(PF_6)$_2$ (525.8 mg, 1.123 mmol) was added in about 1.1 excess to Ru(bpy)$_2$Cl$_2$ · 2H$_2$O (501.1 mg, 1.035 mmol). To the same flask, NaOAc (372.3 mg, 4.539 mmol) was added in about 4-fold excess followed by ethylene glycol (35 mL). The flask was degassed under argon for 15 minutes while stirring and then heated at ~160°C for 4 hours. Reaction was monitored using TLC in 30-minute intervals. After 4 hours, the reaction was stopped and cooled in an ice bath. Aqueous KPF_6 (60 mL), was added to the flask, and the flask was stored in a refrigerator overnight. The precipitate was filtered using vacuum filtration. It was washed 3x with 10 mL portions of both cold deionized water and cold diethyl ether. The precipitate was then dried using vacuum suction. Red crystals were the crude product.

Column chromatography was prepared and performed as stated in **4**. Two bands were observed, the first being a dark purple band and the second being a red-orange band. In total, 12 fractions were collected, and TLC was performed on each. Fractions 2, 3 and 4 were combined. Fractions 6-12 were combined. Fractions 1 and 5 were collected separately. Fractions 6-12 were the desired product. Red crystals were obtained with a 12% yield.

Synthesis of [Ru(bpy)$_2$dmmbi](PF$_6$)$_2$: Trial 2

The reaction was prepared from Ru(bpy)$_2$Cl$_2$ · 2H$_2$O and proceeded as stated in Trial 1. The main differences were an 8-fold excess of NaOAc and a 24-hour reaction time.

For the first 4 hours, the reaction was monitored using TLC in 30-minute intervals. The crude product was isolated as in Trial 1, and red crystals were obtained.

Column chromatography was prepared and performed as stated in **4**. No distinct bands were observed. A total of 9 fractions were collected, and TLC was performed on each. Fractions 1 and 2 were discarded. Fractions 3-9 were combined and evaporated using a rotary evaporator. Red crystals were obtained with a 30% yield.

Synthesis of $[Ru(bpy)_2dmmbi](PF_6)_2$: Trial 3

The reaction was prepared from $Ru(bpy)_2Cl_2 \cdot 2H_2O$ and proceeded as stated in Trial 1. The main difference was a 24-hour reaction time. TLC was not used to monitor the reaction. The crude product was isolated as in Trial 1, and red crystals were obtained.

Column chromatography was prepared and performed as stated in **4**. Two distinct bands were observed: the first was a purple band and the second was an orange band. Excessive dragging occurred as the bands travelled down the column, and a colored solution began to elute out of the column long before the first band had reached the bottom. A second slim purple band was then observed to appear ahead of the orange band as it travelled and disappeared shortly after. After the first purple band eluted almost completely out of the column, the mobile phase was changed to 100% acetonitrile. This helped to push the orange band down the column at a faster rate. A total of 20 fractions were collected, and TLC was performed on each. Fractions 1-12 were discarded as they seemed to contain minimal product and were impure. Fractions 13-20 were combined and evaporated using a rotary evaporator. Red crystals were obtained with a yield of 5.5%.

Synthesis of [Ru(bpy)$_2$dmmbi](PF$_6$)$_2$: Trial 4

To a 150 mL high-pressure vessel, H_2(dmmbi)(PF_6)$_2$ (270.4 mg, 0.5775 mmol) was added in about 1.1 excess to Ru(bpy)$_2$Cl$_2$ · 2H_2O (251.4 mg, 0.4830 mmol). To the same flask, NaOAc (184.9 mg, 2.254 mmol) was added in about 4-fold excess followed by ethylene glycol (20 mL). The contents were degassed under argon for 15 minutes and then heated at ~160°C for 24 hours. After 24 hours, the flask was cooled in an ice bath for 10 minutes while stirring. This was followed by the addition of aqueous KPF_6 (50 mL). The flask was then stored in a refrigerator overnight. The precipitate was filtered via vacuum filtration and washed 3x with 10 mL portions of both cold deionized water and cold diethyl ether. It was then allowed to dry using vacuum suction and stored in a vacuum desiccator.

Column chromatography was prepared and performed as stated in **4**. Two distinct bands were observed. The first was a purple band and the second was an orange band. The bands dragged as they travelled down the column, resulting in unsatisfactory separation between the two. A total of 8 fractions were collected, and TLC was performed on each. Fractions 3-8 were combined and then evaporated using a rotary evaporator. Red crystals were obtained with a yield of 4.0%.

Synthesis of [Ru(bpy)$_2$dmmbi](PF$_6$)$_2$: Trial 5

The reaction was prepared from Ru(bpy)$_2$Cl$_2$ · 2H_2O and proceeded as stated in Trial 4. The main difference was an 8-fold excess of NaOAc. The crude product was isolated as in Trial 4, and red crystals were obtained.

Column chromatography was prepared and performed as stated in **4**. Two distinct bands were observed. The first was a purple band and the second was an orange band. A poor separation between the two bands was observed. Before the first band reached the

bottom of the column, a pink solution began to elute out. A total of 7 fractions were collected, and TLC was performed on each. Fractions 2 and 3 were combined, while fraction 1 was kept separate. Fractions 3-7 were combined and thought to be the desired product. Fractions 3-7 were evaporated using a rotary evaporator. Red crystals were obtained with a yield of 19%.

Synthesis of $[Ru(bpy)_2dmmbi](PF_6)_2$: Trial 6

The reaction was prepared from $Ru(bpy)_2Cl_2 \cdot 2H_2O$ and proceeded as stated in Trial 5. The crude product was isolated as in Trial 4, and red crystals were obtained.

Column chromatography was prepared and performed as stated in **4**. Column chromatography was performed on the crude product. No distinct separation was observed. The band progressed at an extremely slow rate down the column. After little progress, the mobile phase was switched to 100% acetonitrile to drive the band down the column. After doing so, a slight yellow color was observed travelling down the column from the initial band. The initial band did not move. A total of 6 fractions of the yellow solution that eluted out of the column was obtained, and TLC was performed on each. None of the fractions were combined as it was impossible to determine the presence of any product.

Synthesis of $[Ru(bpy)_2dmmbi](PF_6)_2$: Trial 7

The reaction was prepared from $Ru(bpy)_2Cl_2 \cdot 2H_2O$ and proceeded as stated in Trial 5. The crude product was isolated as in Trial 4, and red crystals were obtained. The red filtrate from vacuum filtration was kept.

The red filtrate was added to a separatory funnel and washed with 25 mL portions of DCM. After each wash, the organic layer was extracted. The filtrate was washed until the aqueous layer showed a slight discoloration. The extracted organic layer was then dried

using anhydrous $MgSO_4$ and evaporated using a rotary evaporator. A minimal amount of acetonitrile was then added to dissolve the reddish residue, followed by aqueous KPF_6 (~20 mL) and enough cold deionized water to cause precipitation. The precipitate was isolated via vacuum filtration and was washed once with 10 mL portions of cold deionized water and cold diethyl ether. It was then allowed to dry in a vacuum desiccator.

Column chromatography was prepared and performed as stated in **4**. As the product eluted down the column, two bands were observed: the first being a purple band, the second being a red-orange band. When the purple band had almost eluted completely out of the column, the mobile phase was switched to 100% acetonitrile. A total of 10 fractions were collected, and TLC was performed on each. Fractions 1 and 2 were combined, evaporated using a rotary evaporator, and thought to be the purple band. Fractions 3 and 4 were discarded as they appeared to be impure and contained minimal product. Fractions 5-10 were combined, evaporated using a rotary evaporator, and thought to be the orange-red band, which was the desired product.

A second column was prepared and performed as stated in **4** for the crude product obtained from the filtrate. Two bands were observed. The first was a purple band, and the second was orange. Five fractions were collected in total. Fractions 1-4 were discarded as TLC showed a mix of the two bands. Fraction 5 was evaporated using a rotary evaporator and analyzed via TLC. It was determined to be impure and discarded.

The precipitate of fractions 5-10 from the first column chromatography was obtained using vacuum filtration. It was washed 3x with 10 mL portions of cold diethyl ether and then allowed to dry using vacuum suction. Red crystals were obtained with a 30% yield.

Synthesis of [Ru(bpy)$_2$dmmbi](PF$_6$)$_2$: Trial 8

The reaction was prepared from Ru(bpy)$_2$Cl$_2$ · 2H$_2$O and proceeded as stated in Trial 5. The main difference was a 48-hour reaction time. The crude product was isolated as in Trial 4, and red crystals were obtained. The red filtrate from vacuum filtration was kept. Crude product from the red filtrate was extracted as in Trial 7. Both crude products were combined.

Column chromatography was prepared and performed as stated in **4**. Two bands were observed: the first was purple, and the second was orange. As the bands travelled down the column, substantial dragging was observed, and the column packing contained air bubbles. Five fractions were collected, but all were impure. Most of the product was lost in the column.

Synthesis of [Ru(bpy)$_2$dmmbi](PF$_6$)$_2$: Trial 9

The reaction was prepared from Ru(bpy)$_2$Cl$_2$ · 2H$_2$O and proceeded as stated in Trial 5. The main difference was a 72-hour reaction time. The crude product was isolated as in Trial 4, and red crystals were obtained. The red filtrate from vacuum filtration was kept. Crude product from the red filtrate was extracted as in Trial 7. Both crude products were combined.

Column chromatography was prepared and performed as stated in **4**. Two bands were observed: the first was purple, and the second was orange. As the bands travelled down the column, substantial dragging was observed, and the column packing contained air bubbles. Five fractions were collected, but all were impure. Most of the product was lost in the column.

Synthesis of [Ru(bpy)$_2$dmmbi](PF$_6$)$_2$: Trial 10

The reaction was prepared from Ru(bpy)$_2$Cl$_2$ · 2H$_2$O and proceeded as stated in Trial 5. The main difference was a 96-hour reaction time. The crude product was isolated as in Trial 4, and red crystals were obtained. The red filtrate from vacuum filtration was kept. Crude product from the red filtrate was extracted as in Trial 7. Both crude products were combined.

Column chromatography was prepared and performed as stated in **4**. Two bands were observed. The first was a purple band, and the second was an orange band which was the desired product. A total of 7 fractions were collected, and TLC was performed on each. Fractions 1 and 2 were combined and evaporated using a rotary evaporator. Fractions 3 through 7 were combined and evaporated using a rotary evaporator.

A second column chromatography was prepared and performed as stated in 4 for fractions 1 and 2. The length of the column was 8 inches. A total of five fractions were collected, and TLC was performed on each. Fractions 1, 2, and 3 were determined to be impure and discarded. Fractions 4 and 5 were combined and evaporated using a rotary evaporator.

The precipitates from both column chromatography procedures were determined to be the desired product via TLC and were combined. Red crystals were obtained with a 29% yield.

Synthesis of [Ru(bpy)$_2$dmmbi](PF$_6$)$_2$: Trial 11

The reaction was prepared from Ru(bpy)$_2$Cl$_2$ · 2H$_2$O and proceeded as stated in Trial 5. The main difference was a 12-fold excess of NaOAc. The crude product was isolated as in Trial 4, and red crystals were obtained. The red filtrate from vacuum filtration

was kept. Crude product from the red filtrate was extracted as in Trial 7. Both crude products were combined.

Column chromatography was prepared and performed as stated in **4**. The precipitates were combined and purified via column chromatography. Two bands were observed: the first being a purple band, and the second being an orange band. A total of 9 fractions were collected. Fractions 1-4 were combined, and fractions 5-9 were combined. Fractions 1-4 were determined via TLC to be impure and re-columned using the same conditions. This yielded 8 more fractions, which were labelled 10-17. Fractions 15-17 were combined, and the rest discarded. Fractions 5-9 and 15-17 were determined to be the product and evaporated using a rotary evaporator. However, the precipitate from fractions 15-17 was then determined to be impure via TLC and was discarded. Red crystals were obtained from fractions 5-9. A yield of 20% was recorded.

Synthesis of $[Ru(bpy)_2dmmbi](PF_6)_2$: Trial 12

The reaction was prepared from $Ru(bpy)_2Cl_2 \cdot 2H_2O$ and proceeded as stated in Trial 5. The main difference was a 16-fold excess of NaOAc. The crude product was isolated as in Trial 4, and red crystals were obtained. The red filtrate from vacuum filtration was kept. Crude product from the red filtrate was extracted as in Trial 7. Both crude products were combined.

Column chromatography was prepared and performed as stated in **4**. Three bands were observed: the first was a yellow band, the second was purple, and the third was orange. The orange band was the product. A total of 10 fractions were collected. The yellow band was collected in fractions 1-2. The purple band was collected in fractions 3-7. The

orange band was collected in fractions 8-10. Red crystals were obtained from fractions 8-10. A yield of 42% was obtained.

Synthesis of $[Ru(bpy)_2dmmbi](PF_6)_2$: Trial 13

The reaction was prepared from $Ru(bpy)_2Cl_2 \cdot 2H_2O$ and proceeded as stated in Trial 12. The main difference was a 4-hour reaction time. The crude product was isolated as in Trial 4, and red crystals were obtained. The red filtrate from vacuum filtration was kept.

The red filtrate was added to a 125 mL separatory funnel and washed with 25 mL portions of DCM until the aqueous layer was only slightly discolored. The organic layer was extracted after each wash. The extracted layer was then evaporated using a rotary evaporator. The reddish residue that remained was dissolved in a minimal amount of acetonitrile, followed by the addition of 20 mL of aqueous KPF_6 and 20 mL of cold deionized water to precipitate the product. It was then refrigerated overnight. The precipitate was isolated using vacuum filtration and washed 1x with 10 mL portions of cold deionized water and cold diethyl ether. It was dried using vacuum suction and then added to the previous mass of crude product.

Column chromatography was prepared and performed as stated in **4**. Two bands were observed: a purple band and an orange band. A total of 10 fractions were collected. Fractions 1-5 were discarded as they were confirmed to be impure using TLC and contained minimal product. Fractions 6-10 contained the desired product, were combined, and were evaporated using a rotary evaporator. Red crystals were obtained with a 27% yield.

Synthesis of [Ru(bpy)$_2$dmmbi](PF$_6$)$_2$: Trial 14

The reaction was prepared from Ru(bpy)$_2$Cl$_2$ · 2H$_2$O and proceeded as stated in Trial 12. The main difference was an 8-hour reaction time. The crude product was isolated as in Trial 4, and red crystals were obtained. The red filtrate from vacuum filtration was kept. Crude product from the red filtrate was extracted as in Trial 13. Both crude products were combined.

Column chromatography was prepared and performed as stated in **4**. Two bands were observed: a purple band and an orange band. A total of 6 fractions were collected. Fractions 1-3 were discarded as they were confirmed to be impure using TLC and contained minimal product. Fractions 4-6 contained the desired product. They were combined and evaporated using a rotary evaporator. Red crystals were obtained with a 35% yield.

Synthesis of [Ru(bpy)$_2$dmmbi](PF$_6$)$_2$: Trial 15

The reaction was prepared from Ru(bpy)$_2$Cl$_2$ · 2H$_2$O and proceeded as stated in Trial 12. The main difference was a 12-hour reaction time. The crude product was isolated as in Trial 4, and red crystals were obtained. The red filtrate from vacuum filtration was kept. Crude product from the red filtrate was extracted as in Trial 13. Both crude products were combined.

Column chromatography was prepared and performed as stated in **4**. Two bands were observed: a purple band and an orange band. A total of 6 fractions were collected. Fractions 1-4 were discarded as they were confirmed to be impure using TLC and contained minimal product. Fractions 5 and 6 contained the desired product. They were

combined and evaporated using a rotary evaporator. Red crystals were obtained with a 53% yield.

Synthesis of $[Ru(bpy)_2dmmbi](PF_6)_2$: Trial 16

The reaction was prepared from $Ru(bpy)_2Cl_2 \cdot 2H_2O$ and proceeded as stated in Trial 12. The main difference was a 16-hour reaction time. The crude product was isolated as in Trial 4, and red crystals were obtained. The red filtrate from vacuum filtration was kept. Crude product from the red filtrate was extracted as in Trial 13. Both crude products were combined.

Column chromatography was prepared and performed as stated in **4**. Two bands were observed: a purple band and an orange band. A total of 7 fractions were collected. Fractions 1-4 were discarded as they were confirmed to be impure using TLC and contained minimal product. Fractions 5-7 contained the desired product. They were combined and evaporated using a rotary evaporator. Red crystals were obtained with a 31% yield. The product was determined to be slightly impure using NMR analysis.

Synthesis of $[Ru(bpy)_2dmmbi](PF_6)_2$: Trial 17

The reaction was prepared from $Ru(bpy)_2Cl_2 \cdot 2H_2O$ and proceeded as stated in Trial 16. The main difference was a 2-fold excess of $H_2(dmmbi)(PF_6)_2$. The crude product was isolated as in Trial 4, and red crystals were obtained. The red filtrate from vacuum filtration was kept. Crude product from the red filtrate was extracted as in Trial 13. However, the filtrate crude product was brown and showed to contain more impurities than the product by TLC. It was not added to the total crude product yield.

Column chromatography was prepared and performed as stated in **4**. Two bands were observed: a purple band and an orange band. A total of 6 fractions were collected.

Fractions 1-4 and 5 were discarded as they were confirmed to be impure using TLC and contained minimal product. Fractions 4 and 6 contained the desired product. They were combined and evaporated using a rotary evaporator. Red crystals were obtained with a 33% yield. Slight impurities were found using NMR analysis.

Synthesis of $Ru(dmmbi)_3](PF_6)_2$: Trial 1

The reaction was prepared from $RuCl_3 \cdot 3H_2O$ and proceeded as stated in **5**. The main differences were the use of a 150 mL high pressure vessel, a 3.1-fold excess of $H_2(dmmbi)(PF_6)_2$, a 12-fold excess of NaOAc replacing triethylamine, and a 16-hour reaction time. The product was dissolved in DCM and then precipitated using diethyl ether. The precipitate was collected again using vacuum filtration. It was then washed 3x with 10 mL portions of cold diethyl ether and dried using vacuum suction. Gray crystals were obtained. The product was insoluble and could not be analyzed via NMR. It was determined not to be the desired product.

Synthesis of $Ru(dmmbi)_3](PF_6)_2$: Trial 2

The reaction was prepared and proceeded as stated in **5**. The main differences were the use of a 150 mL high pressure vessel and a 3-fold excess of $H_2(dmmbi)(PF_6)_2$. Gray crystals were obtained. The crystals were insoluble and not the desired product. The brown filtrate was kept.

The filtrate was added to a 125 mL separatory funnel. It was washed with 25 mL portions of DCM, followed by extraction of the organic layer. The organic layer was evaporated using a rotary evaporator, and the remaining residue was dissolved in a minimal amount of acetonitrile followed by the addition of 25 mL of both KPF_6 and cold deionized water. It was then refrigerated overnight. The precipitate was isolated using vacuum

filtration, followed by washing with 10 mL portions of cold deionized water and cold diethyl ether. The precipitate was allowed to dry using vacuum suction and stored in a vacuum desiccator. Gray crystals were obtained. The crystals were insoluble and determined not to be the desired product.

Synthesis of $Ru(dmmbi)_3](PF_6)_2$: Trial 3

The reaction was prepared and proceeded as stated in **5**. The main differences were the use of a 150 mL high pressure vessel and a 12-fold excess of NaOAc replacing triethylamine. Gray crystals were obtained. The crystals were insoluble and could not be analyzed via NMR. It was determined not to be the desired product.

Synthesis of $Ru(dmmbi)_3](PF_6)_2$: Trial 4

The reaction was prepared and proceeded as stated in **5**. The main differences were the use of a 150 mL high pressure vessel and a 100 mg reaction scale. Light brown crystals were obtained.

The crystals were dissolved in a minimal amount of acetonitrile using a sonicator. Vacuum filtration was used to remove any insoluble substances. The filtrate was kept and evaporated using a rotary evaporator. The remaining residue was dissolved in a minimal amount of acetonitrile, followed by the addition of 25 mL of both aqueous KPF_6 and cold deionized water to precipitate the product. It was then stored in a refrigerator for 12 days.

Vacuum filtration was used to isolate the precipitate. This was followed by washing 3x with 10mL portions of cold deionized water and cold diethyl ether. It was then allowed to dry using vacuum suction and stored in a vacuum desiccator. Light brown crystals were obtained in a 28% yield. NMR analysis showed the product to be pure.

Synthesis of $[Ru(bpy)(dmmbi)_2](PF_6)_2$: Trial 1

To a 150 mL high pressure vessel, 2,2'-bipyridine (18.9 mg, 0.121 mmol) was added in 1.1 excess to $[Ru(dmmbi)_3](PF_6)_2$ (96.0 mg, 0.104 mmol). This was followed by the addition of about 8-fold excess of NaOAc (86.2 mg, 1.05 mmol) and 25 mL of ethylene glycol. The reaction mixture was degassed under nitrogen for 15 minutes. It was then heated at 160°C and monitored via TLC every 4 hours. After 8 hours, 40 mL of aqueous KPF_6 was added followed by cooling in an ice bath while stirring for 15 minutes. It was then refrigerated overnight. The mixture was filtered using vacuum filtration. No solid product was obtained.

The red filtrate was kept and added to a 125 mL separatory funnel. It was washed with 25 mL portions of DCM until the aqueous layer was slightly discolored. After each wash, the organic layer was extracted. The combined extracts were then evaporated using a rotary evaporator. A minimal amount of acetonitrile was used to dissolve the remaining residue, followed by the addition of 40 mL of both aqueous KPF_6 and cold deionized water. It was then refrigerated overnight. The precipitate was isolated using vacuum filtration, followed by washing 3x with 10 mL portions of both cold deionized water and cold diethyl ether. It was then allowed to dry using vacuum suction and was stored in a vacuum desiccator. Dark red crystals were obtained.

Synthesis of $[Ru(bpy)(dmmbi)_2](PF_6)_2$: Trial 2

To a 150 mL high pressure vessel, 2,2'-bipyridine (17.5 mg, 0.112 mmol) was added to $[Ru(dmmbi)_3](PF_6)_2$ (102.0 mg, 0.1109 mmol). This was followed by the addition of ethylene glycol (20 mL). The reaction mixture was degassed with nitrogen for 15 minutes and then heated at 160°C for 16 hours. After 16 hours, the flask was cooled in an

ice bath for 15 minutes. Aqueous KPF_6 (50 mL) was added to the flask, and it was refrigerated for 5 days. Vacuum filtration was used to isolate the product, which was then washed 3x with 10 mL portions of cold deionized water followed by cold diethyl ether. It was dried using vacuum suction and stored in a vacuum desiccator. Red crystals were obtained. NMR analysis showed that the major product was $[Ru(bpy)_2(dmmbi)](PF_6)_2$.

Synthesis of $[Ru(bpy)(dmmbi)_2](PF_6)_2$: Trial 3

To a 150 mL high pressure vessel, 2,2'-bipyridine (33.8 mg, 0.2164 mmol) was added to $[Ru(dmmbi)_3](PF_6)_2$ (200.2 mg, 0.2177 mmol). This was followed by the addition of ethylene glycol (40 mL). The reaction mixture was degassed with nitrogen for 15 minutes and then heated at 160°C for 8 hours. After 8 hours, the flask was cooled in an ice bath for 15 minutes. Aqueous KPF_6 (50 mL) was added to the flask, and it was then refrigerated. Vacuum filtration was used to isolate the product, which was then washed 3x with 10 mL portions of both cold deionized water and cold diethyl ether. It was dried using vacuum suction and stored in a vacuum desiccator. Red-brown crystals were obtained. NMR analysis showed the major product to be $[Ru(bpy)_2(dmmbi)](PF_6)_2$.

Synthesis of $[Ru(bpy)(dmmbi)_2](PF_6)_2$: Trial 4

To a 150 mL high pressure vessel, 2,2'-bipyridine (35.0 mg, 0.2241 mmol) was added to $[Ru(dmmbi)_3](PF_6)_2$ (199.5 mg, 0.2169 mmol). This was followed by the addition of ethylene glycol (40 mL). The reaction mixture was degassed with nitrogen for 15 minutes and then heated at 160°C for 1 hour. After 1 hour, the flask was cooled in an ice bath for 15 minutes. Aqueous KPF_6 (60 mL) was added to the flask, and it was then refrigerated. Vacuum filtration was used to isolate the product, which was then washed 3x with 10 mL portions of cold deionized water and cold diethyl ether. It was dried using

vacuum suction and stored in a vacuum desiccator. Red-brown crystals were obtained. NMR analysis determined the product to be impure and contained $[Ru(bpy)_2(dmmbi)](PF_6)_2$.

Synthesis of $[Ru(bpy)(dmmbi)_2](PF_6)_2$: Trial 5

To a 150 mL high pressure vessel, 2,2'-bipyridine (18.4 mg, 0.1178 mmol) was added to $[Ru(dmmbi)_3](PF_6)_2$ (100.4 mg, 0.1092 mmol). This was followed by the addition of ethylene glycol (20 mL). The reaction mixture was degassed with argon for 10 minutes and then heated at 120°C for 4.5 hours. After 4.5 hours, aqueous KPF_6 (40 mL) was added to the flask, and it was cooled in an ice bath for 15 minutes. It was then refrigerated overnight. Vacuum filtration was used to isolate the product, which was then washed 3x with 10 mL portions of both cold deionized water and cold diethyl ether. It was dried using vacuum suction. Red-brown crystals were obtained. NMR analysis determined the product to be $[Ru(bpy)_2(dmmbi)](PF_6)_2$.

Synthesis of $[Ru(bpy)(dmmbi)_2](PF_6)_2$: Trial 6

To a 150 mL high pressure vessel, a 4-fold excess of $H_2(dmmbi)(PF_6)_2$ (376.3 mg, 0.8038 mmol) was added to (2,2'-bipyridine)ruthenium(III)tetrachloride $[Ru(bpy)Cl_4]$ (101.4 mg, 0.1949 mmol). This was followed by the addition of a 32-fold excess of NaOAc (530.7 mg, 6.470 mmol) and ethylene glycol (50 mL). The reaction mixture was degassed for 15 minutes under argon. It was then heated at 160°C for 24 hours. After 24 hours, the reaction stopped. Aqueous KPF_6 (50 mL was added, and the vessel was cooled in an ice bath while stirring for 15 minutes. It was then refrigerated overnight. Vacuum filtration was used to isolate the precipitate. This was followed by washing 3x with 10 mL portions of both cold deionized water and cold diethyl ether. After drying using vacuum suction,

the product was stored in a vacuum desiccator overnight. A red precipitate was obtained. NMR analysis confirmed the product to be $[Ru(bpy)_2(dmmbi)](PF_6)_2$.

Synthesis of $[Ru(bpy)(dmmbi)_2](PF_6)_2$: Trial 7

To a 150 mL high pressure vessel, a 4-fold excess of $H_2(dmmbi)(PF_6)_2$ (479.7 mg, 1.025 mmol) was added to $[Ru(bpy)Cl_4]$ (101.8 mg, 0.2551 mmol). This was followed by the addition of a 32-fold excess of NaOAc (674.2 mg, 8.219 mmol) and ethylene glycol (60 mL). The reaction mixture was degassed for 15 minutes under argon. It was then heated at 160°C for 16 hours. After 16 hours, the reaction stopped. Aqueous KPF_6 (60 mL) was added, and the vessel was cooled in an ice bath while stirring for 30 minutes. It was then refrigerated overnight. Vacuum filtration was used to isolate the precipitate. This was followed by washing 3x with 10 mL portions of both cold deionized water and cold diethyl ether. After drying using vacuum suction, the product was stored in a vacuum desiccator overnight. A rust-colored precipitate was obtained. NMR analysis determined the product to be $[Ru(bpy)_2(dmmbi)](PF_6)_2$.

Synthesis of Diacetatobis(2,2'-bipyridine)ruthenium(II) hexafluorophosphate: $[Ru(OAc)_2(bpy)_2](PF_6)_2$

To a 50 mL Schlenk flask, NaOAc (130.4 mg, 1.590 mmol) was added in 8-fold excess to $[Ru(bpy)_2Cl_2 \cdot 2H_2O]$ (102.2 mg, 0.1964 mmol). This was followed by the addition of ethylene glycol (20 mL). The reaction mixture was degassed under argon while stirring for 10 minutes. It was then heated at 160°C and monitored using TLC in 1-hour intervals for 6 hours. After 6 hours, aqueous KPF_6 was added to the flask, which was then cooled in an ice bath while stirring for 10 minutes. The flask was then stored in a refrigerator overnight. The precipitate was isolated using vacuum filtration, followed by washing 3x with 10 mL portions of cold deionized water and cold diethyl ether. It was

allowed to dry using vacuum suction and stored in a vacuum desiccator. Brown crystals were obtained.

Synthesis of *cis*-bis(3,3'-dimethyl-1,1'-methylenebisimidazolium)ruthenium(II)dichloride dihydrate: [$Ru(dmmbi)_2Cl_2 \cdot 2H_2O$]: Trial 1

To a 100 mL Schlenk flask, $H_2(dmmbi)(PF_6)_2$ (1.8912 g, 4.0396 mmol) was added to $RuCl_3 \cdot 3H_2O$ (526.3 mg, 2.013 mmol). This was followed by the addition of LiCl (604.3 mg, 14.281 mmol) and DMF (20 mL). The reaction mixture was degassed with argon for 15 minutes and then heated at 160°C for 8 hours. After 8 hours, the flask was cooled in an ice bath while stirring, followed by the addition of acetone (25 mL). It was stored in the fridge overnight. The precipitate was isolated by vacuum filtration and washed 3x with 10 mL portions of acetone, cold deionized water, and cold diethyl ether. It was stored in a vacuum desiccator overnight. An insoluble product was obtained.

Synthesis of [$Ru(dmmbi)_2Cl_2 \cdot 2H_2O$]: Trial 2

To a 150 mL high pressure vessel, $H_2(dmmbi)(PF_6)_2$ (462.2 mg, 0.9873 mmol) was added to $RuCl_3 \cdot 3H_2O$ (128.7 mg, 0.4922 mmol). NaOAc (660.8 mg, 8.056 mmol) was added in 16-fold excess. This was followed by the addition of ethylene glycol (60 mL). The reaction mixture was degassed with nitrogen for 10 minutes and then heated at 160°C for 8 hours. After 8 hours, the flask was cooled in an ice bath while stirring, followed by the addition of a solution composed of $Na_2S_2O_4$ (1315.6 mg, 7.5563 mmol) and deionized water (70 mL). It was then refrigerated overnight. Vacuum filtration was used to isolate the product. It was washed 3x with 10 mL portions of both cold deionized water and cold diethyl ether and then dried via vacuum suction. It was stored in a vacuum desiccator overnight. A green solid was obtained.

Synthesis of Hydrogen Tetrachloro(2,2'-bipyridine)ruthenium(II): $H_2[Ru(bpy)Cl_4]$

The reaction was modified from the procedure reported by Krause.[31] To a 25 mL Schlenk flask, 10 mL of 1.00 M HCl was added and degassed with argon for 10 minutes. This was followed by the addition of $RuCl_3 \cdot 3H_2O$ (2.0684 g, 7.9108 mmol) and 2,2'-bipyridine (1.4900 g, 9.5398 mmol) to the flask. The mixture was allowed to stand for 9 days. After 9 days, the precipitate was isolated via vacuum filtration, followed by washing 3x with 10 mL portions of cold deionized water and cold diethyl ether. It was then allowed to dry using vacuum suction and stored in a vacuum desiccator overnight. A yield of 72% was obtained.

RESULTS AND DISCUSSION

Syntheses

Synthesis of $H_2(dmmbi)(PF_6)_2$

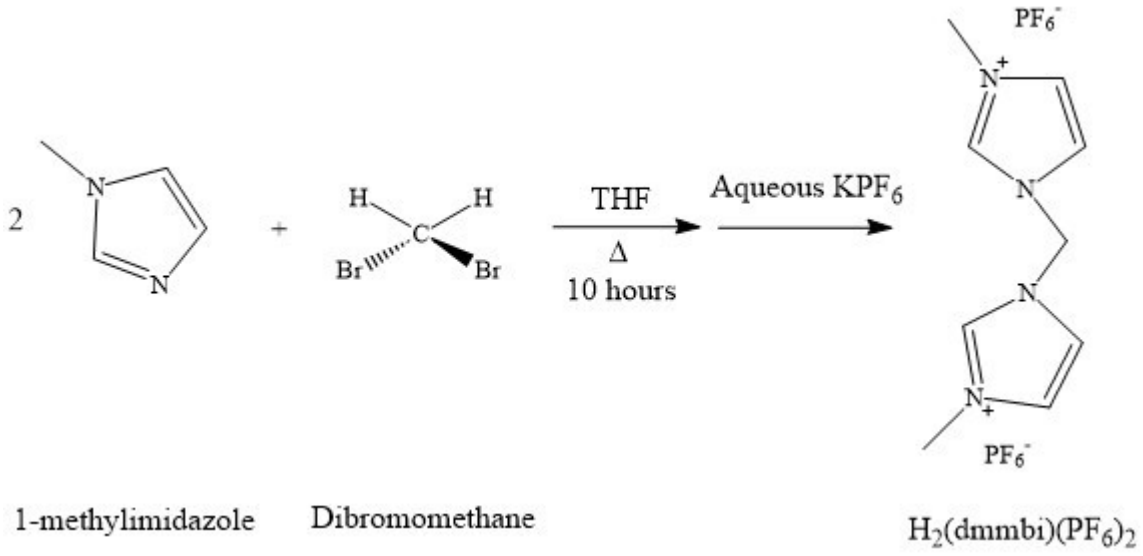

Figure 12. Synthesis of $H_2(dmmbi)(PF_6)_2$.

The reaction proceeded in a 2:1 molar ratio between 1-methylimidazole and dibromomethane. The solvent used was THF, and the reaction mixture was refluxed under pressure at 150°C for 10 hours, after which it was allowed to cool. Initially, water-soluble white crystals were obtained. To obtain the desired water-insoluble product, the crystals were dissolved in a minimal amount of water and precipitated out by ion exchanging Br^- for PF_6^- with the addition of aqueous KPF_6. After washing with cold distilled water, the final product consisted of white crystals. A percent yield of 24% was obtained.

To date, the best yield is 30%. It is unclear as to why the 68% yield recorded by Ryan Mahabir[24] cannot be reproduced. One possibility is that the reaction does not go to completion under these conditions. To circumvent this, a slight excess of 1-

methylimidazole can be tried for the reaction. Another possibility is that not all the product precipitates out of the solution upon the addition of aqueous KPF_6. This could mean that consecutive precipitations are required. No purification was necessary as the obtained samples were confirmed pure via NMR spectroscopy.

Synthesis of $Ru(bpy)_2Cl_2 \cdot 2H_2O$

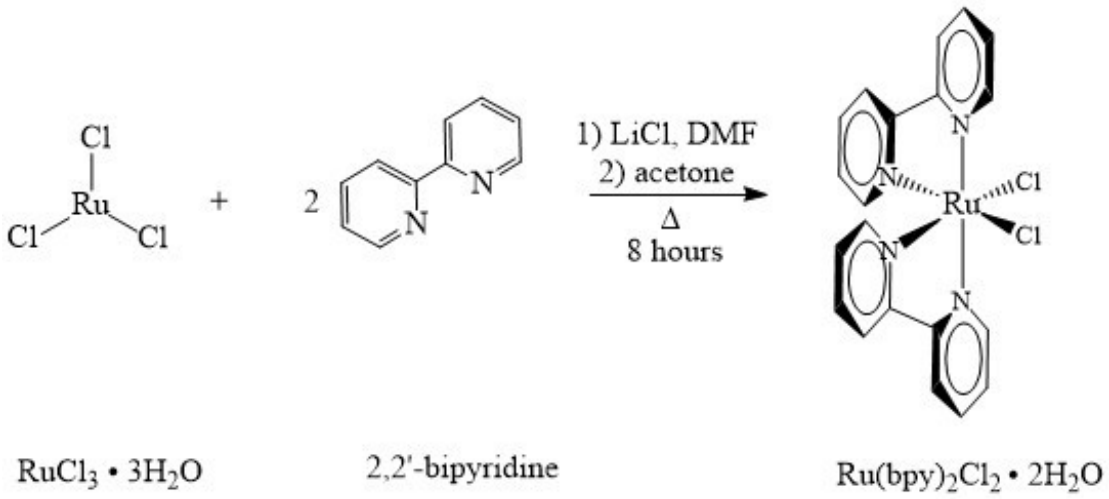

Figure 13. Synthesis of $Ru(bpy)_2Cl_2 \cdot 2H_2O$.

The reaction proceeded with a 2:1 molar ratio between 2,2'-bipyridine and $RuCl_3 \cdot 3H_2O$. The solvent used was DMF, and LiCl was added in a 7-molar excess to $RuCl_3 \cdot 3H_2O$ to prevent two of the chloride ligands from being displaced. The reaction mixture was refluxed at 160°C for 8 hours under an inert atmosphere. The coordination of two 2,2'-bipyridine ligands reduced the ruthenium(III) metal center to ruthenium(II) as observed by NMR. Acetone was used to precipitate the product, and any unreacted starting material was removed by washing with cold distilled water and cold diethyl ether. The overall process resulted in a 69% yield.

The main problem encountered for this synthesis was humidity. It is known that a humid environment causes an insoluble bulk of mass to form in the reaction flask, and it either prevents the reaction from taking place or severely affects the percent yield. This is attributed to the tendency for $RuCl_3 \cdot 3H_2O$ to absorb water from the surrounding atmosphere. Low humidity negates this issue. Heating in an oven for 1 hour before the reaction also helps by removing most of the excess water. No further purification was deemed necessary as the samples were found to be clean via ^1H NMR spectroscopy.

Synthesis of $[Ru(bpy)_3](PF_6)_2$

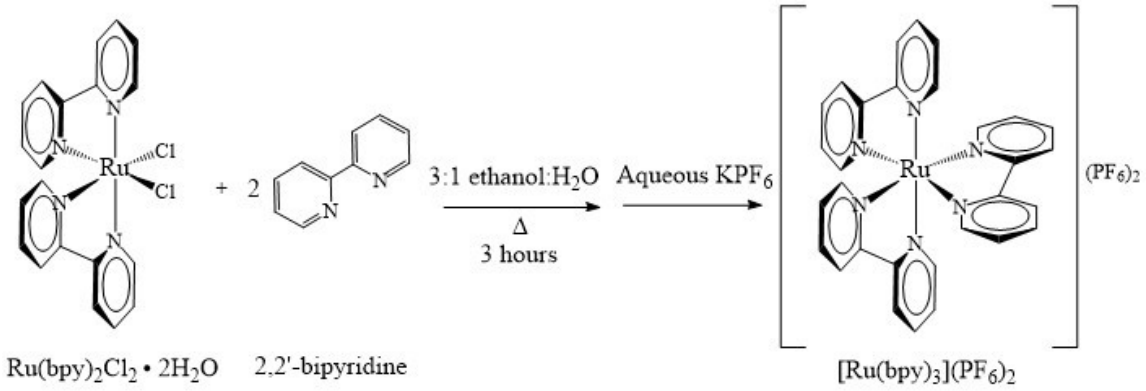

Figure 14. Synthesis of $[Ru(bpy)_3](PF_6)_2$.

The reaction for synthesizing $[Ru(bpy)_3](PF_6)_2$ was modified from the procedure reported by Stanley.[30] The reaction proceeds in a 2:1 molar ratio between 2,2'-bipyridine and $Ru(bpy)_2Cl_2 \cdot 2H_2O$. This was to ensure that the starting material reacted completely. The solvent used was a 3:1 ratio by volume of ethanol and distilled water. The reaction mixture was then refluxed at 80°C under an inert atmosphere for 3 hours. After cooling, aqueous KPF_6 was added to precipitate out the desired product. It was then refrigerated overnight and obtained the following day using vacuum filtration. The precipitate was washed with cold distilled water and cold diethyl ether to remove any starting material. To

remove any remaining impurity, the precipitate was dissolved in a minimal amount of acetonitrile and precipitated out using aqueous KPF_6. Vacuum filtration was used to isolate the desired product. After drying, orange crystals were obtained, and a 62.4% yield was recorded.

The only issue encountered for this synthesis was the lower-than-expected percent yield of 62.4% as compared to that reported, which was 99%. A possible cause for this outcome was the modified purification step. After refluxing and recrystallizing, the literature reported that the solution was evaporated, filtered to remove impurities, and then evaporated again to yield the product. Instead, the purification process for this synthesis involved recrystallization and vacuum filtration twice: once directly after refluxing, and again after the initial filtration. Some product may have been lost during the second filtration of the product. No column chromatography or further purification was required as the sample was found to be clean after performing ^1H NMR spectroscopy.

Synthesis of $[Ru(bpy)_2(dmmbi)](PF_6)_2$

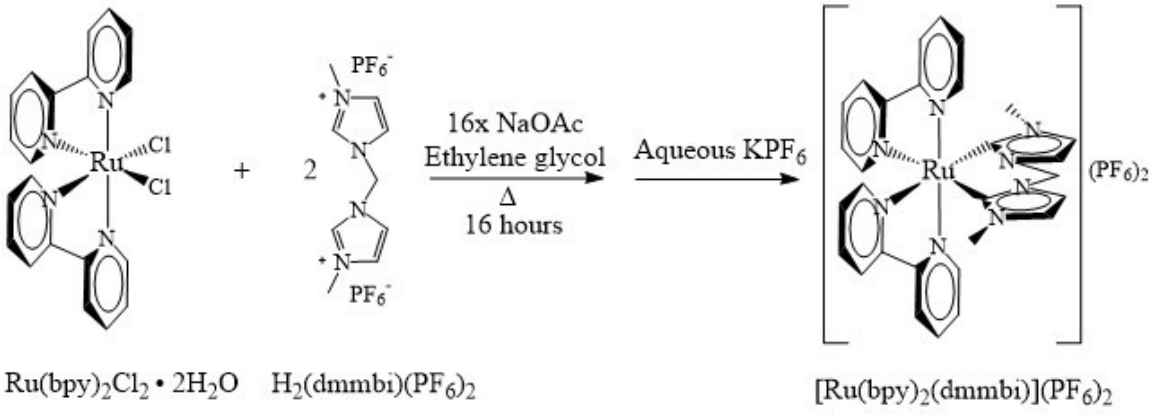

Figure 15. Synthesis of $[Ru(bpy)_2(dmmbi)](PF_6)_2$.

The conditions of the reaction scheme were varied over multiple syntheses to give the greatest yield. The best molar ratio between $H_2(dmmbi)(PF_6)_2$ and $Ru(bpy)_2Cl_2 \cdot 2H_2O$

was 2:1. The amount of NaOAc used ranged from a 2 to 16-fold excess based on $Ru(bpy)_2Cl_2 \cdot 2H_2O$. A 16-fold excess of sodium acetate yielded the greatest results and was used to deprotonate $H_2(dmmbi)(PF_6)_2$, thus generating the free NHC compound and allowing it to coordinate to the metal center. The optimal temperature was found to be 160°C. Reaction times of 4, 8, 12, 16, 24, 48, 72, and 96 hours were tested multiple times. A maximum of 16 hours was found to be sufficient in generating the desired product. Aqueous KPF_6 was used in all cases to precipitate the product. Column chromatography using alumina and a 1:1 acetonitrile:toluene mobile phase proved appropriate for purification. During purification, a purple band and a red band were observed. The first purple band was an impurity, the second red band was the desired product.

Previous attempts in which a 1.1 molar excess of $H_2(dmmbi)(PF_6)_2$ was used increased the presence of purple band impurity and produced a lower yield. It was thought that the 1.1 excess was insufficient in driving the reaction to completion and instead resulted in a mixture of the desired product, unreacted $Ru(bpy)_2Cl_2 \cdot 2H_2O$, and a bridged ligand metal complex (Figure 16). This is based on findings from ^1H NMR spectroscopy. A 2-fold excess of $H_2(dmmbi)(PF_6)_2$ seemed to correct this through the observation of a greatly diminished purple band during column chromatography, which was thought to be the bridged complex. When performing a 250 mg scale reaction, the purple band was completely removed from the crude product after vacuum filtration, as indicated by TLC of the filtrate and the presence of one red band during column chromatography.

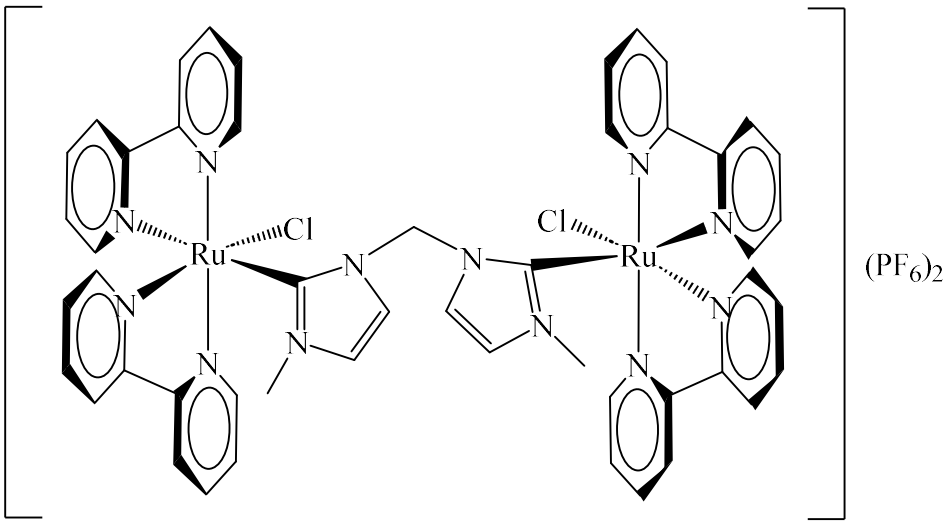

Figure 16. Possible structure of bridged ligand metal complex.

Another outcome for this synthesis is related to time length. In previous syntheses using triethylamine as the base, the reaction time required a minimum of 96 hours.[24] Using sodium acetate, this time length was drastically reduced from 96 to 16 hours with a satisfactory yield of 50%. This is likely a cause of sodium acetate's ability to stay in solution at 160°C as opposed to triethylamine, which would continuously evaporate and need to be replenished. Sodium acetate is also a stronger base than triethylamine.

Table 1. Conditions for all attempted trials to synthesize $[Ru(bpy)_2(dmmbi)](PF_6)_2$.					
Trial	**$H_2(dmmbi)(PF_6)_2$**	**NaOAc**	**Reaction time**	**Yield**	**Purity**
1	1.1-fold excess	4-fold excess	4 hours	12%	Impure
2	1.1-fold excess	8-fold excess	8 hours	30%	Impure
3	1.1-fold excess	4-fold excess	24 hours	5.5%	Impure
4	1.1-fold excess	4-fold excess	24 hours	4.0%	Impure
5	1.1-fold excess	8-fold excess	24 hours	19%	Impure
6	1.1-fold excess	8-fold excess	24 hours	N/A	Impure
7	1.1-fold excess	8-fold excess	24 hours	30%	Impure
8	1.1-fold excess	8-fold excess	48 hours	N/A	Impure
9	1.1-fold excess	8-fold excess	72 hours	N/A	Impure
10	1.1-fold excess	8-fold excess	96 hours	29%	Impure
11	1.1-fold excess	12-fold excess	24 hours	20%	Impure
12	1.1-fold excess	16-fold excess	24 hours	42%	Impure
13	1.1-fold excess	16-fold excess	4 hours	27%	Impure
14	1.1-fold excess	16-fold excess	8 hours	35%	Impure
15	1.1-fold excess	16-fold excess	12 hours	53%	Impure
16	1.1-fold excess	16-fold excess	16 hours	31%	Slightly impure
17	2-fold excess	16-fold excess	16 hours	33%	Slightly impure
18	2-fold excess	16-fold excess	16 hours	50%	Pure

Synthesis of $[Ru(dmmbi)_3](PF_6)_2$

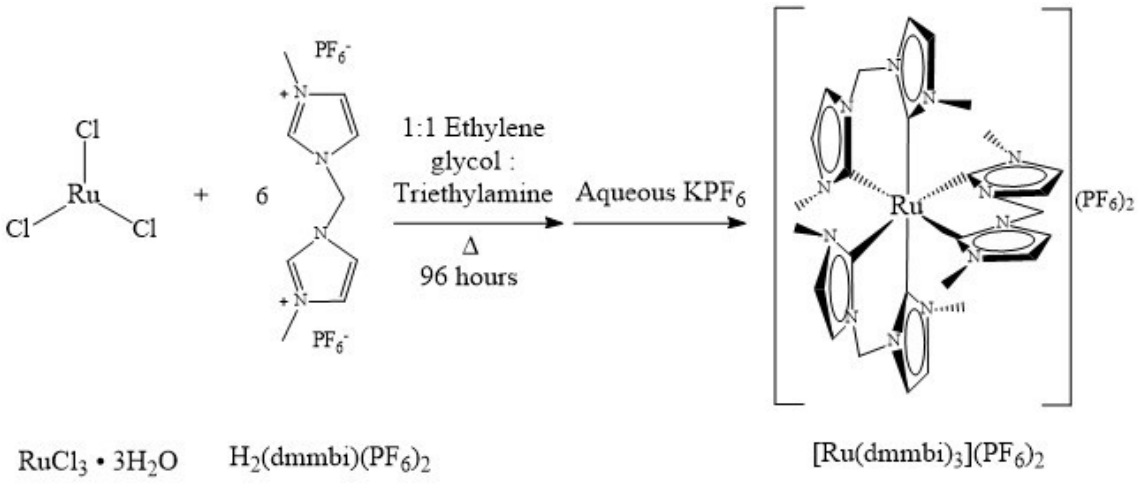

Figure 17. Synthesis of $[Ru(dmmbi)_3](PF_6)_2$.

A 6:1 molar ratio between $H_2(dmmbi)(PF_6)_2$ and $RuCl_3 \cdot 3H_2O$ was used to carry out the reaction. The base used to deprotonate $H_2(dmmbi)(PF_6)_2$ was triethylamine, which occurred over a 96-hour period at 160°C in a Schlenk flask. Using Schlenk techniques required additional triethylamine to be added once more during the reaction. The reaction mixture was not cooled before adding the triethylamine but should be in future syntheses. By using a chiller at 0.1°C, the triethylamine did not escape the condenser as much as in previous attempts. Aqueous KPF_6 was used to precipitate the product. TLC indicated the presence of only one brown band, but column chromatography was still utilized to remove any insoluble material. Column chromatography proceeded with alumina as the stationary phase and 100% acetonitrile as the mobile phase. This eluent was used because there was no need for band separation. Tan-brown crystals were obtained with a yield of 35%.

Initially, the reaction was attempted using sodium acetate as the base instead of triethylamine. Using a 1 to 4-fold excess of NaOAc produced only an ash-white insoluble salt that could not be analyzed. A possible reaction between the acetate ion (OAc^-) itself

and the metal complex may have resulted in this outcome. It was deemed necessary to revert to using triethylamine as the base for the reaction due to its inability to interact with the metal center. However, while significantly more product was obtained via this pathway, a substantial amount of insoluble material was still being produced from the reaction, thus causing lower yields. As was the case in the synthesis of $[Ru(bpy)_2(dmmbi)](PF_6)_2$, it was thought that a bridged ligand complex was forming due to an insufficient amount of $H_2(dmmbi)(PF_6)_2$ in the original reaction mixture. Thus, increasing the amount of $H_2(dmmbi)(PF_6)_2$ to a 6-fold excess compared to $RuCl_3 \cdot 3H_2O$ greatly promoted the formation of $[Ru(dmmbi)_3](PF_6)_2$, and any byproduct could be removed via column chromatography and recrystallization.

With reactions containing 2,2'-bipyridine, the ruthenium(III) metal center can be reduced to ruthenium(II) via coordination of the 2,2'-bipyridine ligand. The successful synthesis of $[Ru(dmmbi)_3](PF_6)_2$ indicates that the reduction does take place after three of the bis-carbene ligands coordinate around the ruthenium metal center to form the octahedral complex. ^1H NMR shows sharp peaks indicative of the diamagnetic Ru(II), and the reduction potential for the Ru(III)/Ru(II) couple is at a positive potential.

Attempted Synthesis of $H_2[Ru(bpy)Cl_4]$

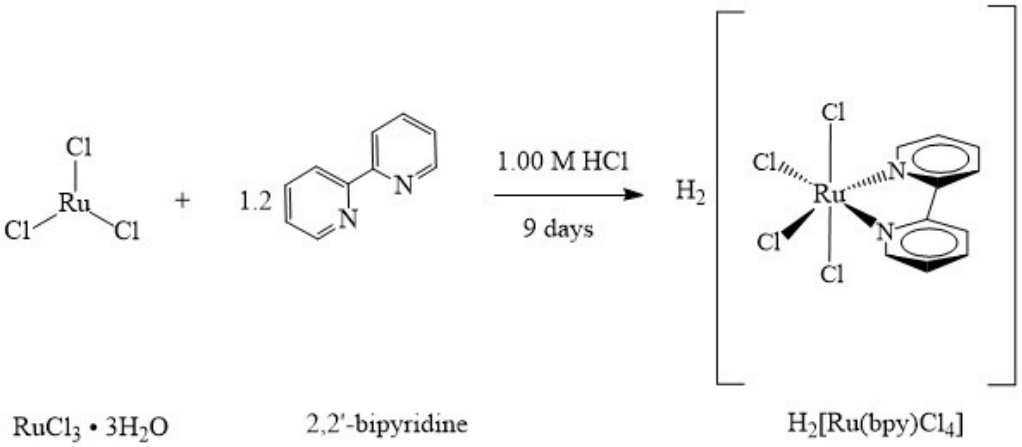

Figure 18. Attempted synthesis of $H_2[Ru(bpy)Cl_4]$.

The reaction was modified from the procedure reported by Krause.[31] A 20% excess of 2,2'-bipyridine was reacted with $RuCl_3 \cdot 3H_2O$. The reagents were added to a 25 mL Schlenk flask containing a 1.00 M HCl solution that had been degassed with argon beforehand. The contents were stirred initially to dissolve the components, and the mixture was allowed to sit for 9 days without stirring. This allowed for one 2,2'-bipyridine ligand to coordinate the metal center. The excess of chloride ions in the solution allowed for the additional binding of one chloride to the ruthenium center and prevented an additional 2,2'-bipyridine ligand from coordinating to the metal center. After 9 days, the precipitate was isolated via vacuum filtration and dried in a vacuum desiccator.

Based on the ability to obtain a ^1H NMR that is not broadened and shifted downfield, we concluded that this is Ru(II) which is d^6 and had no unpaired spins (diamagnetic). Since this is done in a solution of HCl, we assume the counterion is H_3O^+.

Attempted Syntheses of $[Ru(bpy)(dmmbi)_2](PF_6)_2$

Two methods were developed in an attempt to synthesize the last complex, $[Ru(bpy)(dmmbi)_2](PF_6)_2$. The first method involved a ligand exchange between a bound dmmbi and 2,2'-bipyridine. The second method involved deprotonating $H_2(dmmbi)(PF_6)_2$ so that it could coordinate to the ruthenium metal center and displace the chloride ions of the starting material. This second method was similar to the synthesis of $[Ru(bpy)_2(dmmbi)](PF_6)_2$.

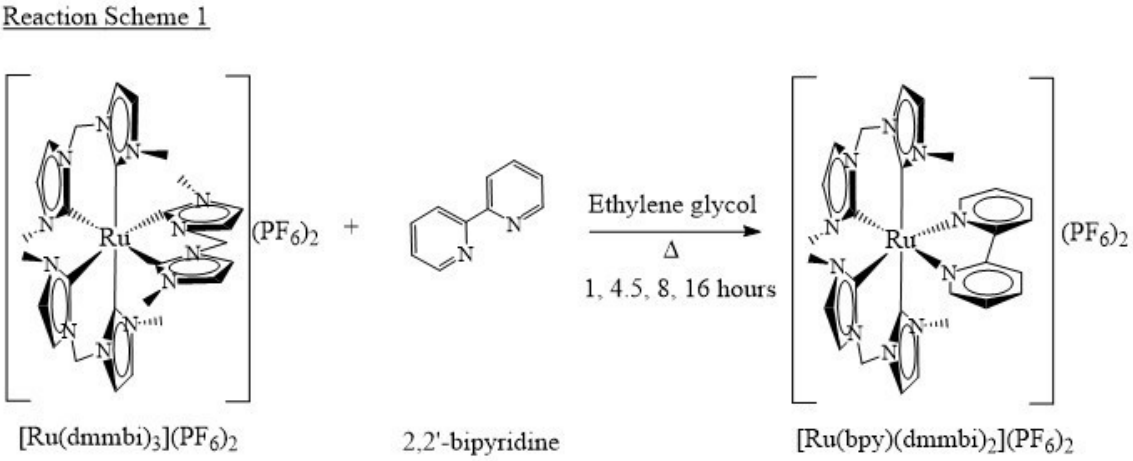

Figure 19. First attempted synthesis of $[Ru(bpy)(dmmbi)_2](PF_6)_2$.

The first reaction scheme used $[Ru(dmmbi)_3](PF_6)_2$ as the starting material and reacted it in a 1:1 molar ratio with 2,2'-bipyridine using a 150 mL high-pressure vessel. It proceeded in a solution of ethylene glycol while heating for a certain amount of time. No base was needed as it was unnecessary to deprotonate the 2,2'-bipyridine so that it could coordinate to the ruthenium metal center. Reaction times of 1, 4.5, 8, and 16 hours were tested. Temperatures of 120°C and 160°C were tested as well. The ratio between $[Ru(dmmbi)_3](PF_6)_2$ and 2,2'-bipyridine was kept the same for each attempt. The major

product for all of these reactions was $[Ru(bpy)_2(dmmbi)](PF_6)_2$, as confirmed by ^1H NMR analysis.

As was observed, 2,2'-bipyridine seems to outcompete the dmmbi ligand in $[Ru(dmmbi)_3](PF_6)_2$, resulting in the formation of $[Ru(bpy)_2(dmmbi)](PF_6)_2$ as the major product. During this process of ligand exchange, the desired complex $[Ru(bpy)(dmmbi)_2](PF_6)_2$ may be an intermediate. Thus, it would be more difficult to isolate. Column chromatography would also prove difficult as $[Ru(bpy)(dmmbi)_2](PF_6)_2$ and $[Ru(bpy)_2(dmmbi)](PF_6)_2$ are similar in charge and structure, causing little to no band separation. One possible change to this reaction scheme would be to add the total mass of 2,2'-bipyridine in portions over time rather than all at once. This could allow for the $[Ru(bpy)(dmmbi)_2](PF_6)_2$ complex to form and stabilize before the addition of more 2,2'-bipyridine.

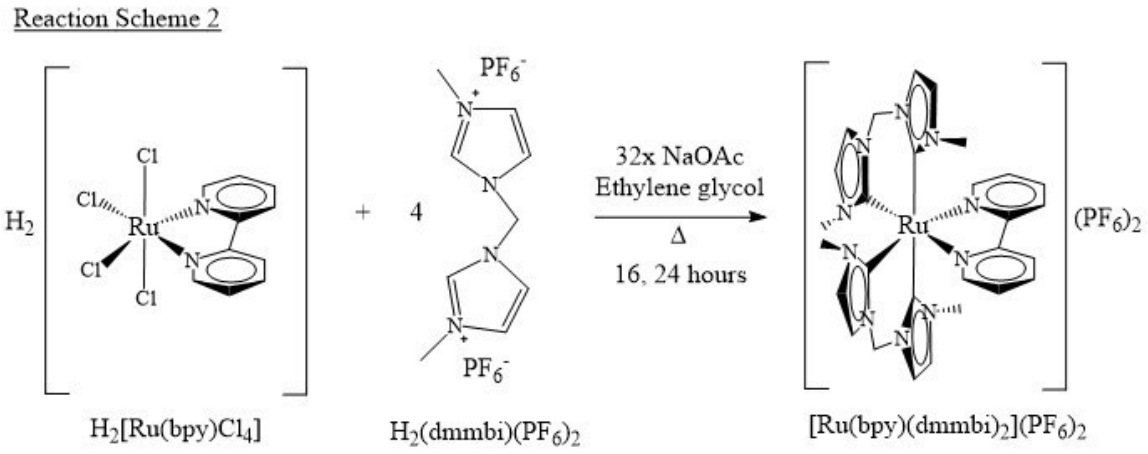

Figure 20. Second attempted synthesis of $[Ru(bpy)(dmmbi)_2](PF_6)_2$.

The second reaction scheme used $H_2[Ru(bpy)Cl_4]$ as the starting material and reacted it in a 1:4 molar ratio with $H_2(dmmbi)(PF_6)_2$ using a 150 mL high-pressure vessel. NaOAc was the base used to deprotonate $H_2(dmmbi)(PF_6)_2$ so that it could coordinate to

the metal center. Ethylene glycol was used as the solvent, and it was heated for either 16 or 24 hours. The temperature was kept at 160°C for all attempts. A 32-fold excess of NaOAc and a 4-fold excess of $H_2(dmmbi)(PF_6)_2$ were used in all cases. The major product was always $[Ru(bpy)_2(dmmbi)](PF_6)_2$, as confirmed by ^1H NMR analysis. It was hoped that the 4-fold excess of $H_2(dmmbi)(PF_6)_2$, rather than the needed 2-fold excess, would force the addition of the second dmmbi ligand. However, this did not appear to be the case. Perhaps an ethylene glycol/water solvent mixture would allow the NaOAc to dissolve more fully and thus increase the amount of dmmbi in the solution.

The use of $H_2[Ru(bpy)Cl_4]$ could potentially eliminate the ability of 2,2'-bipyridine to outcompete the dmmbi ligand as was the case in the first reaction method. However, the major formation of $[Ru(bpy)_2(dmmbi)](PF_6)_2$ demonstrated that an excess of 2,2'-bipyridine could be present in the solution. Since $H_2[Ru(bpy)Cl_4]$ was used as synthesized, it is likely that leftover 2,2'-bipyridine was still part of its composition. Therefore, the starting material would need to be purified through column chromatography prior to any attempted syntheses of the desired product. An attempt to remove the excess 2,2'-bipyridine via recrystallization with diethyl ether proved unsuccessful.

Based on these results, it appears that the $[Ru(bpy)(dmmbi)_2](PF_6)_2$ complex is thermodynamically more stable than $[Ru(bpy)_2(dmmbi)](PF_6)_2$. Additionally, a smaller excess of dmmbi may be needed so that $[Ru(dmmbi)_3](PF_6)_2$ is not formed which would release free bpy into the solution. Furthermore, it may be necessary to exchange the H^+ counter ion in $H_2[Ru(bpy)Cl_4]$ for a less reactive substance such as Na^+ or K^+ to prevent re-protonation of the dmmbi ligand.

Elemental Analysis

CHN elemental analysis provided the percentages of carbon (C), hydrogen (H), and nitrogen (N) atoms contained within the complexes. The actual percentages were contrasted against the expected values (Table 2).

Table 2. Comparison of expected and actual values for elemental analysis.

$[Ru(bpy)_3](PF_6)_2$			
	%C	**%H**	**%N**
Actual	41.73	2.76	9.66
Expected	41.92	2.81	9.78
$[Ru(bpy)_2(dmmbi)](PF_6)_2$			
	%C	**%H**	**%N**
Actual	30.01	2.41	9.75
Expected	39.60	3.21	12.47
Expected w/ 1.5 mol KPF_6	30.14	2.44	9.70
$[Ru(dmmbi)_3](PF_6)_2$			
	%C	**%H**	**%N**
Actual	32.41	3.78	17.20
Expected	35.26	3.95	18.28
Expected w/ 0.4 mol KPF_6	32.65	3.65	16.92

The actual percentages for the $[Ru(bpy)_3](PF_6)_2$ complex were consistent with those expected and fell within the acceptable ±0.40% range. However, $[Ru(bpy)_2(dmmbi)](PF_6)_2$ and $[Ru(dmmbi)_3](PF_6)_2$ exhibited percentages that deviated significantly from the expected values. It was surmised that this was the result of leftover KPF_6 from the recrystallization process. After purification, each of these complexes were recrystallized from a minimal amount of acetonitrile using a large excess of aqueous KPF_6. This likely caused some KPF_6 to precipitate out of the solution along with the complexes. When the extra masses were accounted for (1.5 mol KPF_6 for $[Ru(bpy)_2(dmmbi)](PF_6)_2$ and 0.4 mol

KPF_6 for $[Ru(dmmbi)_3](PF_6)_2]$) the expected %C, %H, and %N values fell within ±0.40% of what was recorded.

To avoid these deviations from the expected values in the future, the recrystallization process could be slightly altered. As stated previously, the errors most likely occurred when precipitating the products using an excess amount of aqueous KPF_6 solution. To circumvent this issue, the complexes could be precipitated from a minimal amount of acetonitrile using deionized water with a small amount of aqueous KPF_6. This would likely remove the excess KPF_6 salt.

Another method could be to dissolve the product in a minimal amount of dichloromethane and vacuum filtering it through a glass frit. Since KPF_6 is insoluble in dichloromethane, any excess present in the sample would be left behind. The product could then be precipitated out of the filtrate using diethyl ether and vacuum filtered again to isolate the desired product.

Nuclear Magnetic Resonance

2,2’-bipyridine

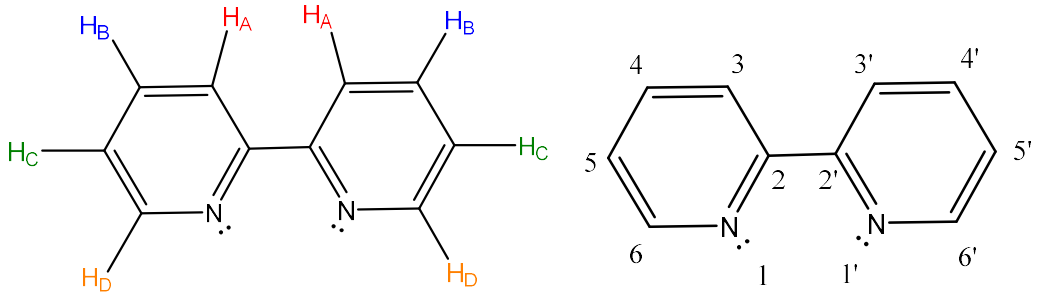

Figure 21. Proton assignments for 2,2’-bipyridine.

^{1}H NMR for 2,2’-bipyridine showed four peaks: two doublets at 8.66 and 8.42 ppm, and two triplets at 7.87 and 7.37 ppm (Figure 21). Integration yielded a total of eight protons when calibrated to the triplet at 7.87 ppm. Since all the protons exist in aromatic rings, the signals appearing in the aromatic ppm range of 9 – 7 ppm were consistent with the structure. Only four signals were obtained due to molecular symmetry – here a plane of symmetry between the two pyridine rings. The two doublets were assigned to the protons adjacent to the nitrogen atoms (H_D) and tertiary carbons (H_A) of the pyridyl rings. The triplets were attributed to the protons on carbon 4 (H_B) and carbon 5 (H_C) on the pyridyl rings.

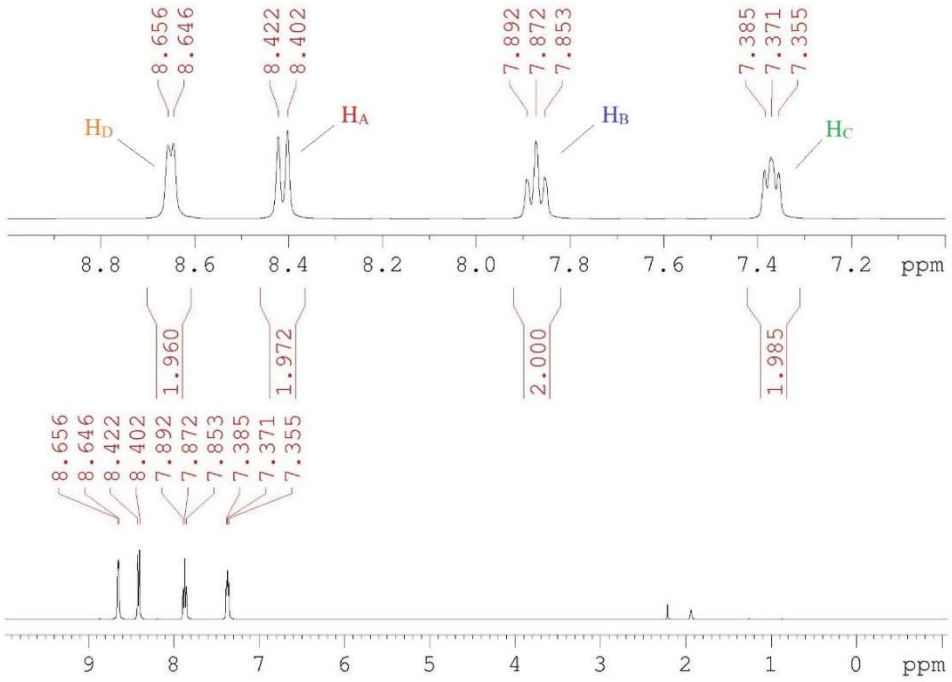

Figure 22. ^{1}H NMR for 2,2'-bipyridine.

COSY NMR clarified the structure further (Figure 22). Strong signals indicated that the triplets at 7.87 and 7.37 ppm were adjacent to each other, which is expected given the proton locations of H_B and H_C and the fact that these are the only triplets. The most deshielded doublet (H_D) was found to be coupled to the least deshielded triplet (H_C), indicating that they are on adjacent carbon atoms. The doublet and triplet at 8.42 and 7.87 ppm, respectively, were also observed to be coupled. This indicates that the doublet was H_A, and the triplet was H_B.

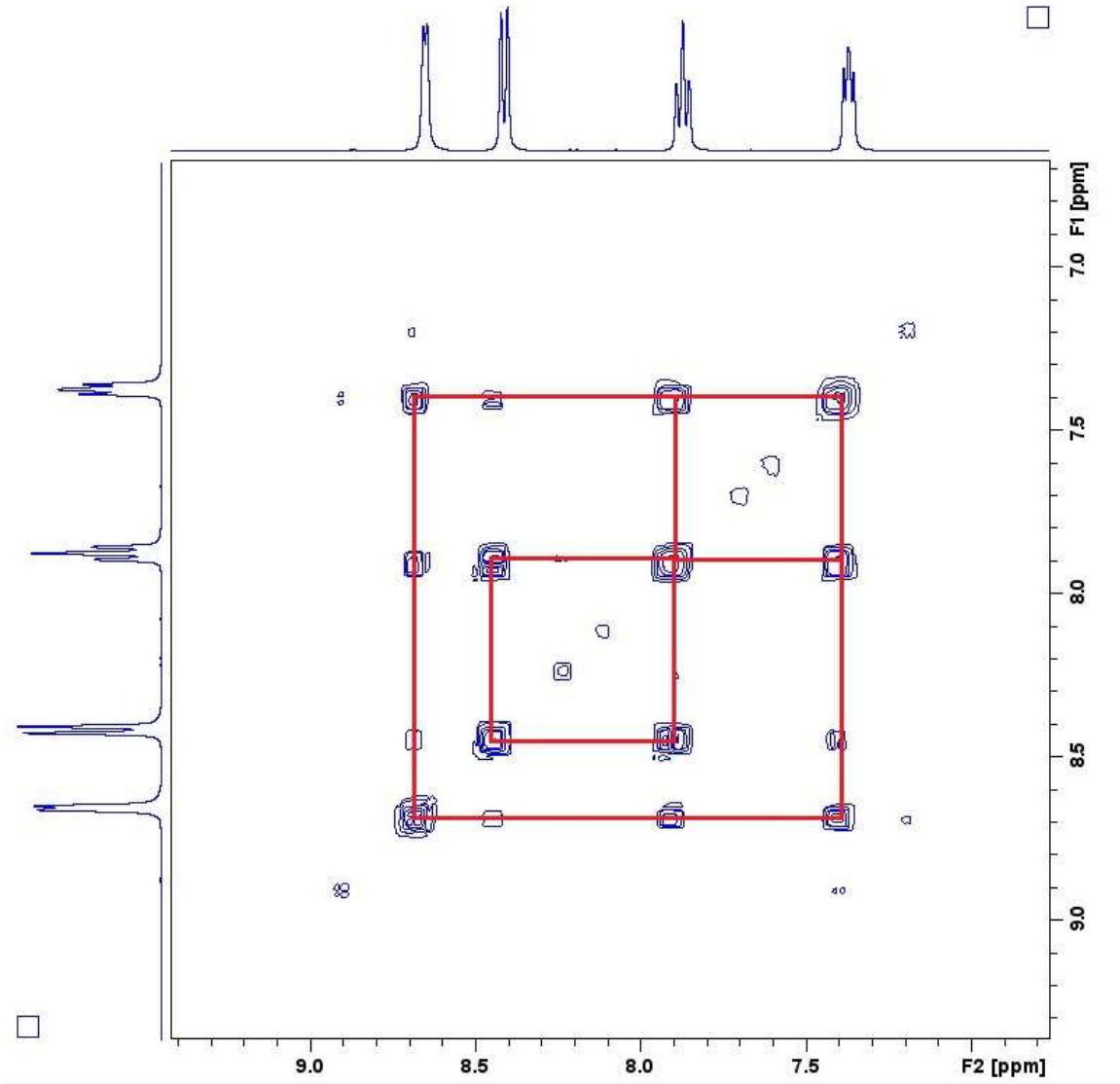

Figure 23. COSY NMR for 2,2'-bipyridine.

^{13}C NMR provided five signal peaks at 157.26, 150.60, 138.42, 125.32, and 121.95 ppm (Figure 23). This is consistent with the structure given that the two pyridine rings are equivalent, meaning that 10 carbons were detected. The signals farthest downfield are expected to be carbons 2 and 6 as the adjacent nitrogen atom would cause significant deshielding. The other three peaks more upfield likely represent carbons 3, 4, and 5. Assuming similar deshielding to that of the protons, carbons 3, 4, and 5 were assigned to the peaks with chemical shifts of 138.42, 125.32, and 121.95 ppm, respectively.

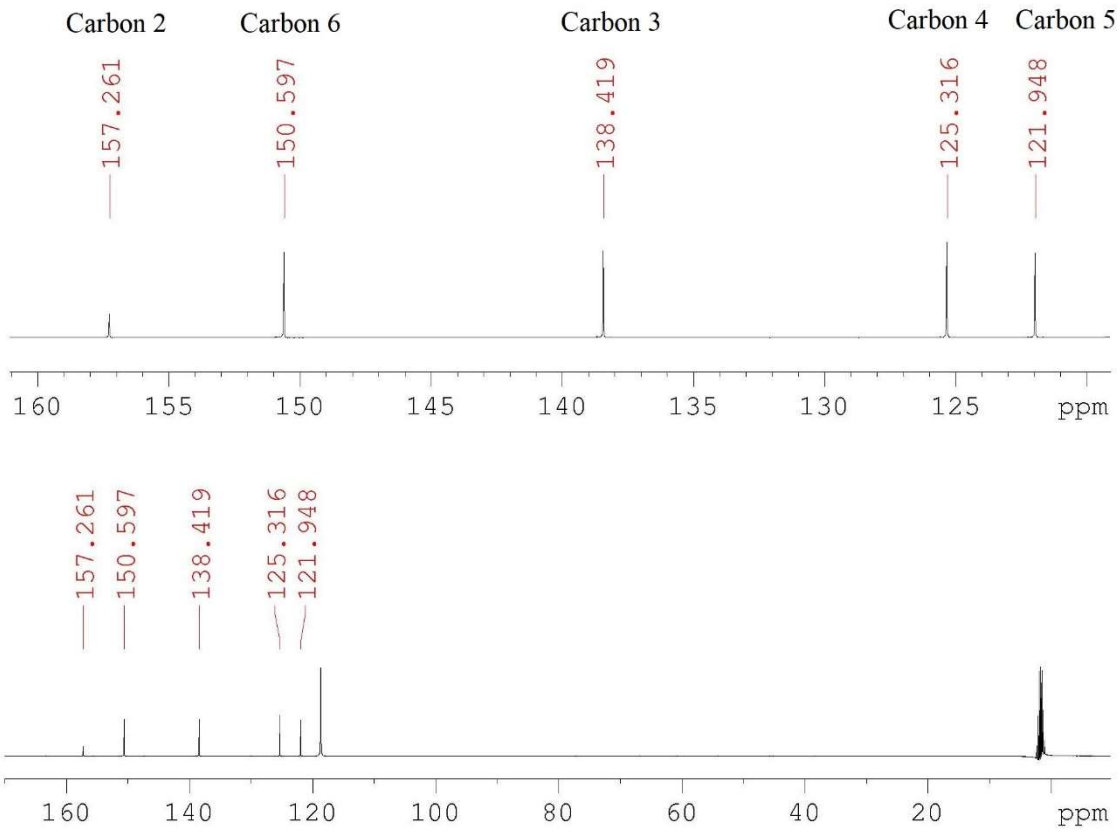

Figure 24. ^{13}C NMR for 2,2'-bipyridine.

[Ru(bpy)$_3$](PF$_6$)$_2$

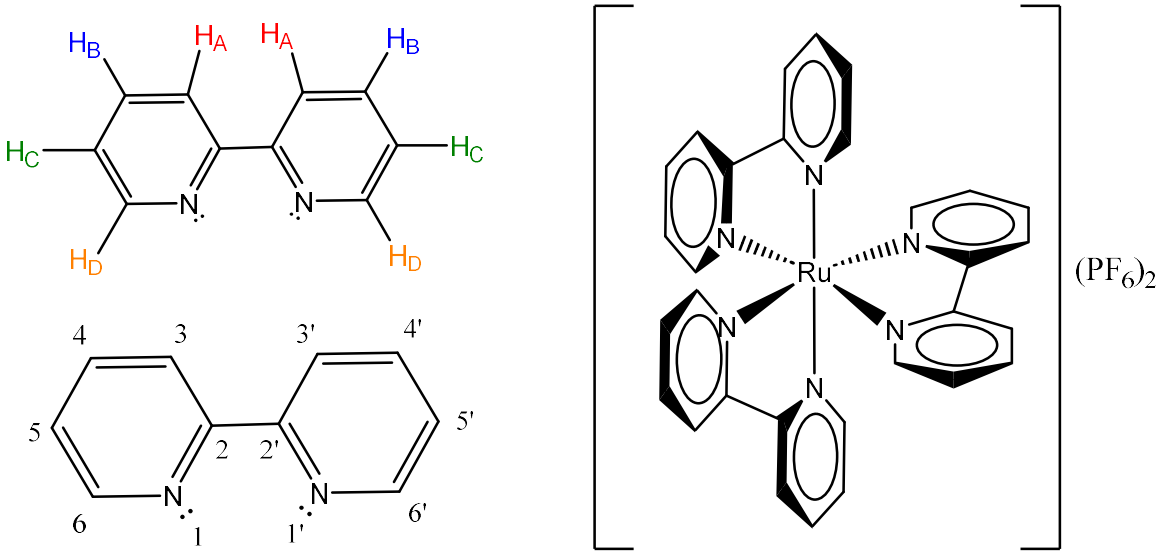

Figure 25. Proton assignments for [Ru(bpy)$_3$](PF$_6$)$_2$.

^{1}H NMR for [Ru(bpy)$_3$](PF$_6$)$_2$ showed four peaks: two doublets at 8.52 and 7.75 ppm, and two triplets at 8.06 and 7.41 ppm (Figure 25). Only four peaks were expected given the symmetry of the ligands and the uniform chemical environment around the metal center. There is a C_3 axis in the molecule that makes the three bipyridine rings equivalent, and each pyridine ring is across the ruthenium from another pyridine ring, making both rings equivalent. Integration yielded a 1:1:1:1 ratio of the four signals or twenty-four protons with calibration of the first peak to six protons. This was expected given that each 2,2'-bipyridine ligand contains eight protons, and three ligands were coordinated around the metal center. The two doublets represent the protons adjacent to the nitrogen atom and the tertiary carbon in the ligand structure (H_A and H_D). The triplets represent the protons on carbons 4 and 5 of the pyridyl rings (H_B and H_C). H_D was most likely the doublet farthest downfield as it would be the most deshielded since it is on a carbon adjacent to a nitrogen

atom, and H_A was the other doublet farther upfield since it is on a carbon adjacent to the bridging carbon.

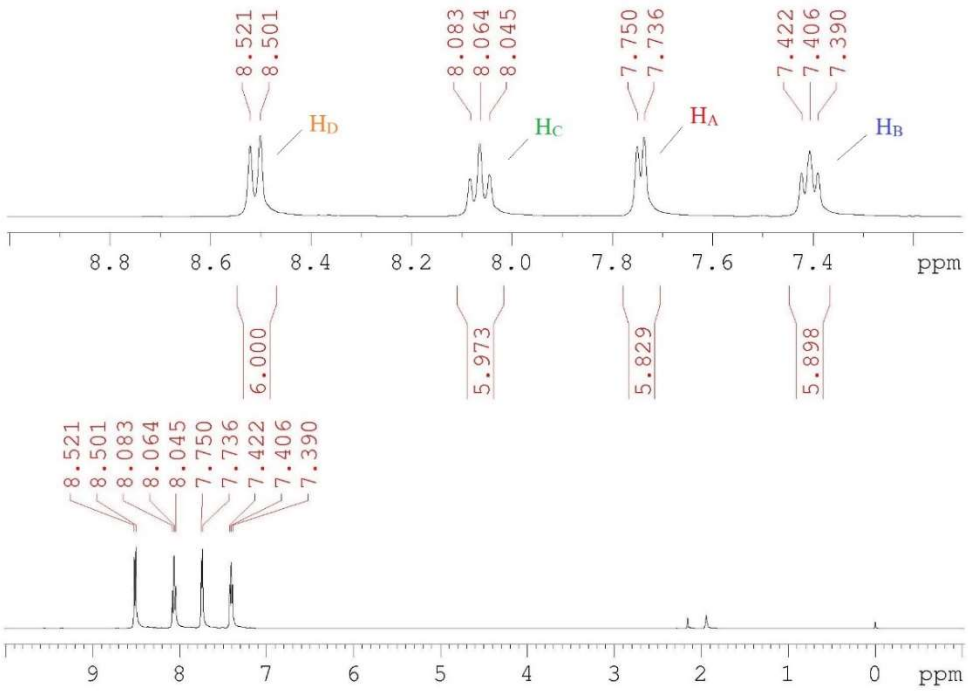

Figure 26. ^{1}H NMR for $[Ru(bpy)_3](PF_6)_2$.

When considering the COSY NMR data for $[Ru(bpy)_3](PF_6)_2$ (Figure 26), it was observed that the first doublet at 8.52 ppm and first triplet at 8.06 ppm were adjacent to each other. From this we can conclude that the triplet at 8.06 ppm must be represented by H_C. The doublet and triplet peaks at 7.75 and 7.41 ppm, respectively, were found to be adjacent as well. This implies that the triplet at 7.41 ppm must be represented by H_B. Some protons were also observed to be weakly coupled to the protons on beta carbons. Such weak signals were observed between the doublet at 8.52 ppm (H_D) and the triplet at 7.41 ppm (H_B), and between the triplet at 8.06 ppm (H_C) and the doublet at 7.75 ppm (H_A).

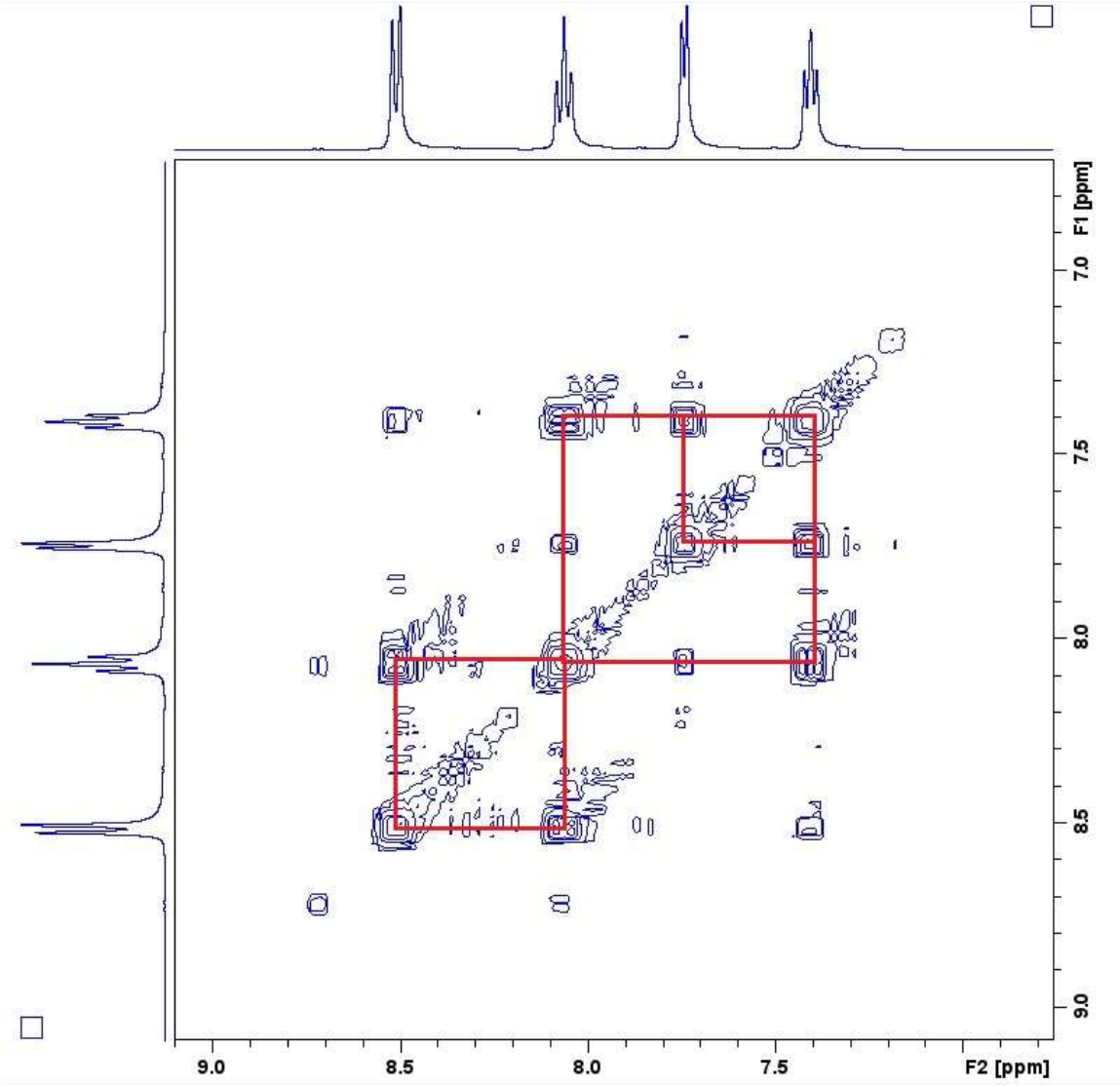

Figure 27. COSY NMR for $[Ru(bpy)_3](PF_6)_2$.

^{13}C NMR provided a total of five peaks at 158.35, 153.04, 139.15, 128.94, and 125.62 ppm (Figure 27). Five peaks and not ten were observed due to the symmetry of the ligands. Given the similarity in the chemical shifts, the carbon assignments for each peak were kept the same as the ^{13}C NMR data for 2,2'-bipyridine. Therefore, carbons 2, 6, 3, 4, and 5 were assigned to the peaks with chemical shifts of 158.35, 153.04, 139.15, 128.94, and 125.62 ppm, respectively.

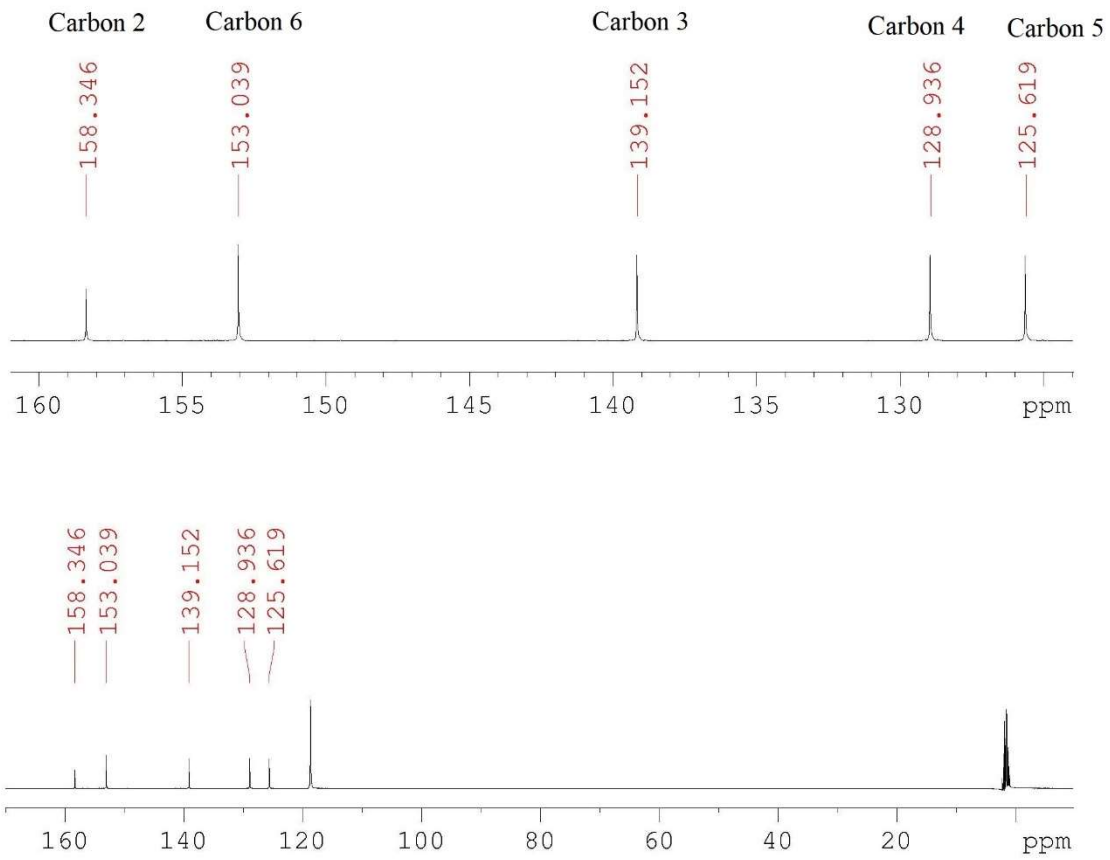

Figure 28. ^{13}C NMR for $[Ru(bpy)_3](PF_6)_2$.

Comparison of 2,2'-bipyridine and $[Ru(bpy)_3](PF_6)_2$ ^{1}H NMR Spectra

It is worthy to note the shift in peak locations when comparing the ^{1}H NMR data of both 2,2'-bipyridine and $[Ru(bpy)_3](PF_6)_2$ (Figure 28). Upon coordination around the metal center, one of the triplet peaks (H_C) becomes more deshielded than the one of the doublet peaks (H_A). When comparing the COSY spectra for 2,2'-bipyridine and $[Ru(bpy)_3](PF_6)_2$, we see strong coupling between the most deshielded doublet (8.66 ppm for 2,2'-bipyridine and 8.52 ppm for $[Ru(bpy)_3](PF_6)_2$) and one of the triplets (farthest upfield for 2,2'-bipyridine at 7.37 ppm and further downfield for $[Ru(bpy)_3](PF_6)_2$ at 8.06 ppm). A possible cause for the greater deshielding of H_C than H_A in $[Ru(bpy)_3](PF_6)_2$ is the change in the electron density near the nitrogen and within the pyridyl rings themselves after coordinating to the ruthenium center. Before coordinating to the ruthenium metal center, the free-floating 2,2'-bipyridine can rotate around the pyridine-pyridine bond. Upon coordination, it becomes fixed in space. This results in the H_A's of both rings to be very close, causing H_A to shift less electron density toward the ruthenium metal center. H_C, the other meta proton of the ring, does not experience this effect. Thus, H_C is more delocalized towards the metal center than H_A.

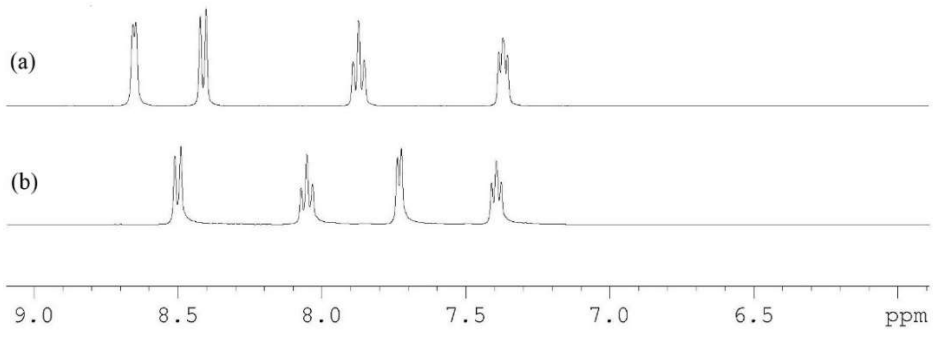

Figure 29. Comparison of ^{1}H NMR data for (a) 2,2'-bipyridine and (b) $[Ru(bpy)_3](PF_6)_2$.

$H_2(dmmbi)(PF_6)_2$

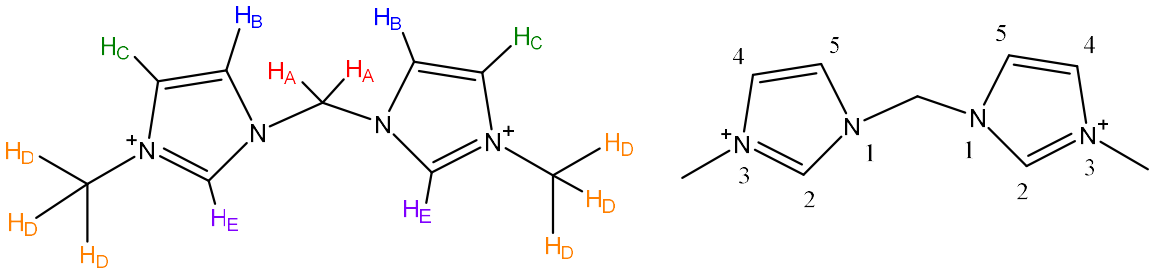

Figure 30. Proton assignments for $H_2(dmmbi)(PF_6)_2$.

^{1}H NMR for $H_2(dmmbi)(PF_6)_2$ showed five peaks at 8.70, 7.56, 7.44, 6.36, and 3.87 ppm (Figure 30). Integration produced a total of fourteen protons when calibrated to two carbene protons (H_E), which is consistent with the molecular structure. The existence of only five peaks as opposed to ten is due to molecular symmetry – in this case a plane of symmetry through the bridging methylene carbon. The four most downfield signals can be attributed to those existing on the ring itself and the methylene group. Of these four, the singlet farthest downfield (most deshielded) at 8.70 ppm was the proton belonging to the imidazolium carbon between the two nitrogens (H_E). The singlet situated least downfield at 6.36 ppm was the proton of the methylene group (H_A) given its lack of conjugation. The two singlets present at 7.56 and 7.44 ppm were those of the carbon-carbon double bond in each ring (H_B and H_C), which occur as singlets and not doublets due to symmetry. The singlet existing farthest upfield (least deshielded) at 3.87 ppm can be assigned to the protons residing on the methyl groups (H_D), which is a characteristic of methyl protons attached to a partially conjugated system. This is also supported by the value given by integration, which is consistent with six protons.

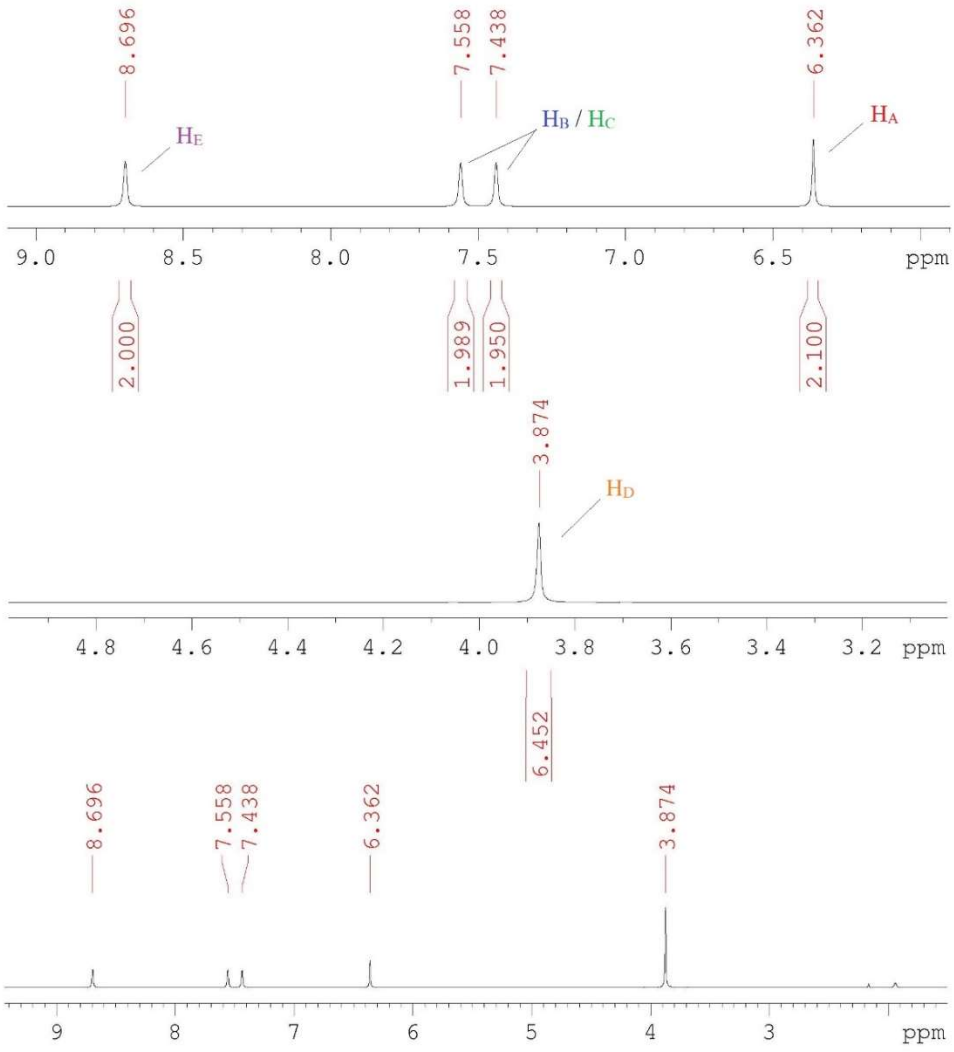

Figure 31. ^{1}H NMR for $H_2(dmmbi)(PF_6)_2$.

COSY NMR showed the proximal relationships between the protons within the compound and gave further insight into the structure (Figure 31). A strong signal showed that the two singlets at 7.56 and 7.44 ppm were coupled, which confirmed them to be the protons on the carbon-carbon double bonds (H_B and H_C) of each ring. Slight coupling

signals were observed for H_A and H_D, H_E and H_B and H_E and H_C. These signals can be attributed to the ability for the molecule to rotate around the methylene carbon which is sp^3 hybridized. By contrast the imidazole rings are essentially planar as there are three sp^2 hybridized carbon atoms and one sp^2 hybridized nitrogen in each ring.

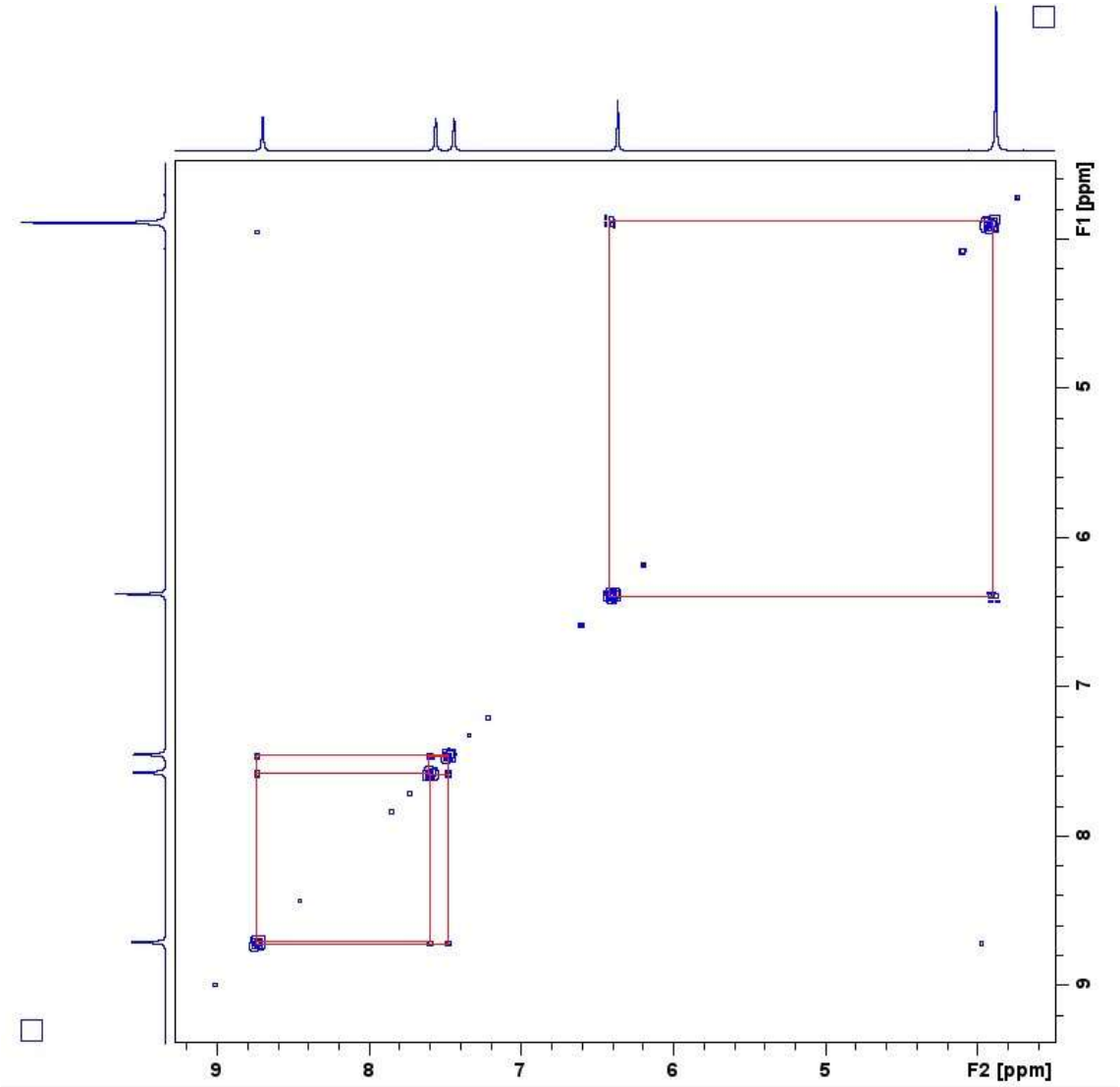

Figure 32. COSY NMR for $H_2(dmmbi)(PF_6)_2$.

^{13}C NMR provided five carbon signals at 138.61, 126.26, 123.30, 59.96, and 37.76 ppm (Figure 32). As with ^1H NMR, only five peaks instead of ten were expected due to molecular symmetry. The peak farthest downfield at 138.61 ppm in the aromatic region

can be attributed to carbon 2 which is between the two nitrogens in the ring. The farthest upfield carbon at 37.76 ppm was the methyl group carbon. The methylene carbon can be assigned to the peak residing at 59.96 ppm, which is supported by its lower intensity (one methylene carbon as compared to each carbon in two imidazole rings). The remaining two peaks at 126.26 and 123.30 ppm can be assigned to the carbons of the carbon-carbon double bond in each ring. This is consistent with H_B/H_C that were observed for the ^1H NMR. The ^{13}C NMR is consistent with the desired compound and lines up with NMRs done by previous researchers.[24]

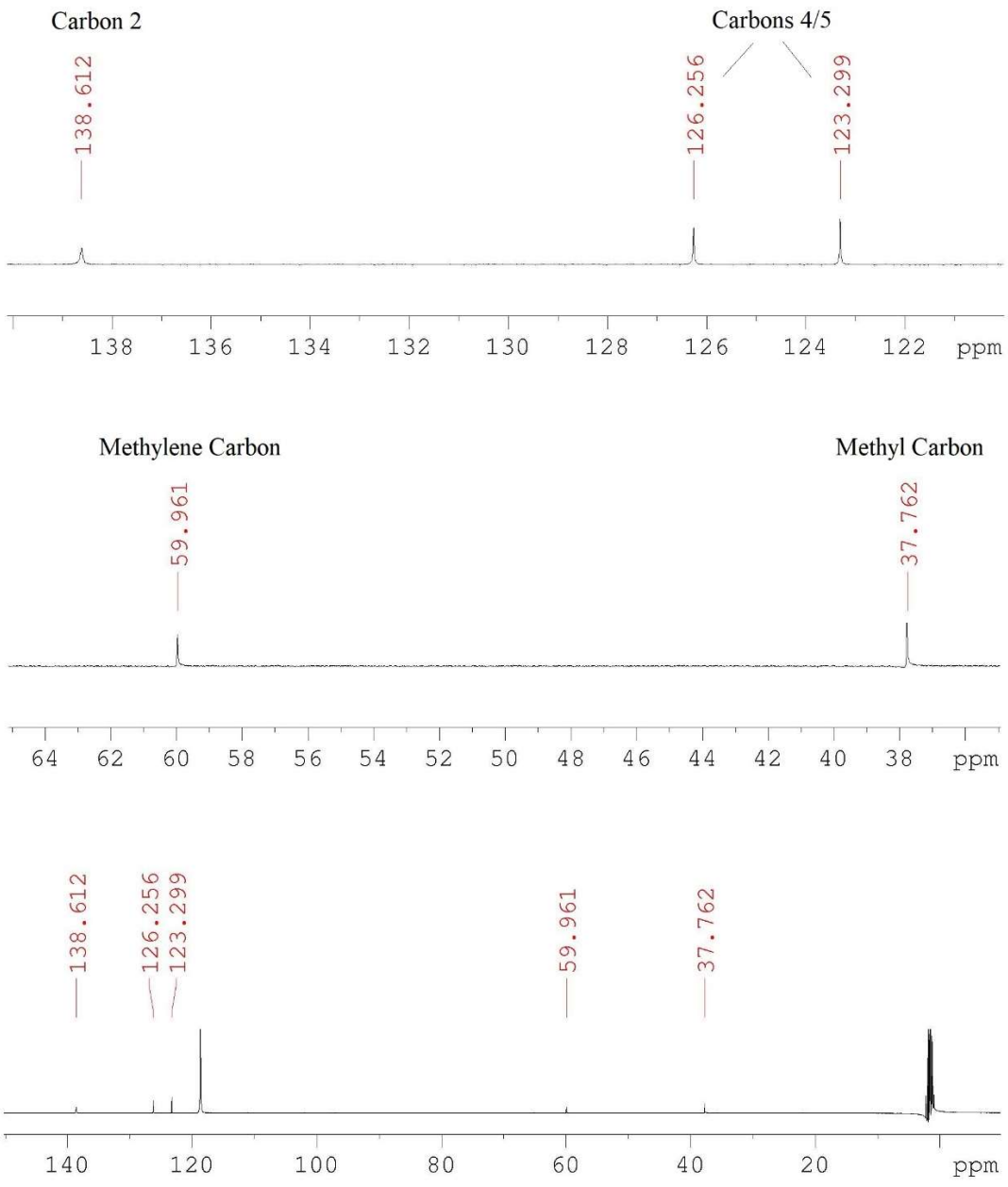

Figure 33. ^{13}C NMR for $H_2(dmmbi)(PF_6)_2$.

[Ru(dmmbi)$_3$](PF$_6$)$_2$

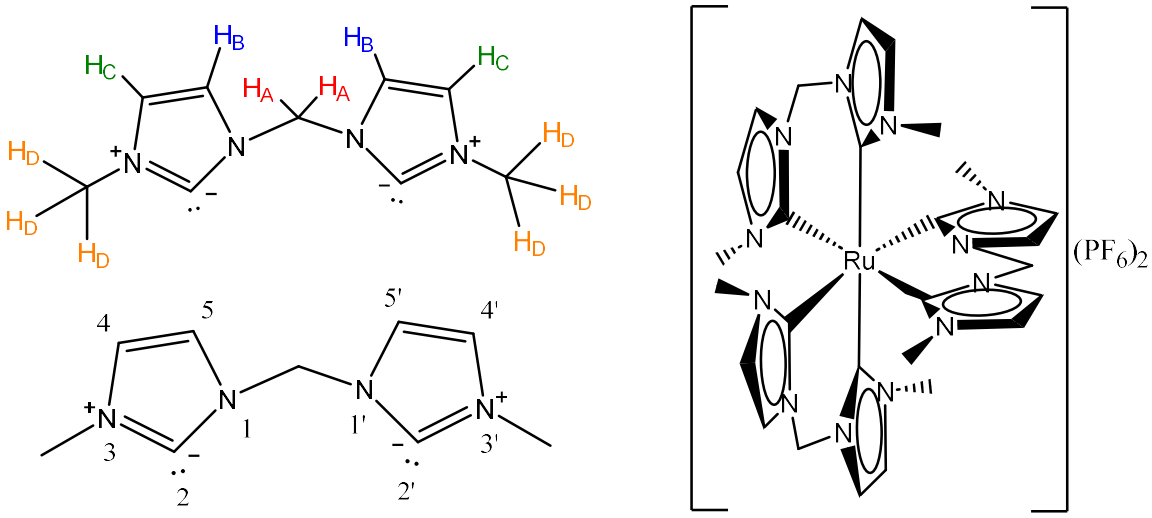

Figure 34. Proton assignments for [Ru(dmmbi)$_3$](PF$_6$)$_2$.

^{1}H NMR for [Ru(dmmbi)$_3$](PF$_6$)$_2$ yielded four singlet peaks at 7.06, 6.88, 6.29, and 3.65 ppm in an integration ratio of 1:1:1:3 (Figure 34). Integration produced thirty-six protons when the singlet at 3.65 ppm was assigned as eighteen protons, which is consistent with the structure of the complex as each dmmbi ligand contains twelve protons after deprotonation of both carbene carbons. Only four peaks are observed because a C_3 axis runs through the ruthenium metal center and each imidazole is across from another imidazole ring, which establishes uniform symmetry through each ligand. The first two singlets farthest downfield (7.06 and 6.88 ppm) represent the protons along the carbon-carbon double bond (H_B and H_C). The methylene protons (H_A) were identified with the singlet at 6.29 ppm. The methyl group protons (H_D) were represented by the singlet peak at 3.65 ppm, which was within a range characteristic of methyl groups attached to a nitrogen atom.

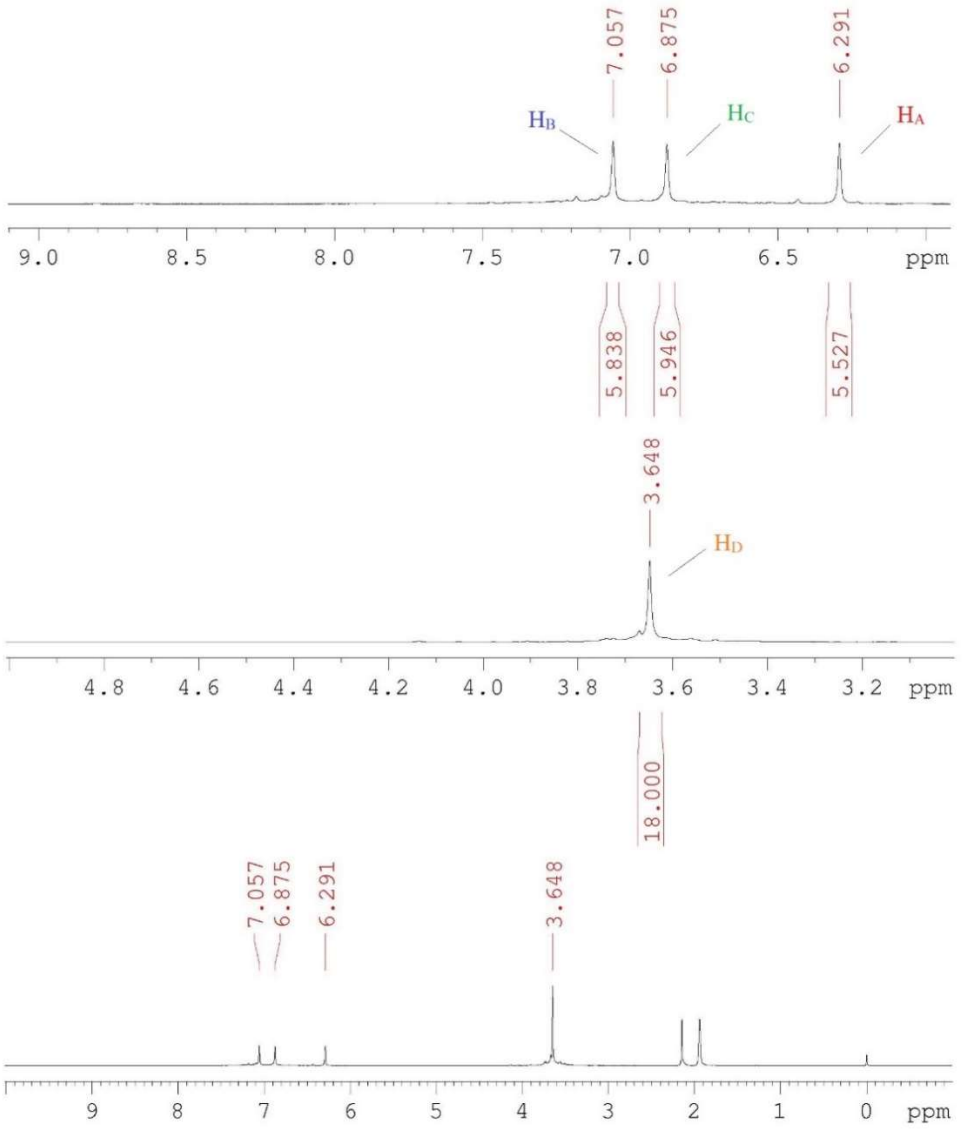

Figure 35. ^{1}H NMR for $[Ru(dmmbi)_3](PF_6)_2$.

COSY NMR further clarified and gave insight into the structure of the $[Ru(dmmbi)_3](PF_6)_2$ complex (Figure 35). A weak signal suggested that the singlets farthest downfield (7.06 and 6.88 ppm) were adjacent and represented H_B and H_C. Another weak signal between the singlets at 7.06 and 6.29 ppm implies a close but nonadjacent proximity, indicating that they represent H_B and H_A, respectively. The methylene carbon

is near H_B in space and is likely coupled through the nitrogen atom. H_D, the methyl group proton, was not found to be adjacent to any other proton. This contrasts to the COSY NMR data for $H_2(dmmbi)(PF_6)_2$ because the coordinated ligand is fixed in place and cannot rotate about the methylene carbon that bridges the two imidazole rings.

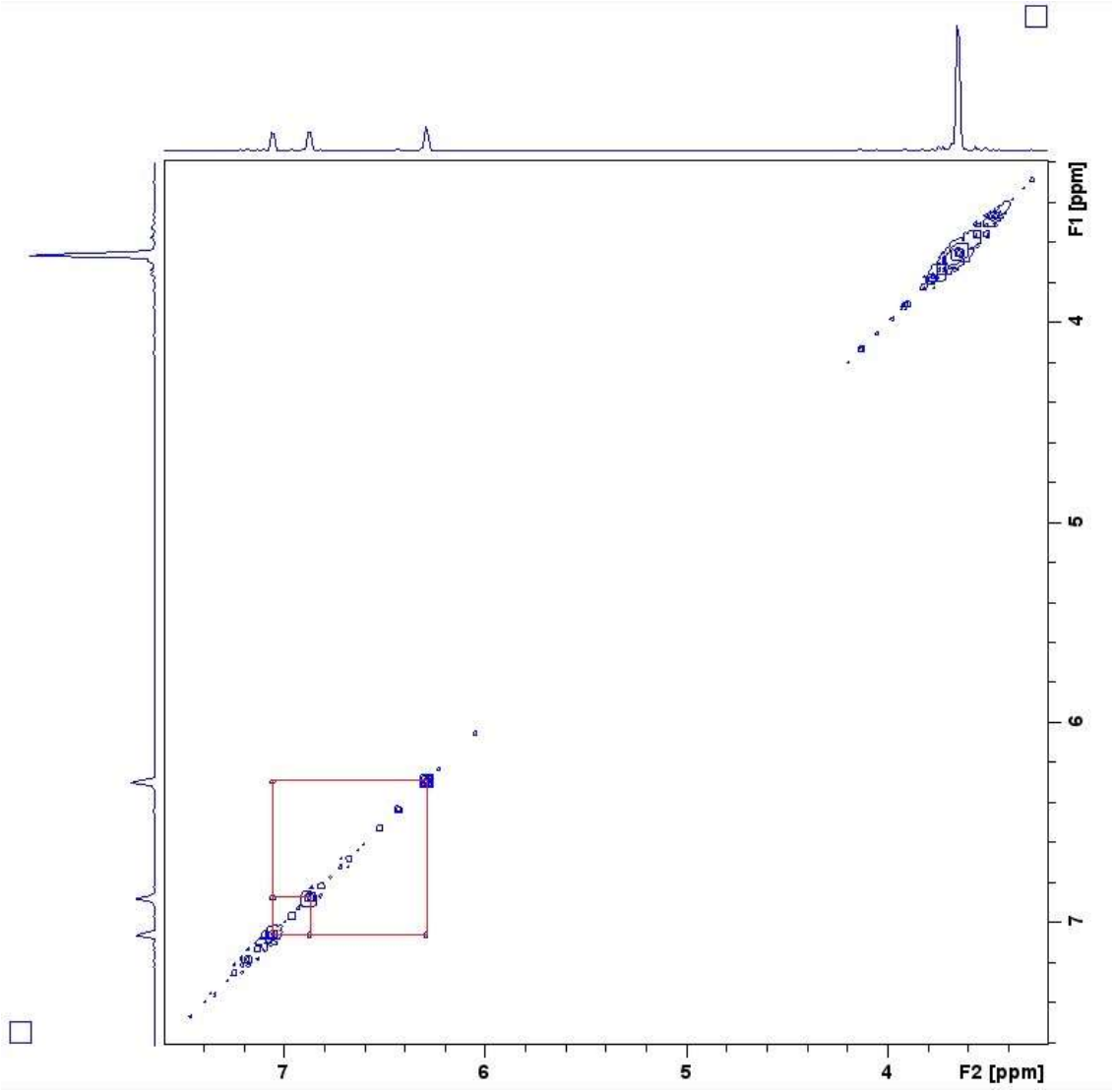

Figure 36. COSY NMR for $[Ru(dmmbi)_3](PF_6)_2$.

^{13}C NMR produced four peaks at 141.46, 131.31, 122.82, and 34.50 ppm (Figure 36). The signal farthest downfield was attributed to the carbene carbon as it would be the most deshielded. The following two signals represent the carbons of the carbon-carbon

double bonds in each imidazole ring. The signal farthest upfield was assigned to the methyl group carbons. The methylene carbon was not identified, regardless of how long we acquired the spectrum up to 16,000 scans. This is likely due to the exceptionally weak signal that would be produced by the methylene carbon, given that only one carbon of that type exists within each ligand and the molecular mass of the complex is far greater than that of $H_2(dmmbi)(PF_6)_2$ alone. This is consistent with the ^{13}C NMR data collected by Ryan Mahabir.[24]

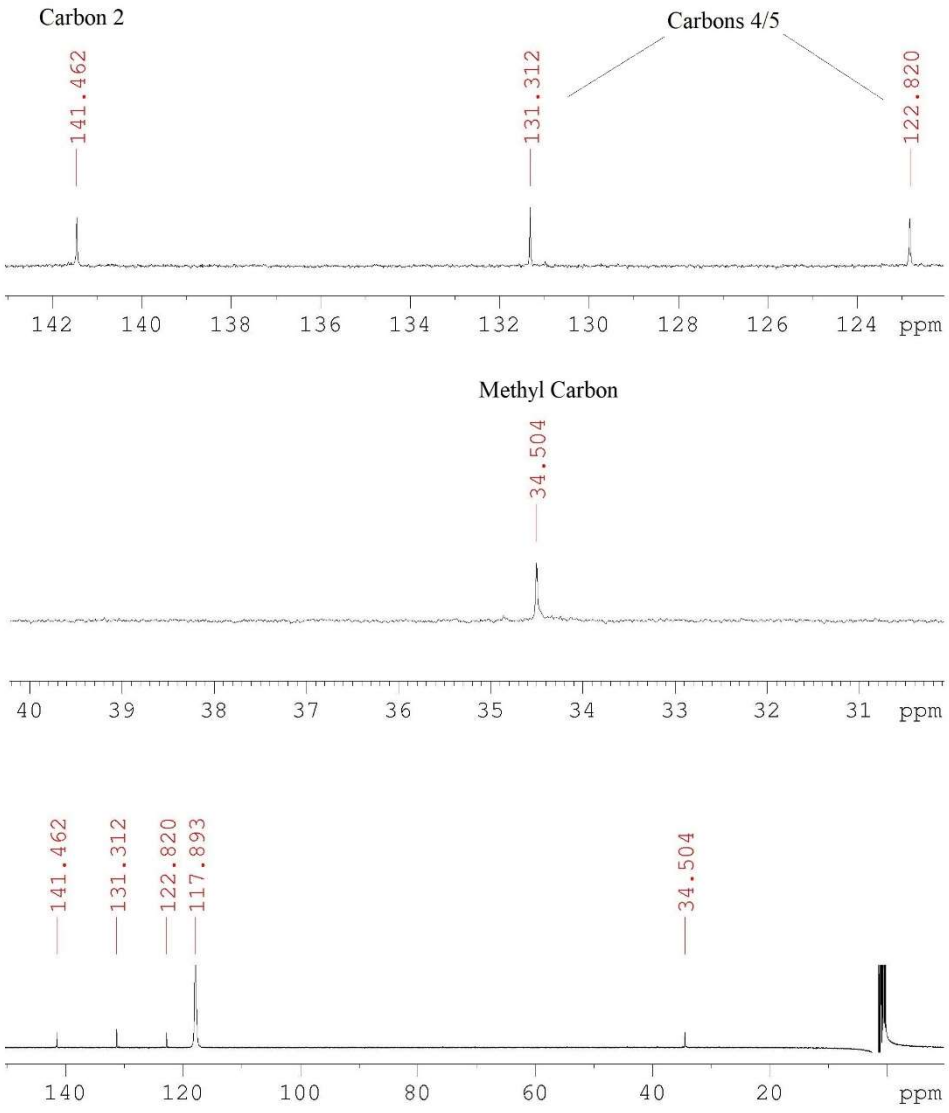

Figure 37. ^{13}C NMR for $[Ru(dmmbi)_3](PF_6)_2$.

Comparison of $H_2(dmmbi)(PF_6)_2$ and $[Ru(dmmbi)_3](PF_6)_2$ ^1H NMR Spectra

The most notable change in the ^1H NMR data is the loss of the most deshielded singlet proton, H_E, around 8.70 ppm for $[Ru(dmmbi)_3](PF_6)_2$ (Figure 37). This is due to deprotonation of the carbene carbons so that they can be bound to the metal center. Therefore, the four singlet peaks in $[Ru(dmmbi)_3](PF_6)_2$ and the five singlet peaks in $H_2(dmmbi)(PF_6)_2$ were proof that three bis-NHC were attached to the ruthenium(II) metal center. Another change observed is the shift in location of the protons attached to the carbon-carbon double bonds in the imidazole rings (H_B and H_C). These protons are more deshielded in $H_2(dmmbi)(PF_6)_2$ than they are in $[Ru(dmmbi)_3](PF_6)_2$, which could be attributed to the effect that π-backbonding between the ruthenium metal center and the metal-bound carbon would have within the imidazole rings. The only other singlet peak that shows a significant shift between the two compounds is that belonging to the methyl groups. The methyl protons for $[Ru(dmmbi)_3](PF_6)_2$ exhibit slightly less deshielding than in $H_2(dmmbi)(PF_6)_2$, which could also be due to introducing π-backbonding within the system.

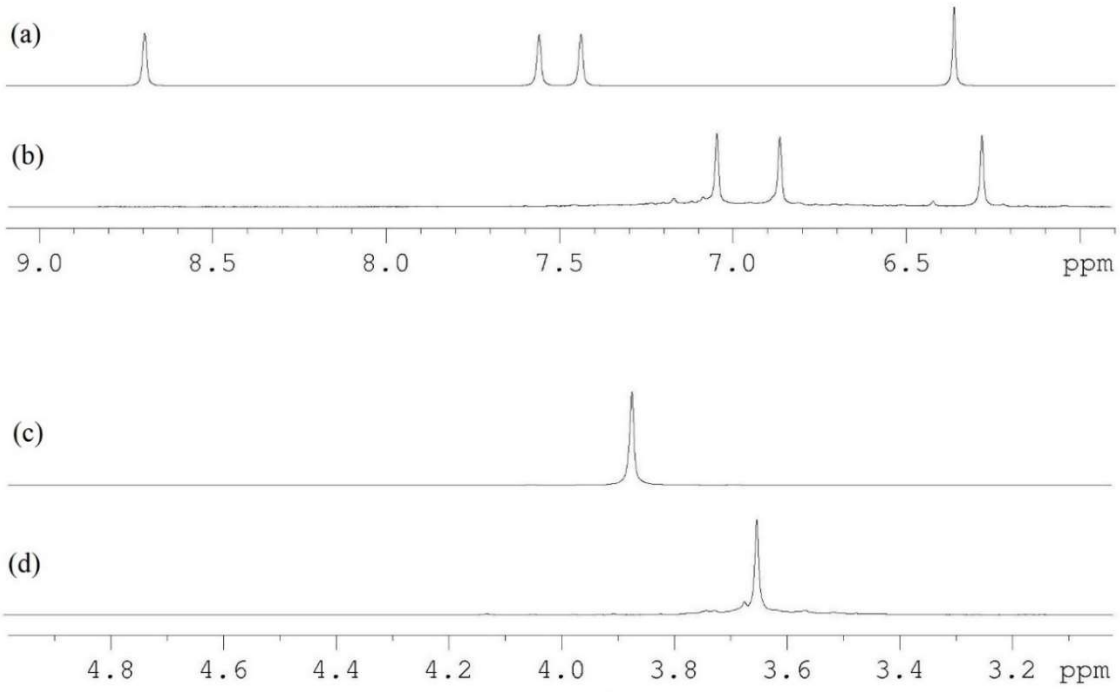

Figure 38. Comparison of ^{1}H NMR data: downfield regions for (a) $H_2(dmmbi)(PF_6)_2$ and (b) $[Ru(dmmbi)_3](PF_6)_2$, upfield regions for (c) $H_2(dmmbi)(PF_6)_2$ and (d) $[Ru(dmmbi)_3](PF_6)_2$.

[Ru(bpy)$_2$(dmmbi)](PF$_6$)$_2$

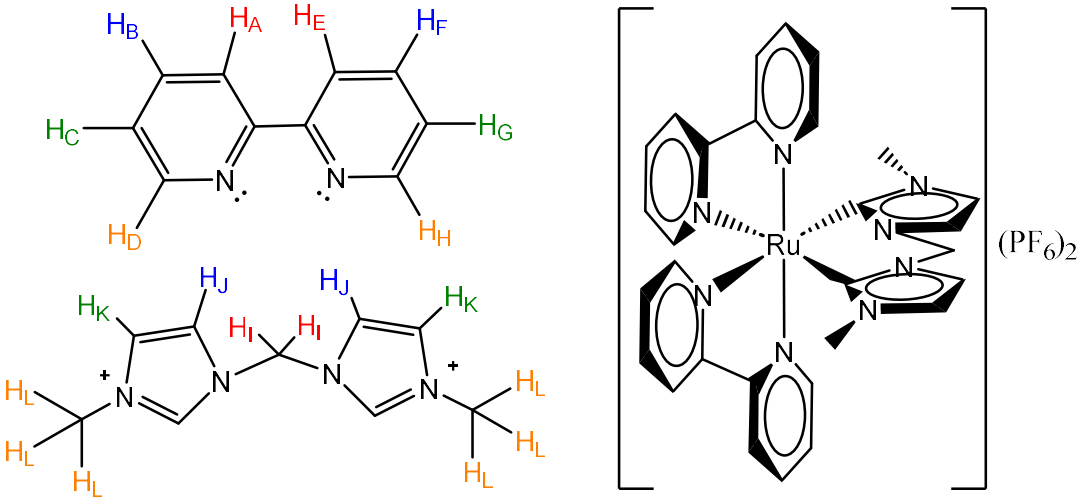

Figure 39. Proton assignments for [Ru(bpy)$_2$(dmmbi)](PF$_6$)$_2$.

^{1}H NMR for [Ru(bpy)$_2$(dmmbi)](PF$_6$)$_2$ produced a total of eleven peaks (Figure 39). Three doublets were observed at 8.92, 8.36, and 8.27 ppm. Three triplets were observed at 8.07, 7.68, and 7.27 ppm. Four singlets were observed at 7.37, 6.98, 6.64, and 3.57 ppm. A multiplet peak was found at 7.87 ppm which integrated to twice the number of protons as the isolated doublets and triplets. Based on the expected signals for each bipyridine, this is likely an overlapping of a doublet and a triplet. Integration yielded a total of twenty-eight protons when the doublet farthest downfield was assigned as two protons, which is consistent with the structure of the complex. The singlets were attributed to the dmmbi ligand and yielded four peaks instead of eight due to molecular symmetry. The locations of the peaks were consistent with the ^{1}H NMR data of the H$_2$(dmmbi)(PF$_6$)$_2$ itself. The 2,2'-bipyridine peaks, consisting of the doublets and triplets in the spectrum, were split into two sets of four because of the chemically different environments that each pyridyl ring experiences upon coordination around the metal center. One ring is oriented across from the dmmbi ligand, while the other is oriented across from another 2,2'-bipyridine

ligand. This causes the protons of each pyridyl ring to encounter different scales of deshielding.

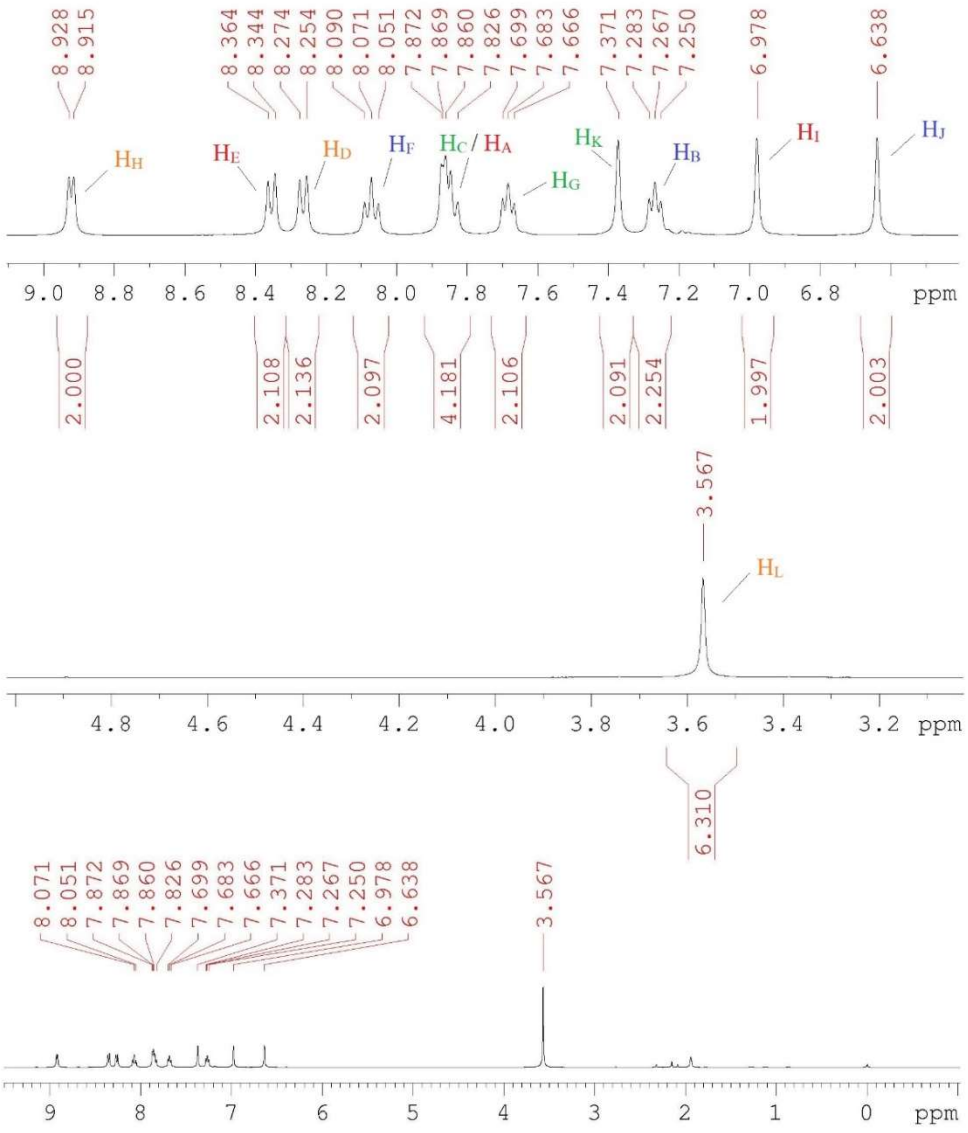

Figure 40. ^{1}H NMR for $[Ru(bpy)_2(dmmbi)](PF_6)_2$.

COSY NMR was difficult to decipher given the splitting of the 2,2'-bipyridine proton peaks (Figure 40). It was determined that the two triplets at 8.07 and 7.68 ppm were adjacent protons, and the two triplets at 7.87 and 7.27 ppm were adjacent protons. Adjacent

protons were also found between the doublets and triplets at 8.92 and 7.68 ppm, 8.36 and 8.07 ppm, 8.27 and 7.87 ppm, and 7.68 and 7.27 ppm, respectively. It was surmised that the doublet farthest downfield represented H_H as its proximity to the dmmbi ligand would cause greater deshielding. The triplet coupled to H_H at 7.68 ppm was assigned to H_G. This indicated that the triplet coupled to H_G at 8.07 ppm represented H_F. The doublet coupled to H_F at 8.36 ppm could then be assigned to H_E. Following this same line of logic, the signals for the other bipyridyl ring at 8.27, 7.87, and 7.27 ppm could be assigned to H_D, H_C/H_A, and H_B, respectively.

The COSY for the dmmbi portion showed a total of three singlets (Figure 40). The singlet farthest upfield at 3.57 ppm was absent from the figure due to its lack of coupling to the other peaks. For this reason, H_L was assigned to the 3.57 ppm peak as it represents the protons of the methyl group. The three singlets farther downfield would then represent H_I, H_K, and H_J. The singlets at 7.37 and 6.34 ppm were assigned as H_K and H_J, respectively, which are the protons on the carbon-carbon double bond. This resulted in the singlet at 6.98 ppm being labelled as H_I, the protons on the methylene carbon, since it was only very weakly coupled to the singlet representing H_J (6.34 pppm) and showed no coupling to the other singlet assigned as H_K (7.37 ppm).

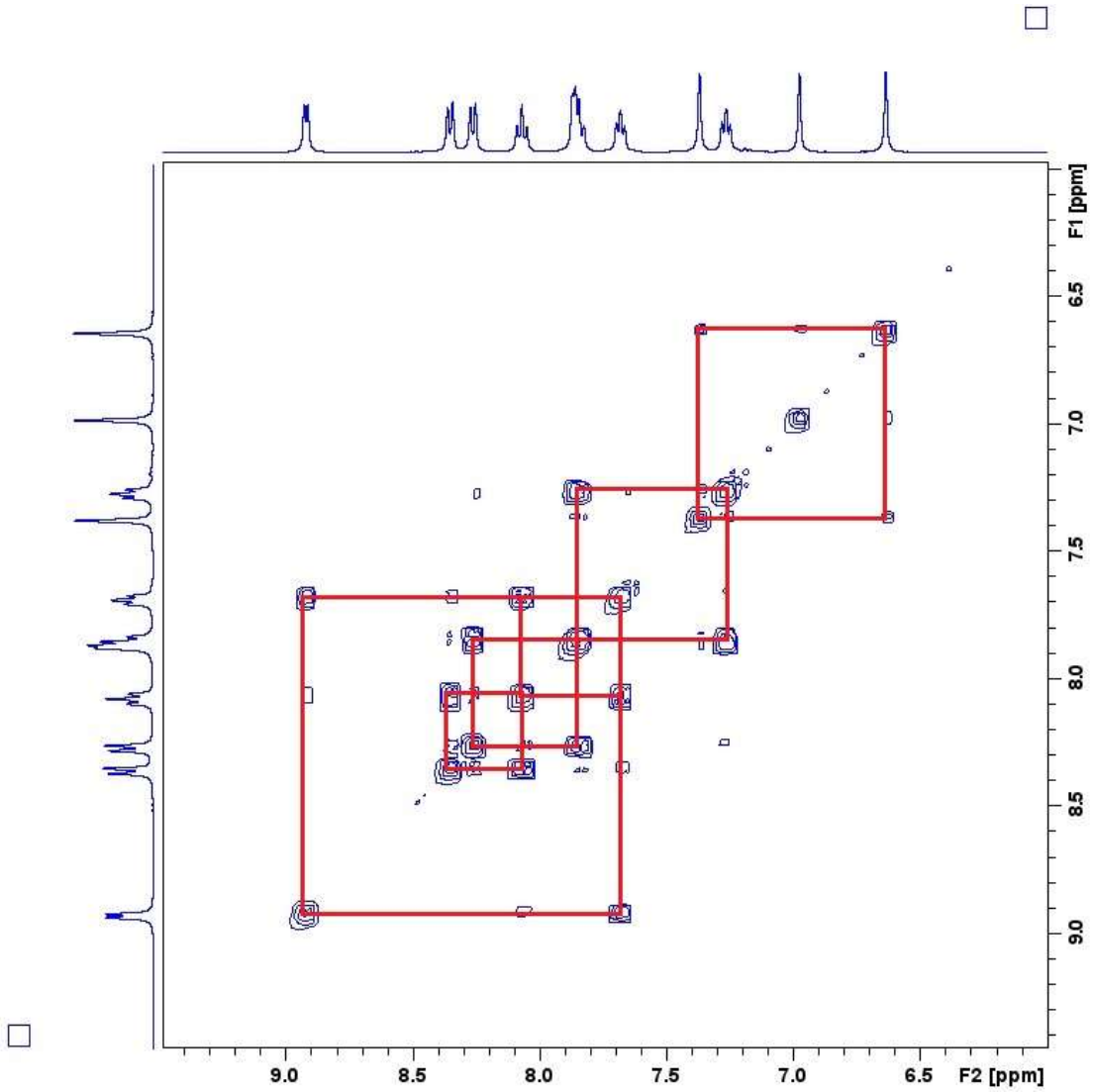

Figure 41. COSY NMR for $[Ru(bpy)_2(dmmbi)](PF_6)_2$.

^{13}C NMR produced at total of fourteen peaks at 159.49, 159.96, 153.76, 153.72, 141.57, 138.08, 137.74, 130.73, 128.54, 128.22, 124.85, 124.68, 123.90, and 35.35 ppm (Figure 41). Although fifteen peaks were expected, the loss of one peak can be attributed to that of the methylene carbon. The reasoning for this is the same as that for the ^{13}C NMR data of $[Ru(dmmbi)_3](PF_6)_2$. The total mass of the complex and the single methylene carbon of the ligand would contribute to this result. This essentially made it undetectable to the instrumentation even after 16,000 scans.

The signals that showed minimal separations between each other exhibited chemical shifts similar to those in the ^{13}C NMR data for $[Ru(bpy)_3](PF_6)_2$ and were thought to be the signals from the bpy portion of the complex. Therefore, these signals were assigned similarly. Carbons 2/2' were assigned to the signals at 159.49 and 158.96 ppm. Carbons 6/6' were assigned to the signals at 153.76 and 153.72 ppm. Carbons 3/3' were assigned to the signals at 138.09 and 137.74 ppm. Carbons 4/4' were assigned to the signals at 128.54 and 128.22 ppm. Finally, carbons 5/5' were assigned to the signals at 124.85 and 124.68 ppm.

The remaining isolated peaks were thought to originate from the dmmbi portion of the complex. Assuming the carbons would experience deshielding similar to the protons in the ^{1}H NMR data for this complex, the carbons were assigned accordingly. Carbons 2, 4, and 5 were assigned to the signals at 141.57, 130.73, and 123.09 ppm, respectively. The signal farthest upfield (35.35 ppm) could be assigned to the carbon of the methyl group.

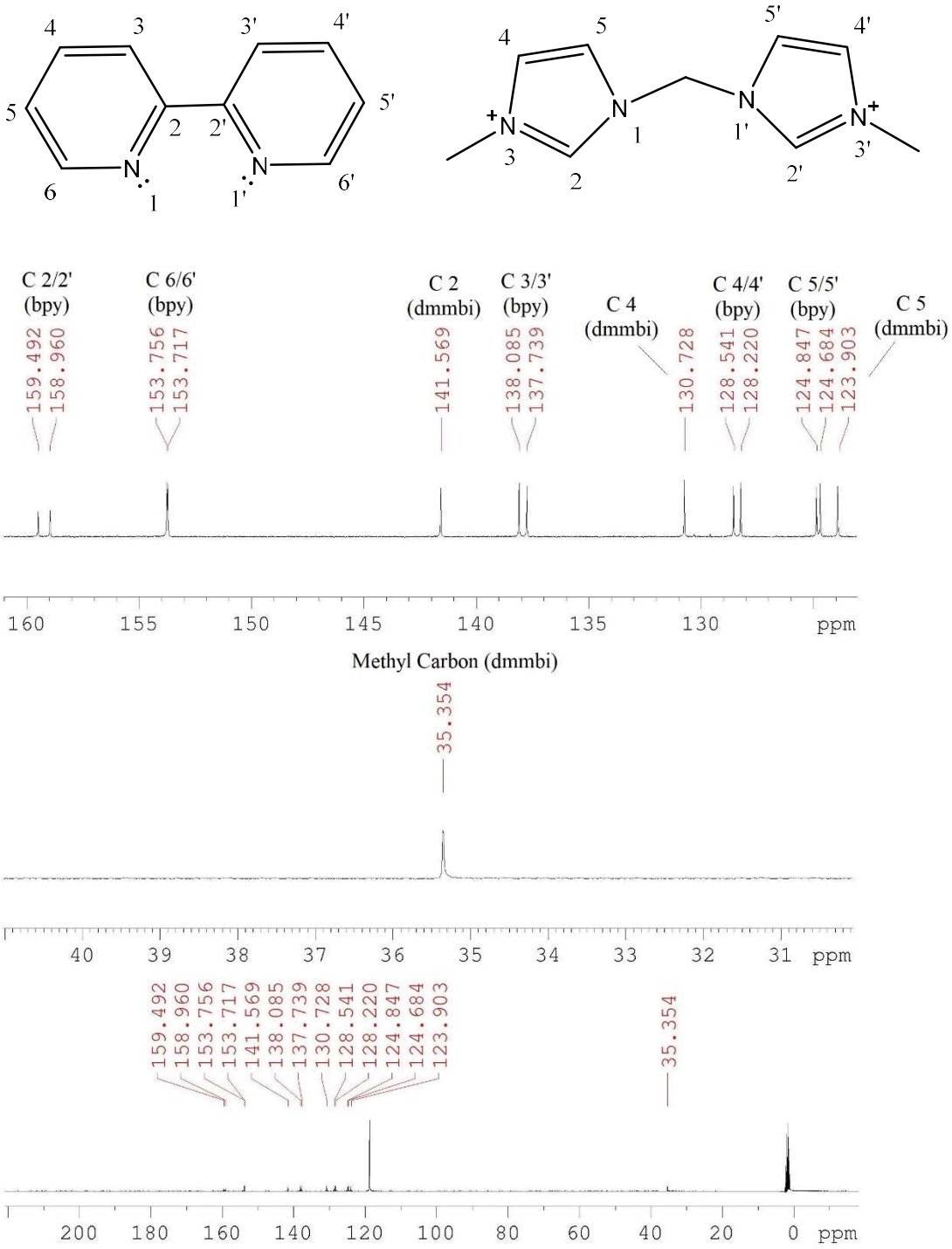

Figure 42. ^{13}C NMR for $[Ru(bpy)_2(dmmbi)](PF_6)_2$.

Comparison of $[Ru(bpy)_2(dmmbi)](PF_6)_2$, $[Ru(bpy)_3](PF_6)_2$, and $[Ru(dmmbi)_3](PF_6)_2$ ^{1}H NMR Spectra

The ^{1}H NMR spectra for all three metal complexes were consistent in the chemical shift regions ranging from 9.0 – 6.7 ppm and 4.9 – 3.1 ppm (Figure 42). All 2,2'-bipyridine ligand and dmmbi imidazole/methylene protons were situated in the downfield range, while the only peak upfield was that of the dmmbi methyl protons.

For $[Ru(bpy)_2(dmmbi)](PF_6)_2$, the 2,2'-bipyridine protons exhibited wide shifts both downfield and upfield as opposed to the peaks from $[Ru(bpy)_3](PF_6)_2$. As discussed previously, this is a result of the orientation of the pyridyl rings around the metal center.

The proton dmmbi singlets in the downfield region were in the same general area as those from $[Ru(dmmbi)_3](PF_6)_2$ with the exception being that the two singlets at 6.98 ppm (H_I) and 6.64 ppm (H_J) were swapped. This means that the methylene proton is now between the two carbon-carbon double bond protons. A likely explanation for this is that π-backbonding in $[Ru(dmmbi)_3](PF_6)_2$ is uniform throughout the complex, but only significant from one dmmbi to the metal in $[Ru(bpy)_2(dmmbi)](PF_6)_2$. Nitrogen does not exhibit nearly as much π-backbonding as the carbene carbon.

Finally, the singlet representing the methyl proton was only slightly more shielded in $[Ru(bpy)_2(dmmbi)](PF_6)_2$ than in $[Ru(dmmbi)_3](PF_6)_2$, but stayed within the general area.

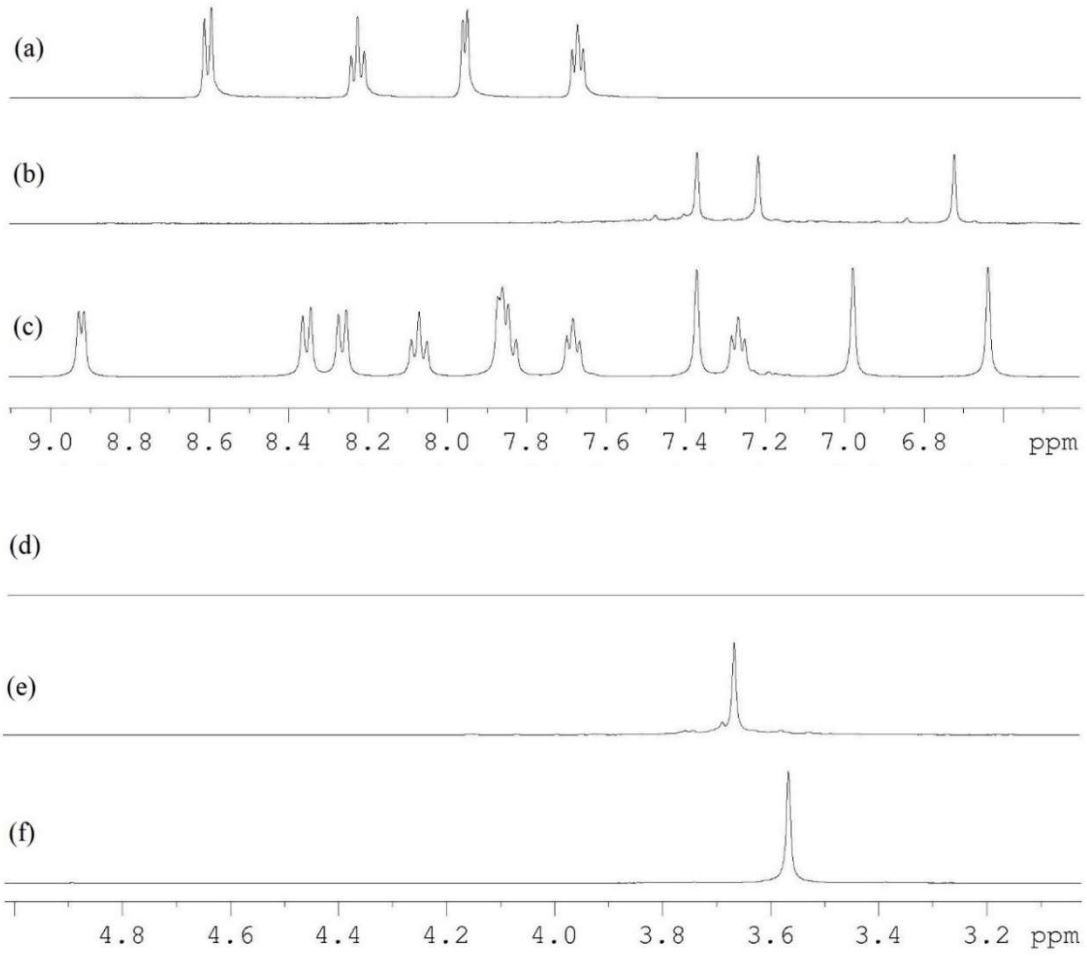

Figure 43. Comparison of ^{1}H NMR data: (a-c) downfield regions for (a) $[Ru(bpy)_3](PF_6)_2$, (b) $[Ru(dmmbi)_3](PF_6)_2$, and (c) $[Ru(bpy)_2(dmmbi)](PF_6)_2$, (d-f) upfield regions for (d) $[Ru(bpy)_3](PF_6)_2$, (e) $[Ru(dmmbi)_3](PF_6)_2$, and (f) $[Ru(bpy)_2(dmmbi)](PF_6)_2$.

Infrared Spectroscopy

IR spectra were obtained for 2,2'-bipyridine, $[Ru(bpy)_3](PF_6)_2$, $H_2(dmmbi)(PF_6)_2$, $[Ru(dmmbi)_3](PF_6)_2$, and $[Ru(bpy)_2(dmmbi)](PF_6)_2$. The data was split into two graphs: one for the functional group region between 4000 and 1500 cm^{-1} (Figure 43), and another for the fingerprint region between 1500 and 600 cm^{-1} (Figure 44).

For the functional group region (Figure 43), CH single-bond stretching from 3200 – 2800 cm^{-1} was observed for all five molecules. CC and CN double-bond stretching frequencies were observed for all five compounds between 1650 – 1500 cm^{-1}. Weak aromatic CH bending was found from 2000 – 1650 cm^{-1} for 2,2'-bipyridine and $[Ru(bpy)_3](PF_6)_2$. The lack of this vibrational mode in $H_2(dmmbi)(PF_6)_2$ clarified that the imidazolium rings are nonaromatic and that the nitrogen atoms in each ring are sp^2 hybridized. A broad peak for both $[Ru(bpy)_3](PF_6)_2$ and $[Ru(dmmbi)_3](PF_6)_2$ was found between 2000 and 1900 cm^{-1}, but could not be identified with a specific vibrational mode. It is possible that a symmetric/asymmetric stretch occurs after three of the same ligands coordinate around the ruthenium metal center. Another similarity between $[Ru(bpy)_3](PF_6)_2$, $[Ru(dmmbi)_3](PF_6)_2$, and $[Ru(bpy)_2(dmmbi)](PF_6)_2$ was the broad OH single bond stretch that occurred between 3550 and 3200 cm^{-1}, which was due to the presence of water within each sample as determined by ^1H NMR. One observation worthy of note is the lack of aromatic CH stretching for $[Ru(bpy)_2(dmmbi)](PF_6)_2$ towards the end of the functional group region. This could be attributed to the greater molecular mass of the compound as opposed to that of $[Ru(bpy)_3](PF_6)_2$ and the replacement of one aromatic 2,2'-bipyridine ligand by dmmbi. This is also supported by the weaker intensity in general of the entire spectrum as opposed to the four other spectra.

For the fingerprint region (Figure 31), an aromatic amine CN stretch was found at approximately 1250 cm^{-1} for 2,2'-bipyridine, $[Ru(bpy)_3](PF_6)_2$, and $[Ru(bpy)_2(dmmbi)](PF_6)_2$. A methylene group and methyl group CH bend was observed for $H_2(dmmbi)(PF_6)_2$, $[Ru(dmmbi)_3](PF_6)_2$, and $[Ru(bpy)_2(dmmbi)](PF_6)_2$ at approximately 1450 cm^{-1}. For $[Ru(bpy)_3](PF_6)_2$, $[Ru(dmmbi)_3](PF_6)_2$, and $[Ru(bpy)_2(dmmbi)](PF_6)_2$, an OH stretch was found at 1300 cm^{-1}, which was expected given the presence of water within the samples. One broad peak common between $[Ru(bpy)_3](PF_6)_2$, $H_2(dmmbi)(PF_6)_2$, $[Ru(dmmbi)_3](PF_6)_2$, and $[Ru(bpy)_2(dmmbi)](PF_6)_2$ was observed between 875 and 800 cm^{-1}. Given that the main similarity between these molecules is the PF_6^- counterion, it is possible that this interaction comes from the counterion itself. The other peaks within this region could be attributed to other CC and CN single bond stretches that are specific to each molecule.

The spectrum for $[Ru(bpy)_2(dmmbi)](PF_6)_2$ provided interesting insight into the structure of the complex itself. Many of the vibrational modes that were detected could be described as combinations of peaks from the other two metal complexes: $[Ru(bpy)_3](PF_6)_2$ and $[Ru(dmmbi)_3](PF_6)_2$. Such combinations were observed from 3300 – 2800 cm^{-1}, 1650 – 1500 cm^{-1}, 1350 – 1200 cm^{-1}, 775 – 700 cm^{-1}, and 690 – 600 cm^{-1}. These data in conjunction with the NMR data confirm the presence of the specified ligand(s) in each compound.

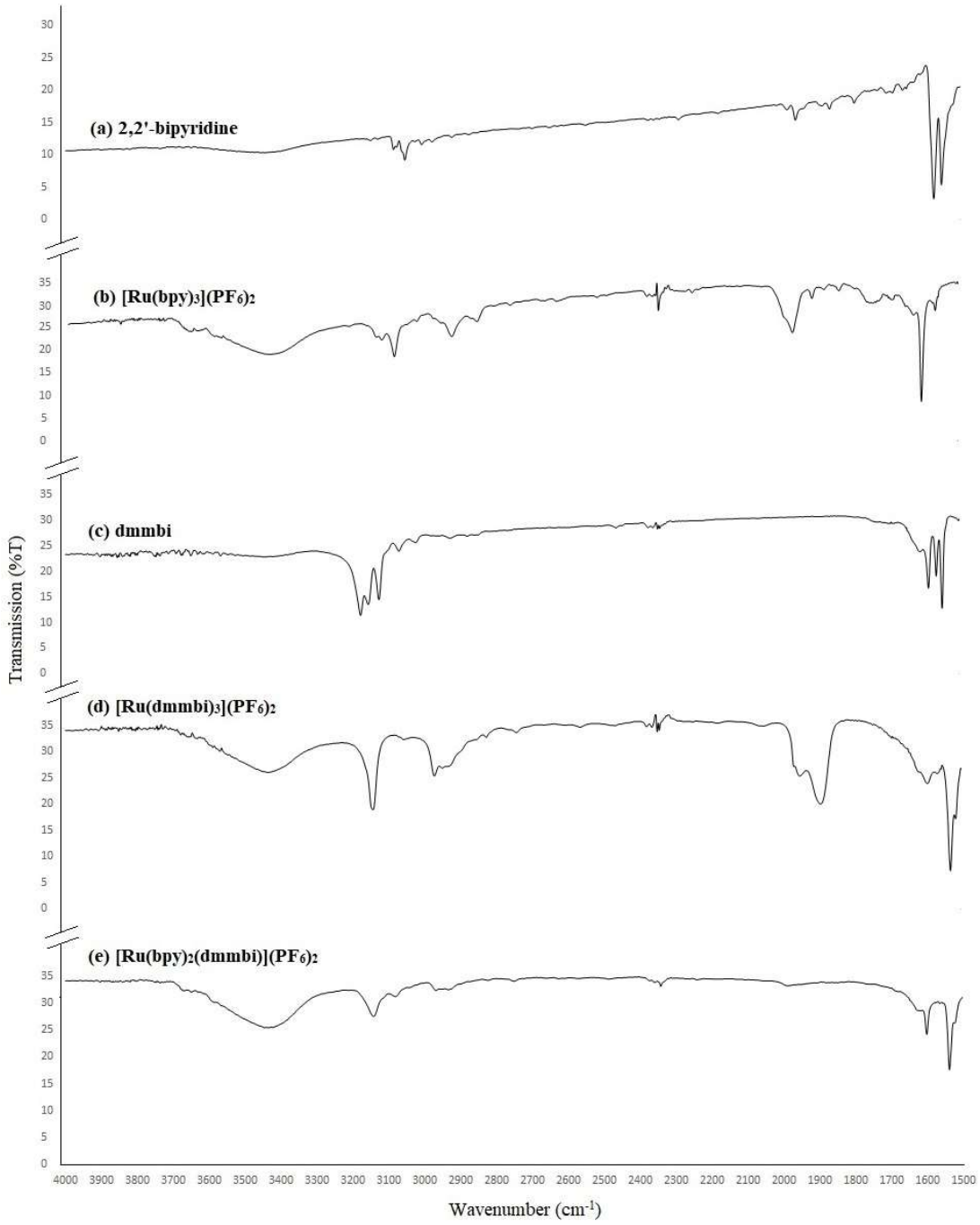

Figure 44. Infrared spectroscopy for all five compounds in the functional group region: (a) 2,2'-bipyridine, (b) $[Ru(bpy)_3](PF_6)_2$, (c) dmmbi, (d) $[Ru(dmmbi)_3](PF_6)_2$, and (e) $[Ru(bpy)_2(dmmbi)](PF_6)_2$.

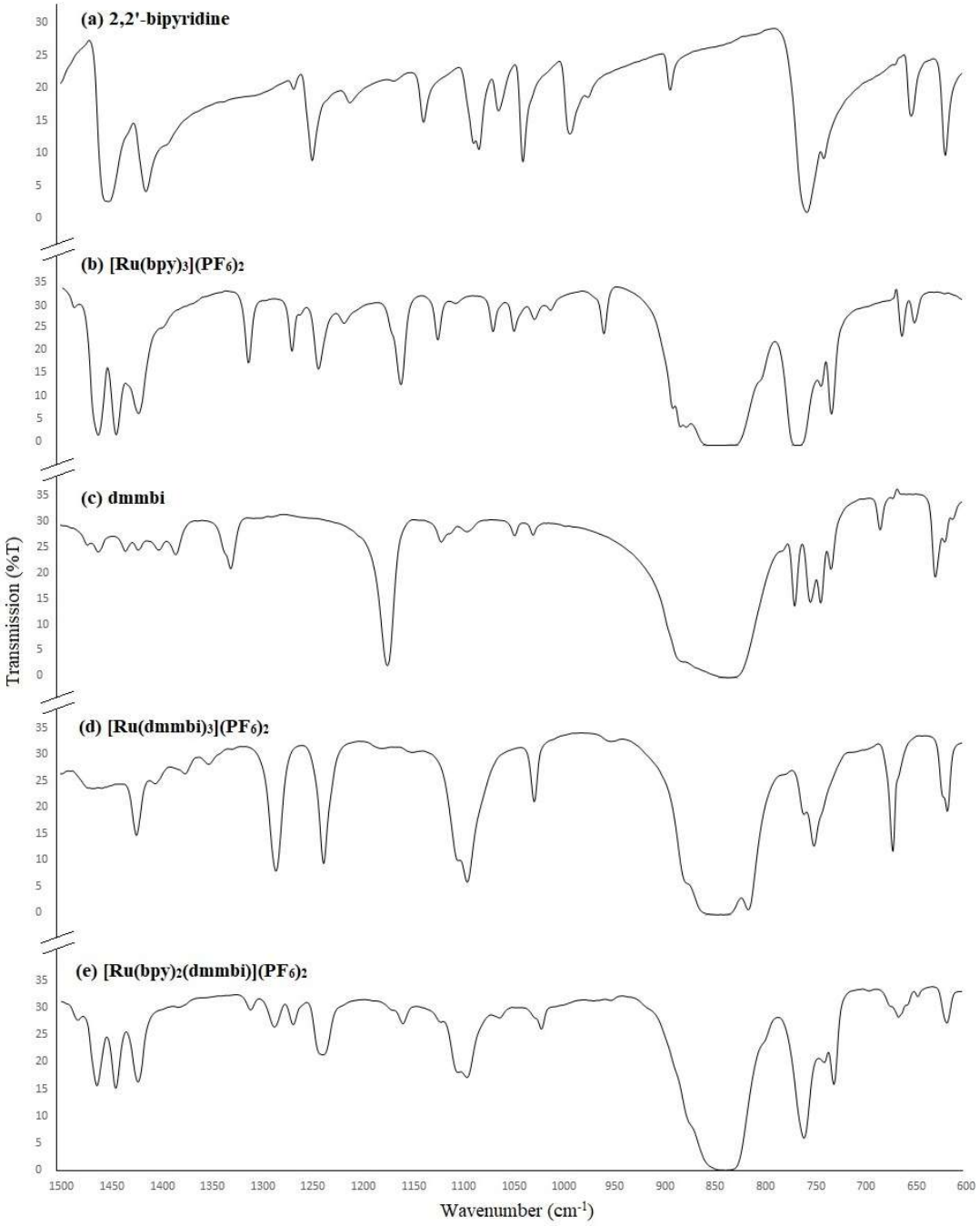

Figure 45. Infrared spectroscopy for all five compounds in the fingerprint region: (a) 2,2'-bipyridine, (b) $[Ru(bpy)_3](PF_6)_2$, (c) $H_2(dmmbi)(PF_6)_2$, (d) $[Ru(dmmbi)_3](PF_6)_2$, and (e) $[Ru(bpy)_2(dmmbi)](PF_6)_2$.

Ultraviolet-Visible Spectroscopy

Ultraviolet-visible (UV-Vis) spectroscopy was used to determine the molar absorptivities (ε) and wavelength maxima of the absorption bands for each compound. The observed bands were indicative of π–π*, *d*–π*, and π–*d* electron transitions with calculated R^2 values above 0.998 for the molar absorptivity of each band. The type of transition taking place is determined by a combination of the energy of the transition and the intensity of the molar absorptivity.

Upon irradiation, an electron transitions from one state to another. This results in a transition dipole moment, which measures the strength of the coupling between the electromagnetic field and the metal complex. These transitions can be characterized in two ways: allowed and forbidden. The difference between the two are a nonzero transition dipole moment producing a nonzero intensity (allowed) and a zero-transition dipole moment producing zero intensity (forbidden).[16] As a result, allowed transitions are greater in ε intensity than forbidden ones. Spectroscopic selection rules govern how a transition is characterized. The spin selection rule states that the orientations of the spins of the electrons cannot change during a transition. This results in spin-allowed and spin-forbidden transitions.[16] The Laporte selection rule states that the only allowed transition is one that changes parity. These transitions can be classified as symmetry-allowed or symmetry-forbidden. As such, transitions can occur between g terms and u terms, whereas transitions between two of the same terms (g ↔ g or u ↔ u) are forbidden. Therefore, the following transitions are allowed: *s*–*p*, *p*–*d*, and *d*–*f*. Likewise, the following would be forbidden: *s*–*s*, *p*–*p*, *d*–*d*, *f*–*f*, *s*–*d*, and *p*–*f*.[16] Combinations between the spin selection rule and the

Laporte selection rule produce different transitions varying in ε intensity, as depicted in Table 3.

Table 3. Selection rules governing the types of transitions and ε intensity.[33, 34, 35]

Type of Transition		**ε ($M^{-1}cm^{-1}$)**	**Selection Rules**
Ligand	π–π*	$10^4 – 10^5$	Spin- and symmetry-allowed u → g, g → u, ΔS = 0
Charge Transfer	MLCT, LMCT	$10^3 – 10^4$	Spin- and symmetry-allowed May involve spin flip (ΔS ≠ 0, ↓ε_λ)
Metal	d–d	10 – 1000	Depends on geometry and e^- spin
	Octahedral	(M^{2+}) ~10 (M^{3+}) ~50	Symmetry-forbidden (g ↔ g)
		$10^{-3} – 10^{-2}$	Spin- and symmetry-forbidden (ΔS ≠ 0)
	Tetrahedral	100 – 1000	Allowed (no *i*)

Larger ε values indicate transitions that are more allowed, while smaller ε values indicate more forbidden ones. As seen in Figure 45, the highest energy transitions are typically ligand based π–π* transitions. The lowest energy transitions are usually metal based *d*–*d** transitions. This is consistent with the selection rules, as the π–π* transitions are both symmetry- and spin-allowed while the *d*–*d** transitions are symmetry forbidden. Transitions between *d* and *d** molecular orbitals are frequently not seen as they are under the tail of the broad MLCT or LMCT bands.

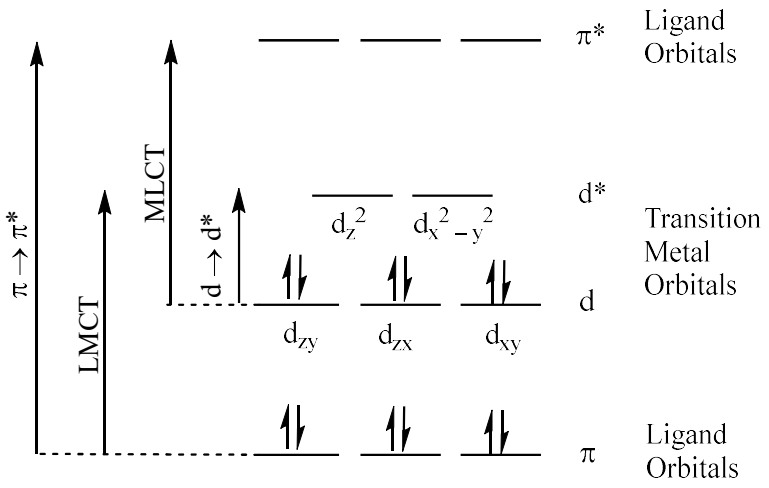

Figure 46. Possible electron transition within an octahedral complex.

For reference, the absorption spectra for the ligand compounds {2,2-bipyridine and $H_2(dmmbi)(PF_6)_2$} were obtained. As expected for compounds exhibiting conjugated π systems, absorption bands occurred within the near-ultraviolet region (approximately 200 – 400 nm). Specifically, 2,2'-bipyridine demonstrated such bands at 236 and 281 nm, with ε values of 11,200 and 14,400 $M^{-1}cm^{-1}$, respectively. For $H_2(dmmbi)(PF_6)_2$, one band was observed at 223 nm with ε = 4030 $M^{-1}cm^{-1}$ (Table 4).

Table 4. Molar absorptivity data for all five compounds.

Compound	**Wavelength (λ) (nm), Molar Absorptivity (ε) ($10^3 \cdot M^{-1} \cdot cm^{-1}$)**		
	π*–*π*	***d*–*π** (MLCT)**	***π*–*d* (LMCT)**
2,2'-Bipyridine	236, 11.2 281, 14.4		
$H_2(dmmbi)(PF_6)_2$	223, 4.03		
$[Ru(bpy)_3](PF_6)_2$	244, 26.0 286, 82.3	450, 14.4	
$[Ru(bpy)_2(dmmbi)](PF_6)_2$	223, 15.9 244, 18.5 292, 44.3	344, 6.23 492, 6.72	
$[Ru(dmmbi)_3](PF_6)_2$	225, 18.6 277, 9.94		473, 1.03

The absorption spectrum of $[Ru(bpy)_3](PF_6)_2$ was consistent with that of the free 2,2'-bipyridine compound. Two π–π* transitions were observed at 244 and 286 nm, with ε values of 26,000 and 82,300 $M^{-1}cm^{-1}$, respectively. One MLCT band is observed in the visible region at 450 nm with ε = 14,400 $M^{-1}cm^{-1}$. The coordination of three 2,2'-bipyridine ligands around the ruthenium metal center further increases the extent to which ultraviolet light at the specified wavelengths is absorbed, as indicated by the vastly greater molar absorptivities. This is expected as the $[Ru(bpy)_3](PF_6)_2$ complex effectively has three times the concentration of 2,2'-bipyridine.

The replacement of one 2,2'-bipyridine ligand with dmmbi, $[Ru(bpy)_2(dmmbi)](PF_6)_2$, yields three π–π* absorption bands and two MLCT bands. The π–π* transition bands occurred at 223, 244, and 292 nm with ε values of 15,900, 18,500, and 44,300 $M^{-1}cm^{-1}$, respectively. This is consistent with the presence of π–π* bands at these wavelengths for both 2,2'-bipyridine (244 and 292 nm) and $H_2(dmmbi)(PF_6)_2$ (223 nm). The MLCT bands occurred at wavelengths of 344 and 492 nm, with ε values of 6230 and 6720 $M^{-1}cm^{-1}$, respectively. When compared to $[Ru(bpy)_3](PF_6)_2$, the addition of one dmmbi ligand splits the MLCT band originally observed at 450 nm to the two previously mentioned transitions with significantly lower molar absorptivites for each. This can be explained by a change in symmetry. Assuming a pseudo–octahedral symmetry in $[Ru(bpy)_3](PF_6)_2$, the symmetry of the complex changes from octahedral (O_h) to C_{2v} in $[Ru(bpy)_2(dmmbi)](PF_6)_2$. This kind of a shift in symmetry reorganizes the energies of the d orbitals in a way that allows for two *d*–π* transitions to occur: one from the new higher energy *d* orbital, and one from the two remaining degenerate d orbitals that are lower in energy (Figure 46).

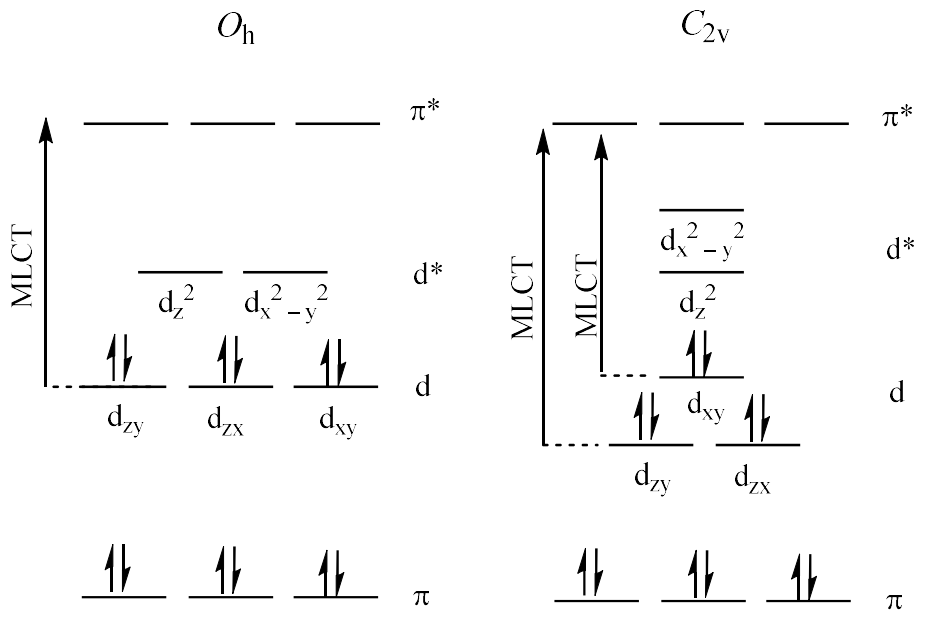

Figure 47. Possible change in electron transition from (pseudo–)O_h to C_{2v} symmetry.

The cyclometallation of three dmmbi ligands around the ruthenium metal center, $[Ru(dmmbi)_3](PF_6)_2$, produced π–π* absorption bands at 225 and 277 nm. The ε values for each were 18,600 and 9940 $M^{-1}cm^{-1}$, respectively. The presence of the band at 225 nm is consistent with the one observed at 223 nm for $H_2(dmmbi)(PF_6)_2$. The band at 277 nm is thought to be a result of both the presence of the metal and the loss of $2H^+$ from the bis-NHC. This could remove the degeneracy of the π orbitals on the dmmbi, causing a second lower energy π–π* transition. It could also be the outcome of π-backbonding within the imidazole rings. Another new absorption band is observed at 473 nm with ε = 1030 $M^{-1}cm^{-1}$. This is likely not an MLCT band as the dmmbi ligand is not an electron withdrawing group due to the presence of the carbons bound to the ruthenium metal center. A more plausible explanation is that the band is a result of a ligand-to-metal charge transfer (LMCT). LMCT phenomena can occur because of the high energy lone pairs on the carbons that coordinate to the metal center, allowing for a π–*d* electron transfer. This would

be the case with the ruthenium bound carbene generated after deprotonation. As a result, the lone pairs on these carbene carbons would be higher in energy compared to those of the ruthenium bound nitrogen atoms in the 2,2'-bipyridine ligands. The molar absorptivity also supports this observation as its magnitude falls within range of LMCT bands.

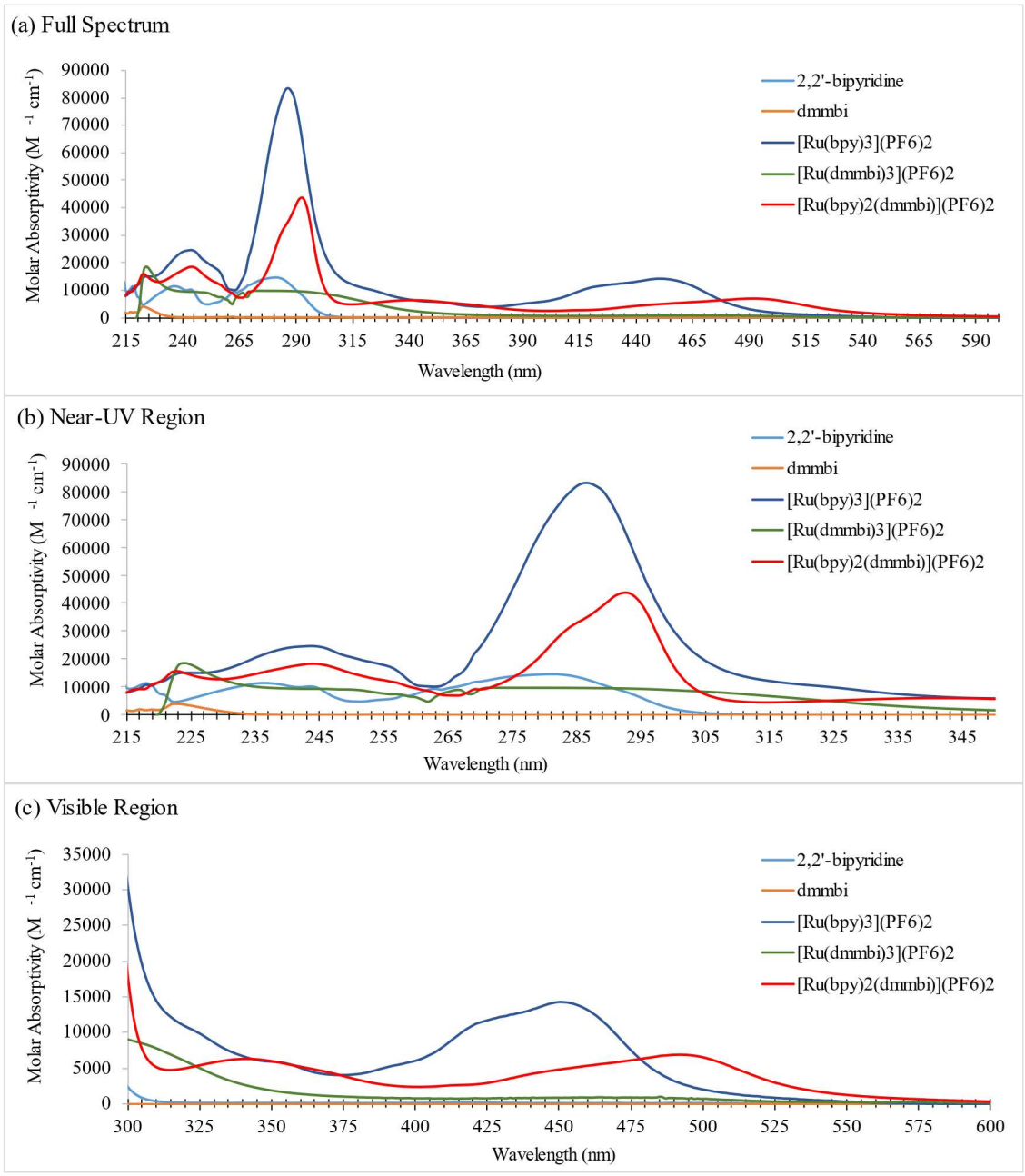

Figure 48. Absorption spectra for all five compounds. (a) Full spectrum, (b) Near-UV region, and (c) Visible region.

Cyclic Voltammetry

Cyclic voltammograms give direct insight into the electron transfer capabilities of organometallic molecules. Such electron transfer characteristics are dependent on the transition metal center in the complex and the types of ligands coordinated around that center. Figure 48 shows a simple voltammogram for ferrocene (Fc). In a typical cyclic voltammogram (US convention), the potential will undergo three cycles from 0 V to negative potentials (–) on the right to positive potentials (+) on the left and back to 0 V. Ferrocene undergoes reduction in the positive potential range, so only a two-point potential scan from 0 V to positive potentials and back to 0 V is required. As shown, the voltammogram begins at point A and increases in potential to point C. In between A and C, ferrocene is oxidized ($Fc \rightarrow Fc^+ + e^-$) at point B. From point C, the voltage is cycled back to a lower potential from point D to F. In between D and F, ferrocene is reduced ($Fc^+ + e^- \rightarrow Fc$) at point E. Upon reaching 0 V again, the voltammogram is completed. The main points of interest for analyzing electron transfer in ferrocene are B and E. It is at these points where the cathodic and anodic potentials are obtained. I_{pc} and E_{pc} refer to the cathodic current and peak potential, respectively. Similarly, I_{pa} and E_{pa} refer to the anodic current and peak potential, respectively.[32]

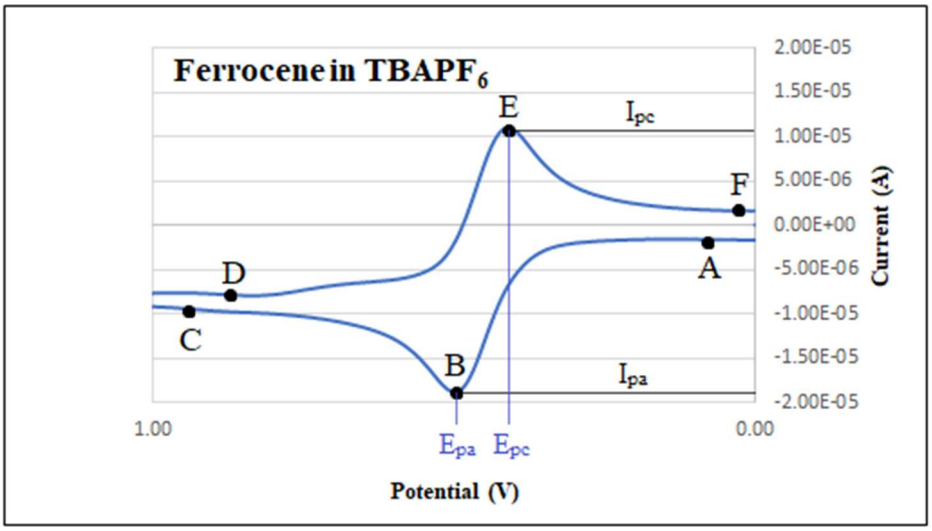

Figure 49. Cyclic voltammogram for ferrocene in a 1 M solution of $TBAPF_6$ in dry acetonitrile.

The reduction potential (E°) of a species can be obtained via E_{pc} and E_{pa}. An approximation of the reduction potential can first be obtained from the average potential ($E_{1/2}$) of E_{pc} and E_{pa} as shown in Equation 1. Using an internal standard such as ferrocene, the corrected reduction potential can then be determined as depicted in Equation 2. Here, E_{Fc} represents the average reduction potential calculated for ferrocene within the sample. Theoretically, reversible reductions for a one electron transfer should exhibit a difference (ΔE) between E_{pc} and E_{pa} of approximately 59 mV (Equation 3). However, the exact value of this difference may vary depending on the solvent used because some solvents are more resistant to current flow and to the concentration of the electrolyte.[32]

$$E_{1/2} = \frac{E_{pc}+E_{pa}}{2} \quad (1)$$

$$E° = E_{1/2} + E_{Fc} \quad (2)$$

$$\Delta E = \left|E_{pc} - E_{pa}\right| \quad (3)$$

The reduction potential indicates the difficulty in reducing a given chemical species. Reduction potentials that are more positive demonstrate that the species is easier

to reduce (or harder to oxidize). A less positive potential indicates more difficulty in reducing (or easier in oxidizing) the species. This relationship is important in organometallic chemistry as the ligands coordinated around a metal center vary the nature of the chemical species. Typically, electron-donating ligands make it harder to reduce the metal and electron-withdrawing ligands make it easier to reduce the metal.

Four cyclic voltammograms were obtained (Figure 49): a background scan containing only $TBAPF_6$ and one each for $[Ru(bpy)_3](PF_6)_2$, $[Ru(bpy)_2(dmmbi)](PF_6)_2$, and $[Ru(dmmbi)_3](PF_6)_2$. The reduction potentials of each were calculated as shown in Table 5. For this class of compounds, reduction occurred within the positive potential range for the ruthenium metal center and within the negative potential range for the 2,2'-bipyridine ligands. No reduction potentials were seen within the voltage range (–2.0 to +2.0 V) for the dmmbi ligands – free or bound. In addition, free-floating 2,2'-bipyridine does not show a reduction potential within the given voltage limits. Only when bound to the metal center are the reduction potentials observed for the 2,2'-bipyridine ligands. This indicates that the ruthenium(II) metal center makes the bipyridine ligand easier to reduce; most likely because it is easier to transfer an electron to the bpy ligand when bound to the metal.

Table 5. Calculated reduction potentials for each ruthenium(II) complex. All values are reduction potentials referenced to the ferrocene/ferrocenium cation potential.[a]

Complex/Potential	E(V) Ru(III) → Ru(II)	E(V) 1st bpy	E(V) 2nd bpy	E(V) 3rd bpy
$[Ru(bpy)_3](PF_6)_2$	1.78	–0.843	–1.04	–1.27
$[Ru(bpy)_2(dmmbi)](PF_6)_2$	1.49	–0.959	–1.20	–
$[Ru(dmmbi)_3](PF_6)_2$	0.770	–	–	–

[a] All samples were ~1 mM of sample and 0.1 M in $TBAPF_6$ in dry acetonitrile. A platinum disk working electrode, a platinum wire auxiliary electrode, a Ag/AgCl reference electrode, and a scan rate of 200 mV/sec were used.

Upon cycling from a negative potential to a positive one, the ruthenium metal center was first oxidized (Ru(II) → Ru(III)) and then reduced (Ru(III) → Ru(II)) after cycling back to 0 V. This confirmed the oxidation state of the metal in each complex to be Ru(II). The reduction potentials for each metal center varied depending on the number of bpy ligands replaced with dmmbi. As each dmmbi ligand was added, the ruthenium reduction potentials shifted from 1.78 V to 1.49 V to 0.770 V. The steady move to less positive reductions indicates that dmmbi inhibits reduction of the ruthenium metal center.

The 2,2'-bipyridine ligands underwent reduction and oxidation when cycling in the negative potential range. The number of reduction couples agree with the number of bpy ligands coordinated around the metal center. Three peaks were therefore seen in $[Ru(bpy)_3](PF_6)_2$, two peaks were seen in $[Ru(bpy)_2(dmmbi)](PF_6)_2$, and zero for $[Ru(dmmbi)_3](PF_6)_2$. As each bipyridine ligand was reduced, the reduction potential became more negative demonstrating that each reduction was significantly more difficult to achieve. The substitution of one bipyridine by dmmbi caused the reduction potentials for each bpy ligand to become even more negative. For example, when comparing

$[Ru(bpy)_3](PF_6)_2$ to $[Ru(bpy)_2(dmmbi)](PF_6)_2$, the reduction potential decreased from –0.843 V to –0.959 V for the 1st bpy ligand and from –1.04 V to –1.20 V for the 2nd bpy ligand. As with the ruthenium metal centers, the reductions of the bpy ligands were inhibited by the presence of the dmmbi ligand.

The capacity for the dmmbi ligand to inhibit reduction of the ruthenium metal centers and the bpy ligands demonstrated dmmbi to be an electron donating group. This is likely the result of π-backbonding within the dmmbi-containing complexes. Through this phenomenon, electron density from the dmmbi ligand is donated to the metal center, making the metal electron rich and causing it to shift some of that electron density to all the ligands. The relation, therefore, is: the more dmmbi ligands that are substituted in for bpy, the greater the electron distribution throughout the complex and the more difficult it is for reduction to occur.

The main issue that occurred while performing CV was the reduction of the solvent in the negative potential range. Given that the bpy ligands have negative reduction potentials, it proved difficult to analyze the data. Oftentimes, the reduction peak of the last bpy ligand in the complex would be masked by the curve produced by the reduction of the solvent. Therefore, the best possible maximum for the reduction peak was obtained for the last bpy ligand in each complex. This likely resulted in a somewhat higher experimental error. Another issue that occurred was the masking of the Ru(II)/Ru(III) reduction and oxidation peaks in $[Ru(dmmbi)_3](PF_6)_2$ by those produced from ferrocene. For both these reasons, CV were obtained without and with added ferrocene as an internal standard.

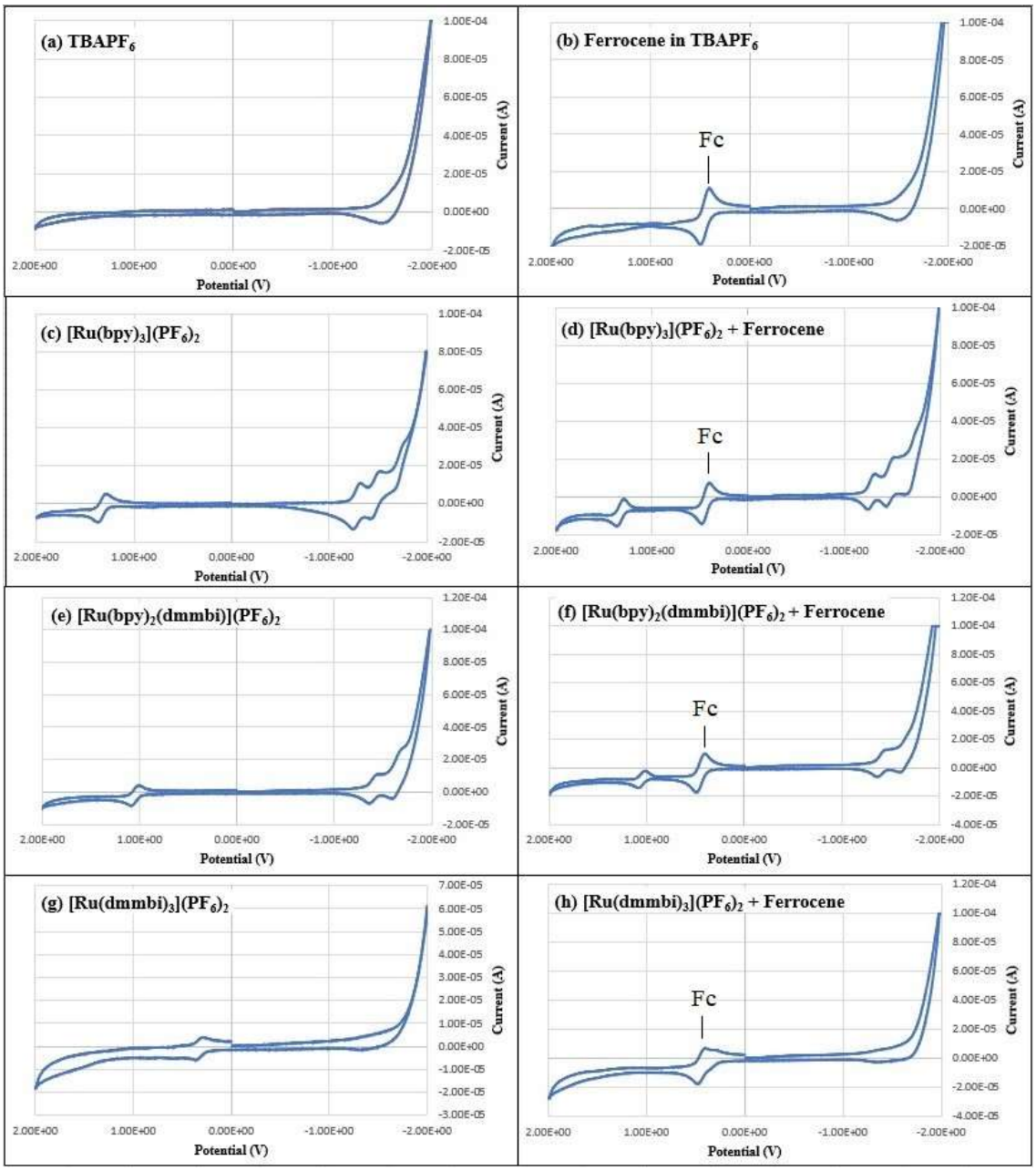

Figure 50. Cyclic voltammograms for all three complexes obtained using 1 mM of compound in 0.1 M $TBAPF_6$ solutions in dry acetonitrile. (a) $TBAPF_6$ alone (b) $TBAPF_6$ + Ferrocene (c) $[Ru(bpy)_3](PF_6)_2$ (d) $[Ru(bpy)_3](PF_6)_2$ + Ferrocene (e) $[Ru(bpy)_2(dmmbi)](PF_6)_2$ (f) $[Ru(bpy)_2(dmmbi)](PF_6)_2$ + Ferrocene (g) $[Ru(dmmb)_3](PF_6)_2$ (h) $[Ru(dmmb)_3](PF_6)_2$ + Ferrocene.

CONCLUSION

Mixed ligand complexes containing 2,2'-bipyridine and $H_2(dmmbi)(PF_6)_2$ were synthesized and characterized by elemental analysis, NMR spectroscopy, IR spectroscopy, UV-Vis spectroscopy, and cyclic voltammetry. Three of the four targeted complexes were produced successfully: $[Ru(bpy)_3](PF_6)_2$, $[Ru(bpy)_2(dmmbi)](PF_6)_2$, and $[Ru(dmmbi)_3](PF_6)_2$. The reaction methods for $[Ru(bpy)_2(dmmbi)](PF_6)_2$ and $[Ru(dmmbi)_3](PF_6)_2$ were optimized and built upon work done by previous researchers in the lab.[24,29] $[Ru(bpy)(dmmbi)_2](PF_6)_2$ was not successfully synthesized, but our attempts to do so provide future insight into possible reaction conditions.

First and foremost, the reaction procedure for $[Ru(bpy)_2(dmmbi)](PF_6)_2$ was enhanced via a new synthetic approach. This new method utilized NaOAc as the base for deprotonating $H_2(dmmbi)(PF_6)_2$ and forming the free bidentate NHC ligand (dmmbi) that could coordinate to the ruthenium metal center. The optimal conditions were found over a course of eighteen trials. This synthesis also played a key role in discovering the need for a 2-fold excess of $H_2(dmmbi)(PF_6)_2$ in the reaction mixture to further increase the desired product yield and eliminate a substantial amount of impurity. Doing so on a 250 mg scale drastically eliminated the amount of impurity to the point of only seeing one band (red) while purifying via column chromatography. These results along with the ability to use a high-pressure vessel instead of a Schlenk flask simplified the procedure and produced high yields.

The synthesis of $[Ru(dmmbi)_3](PF_6)_2$ followed the successful production of $[Ru(bpy)_2(dmmbi)](PF_6)_2$. Attempts to synthesize $[Ru(dmmbi)_3](PF_6)_2$ using NaOAc as a base produced an insoluble material. After various attempts, triethylamine was reverted to

being used as the base which resulted in significantly less insoluble material being produced. Similar to the synthesis of $[Ru(bpy)_2(dmmbi)](PF_6)_2$, it was found that using a 6-fold excess of $H_2(dmmbi)(PF_6)_2$ in the reaction mixture increased the yield of the desired product and decreased the amount of insoluble material. Any insoluble substances could then be removed via column chromatography in which no separation was required as only one band was present. Although the new synthetic approach utilizing NaOAc was unsuccessful, the finding of the need for a 6-fold excess as opposed to a 3.3-fold excess of $H_2(dmmbi)(PF_6)_2$ was crucial in increasing the yield of $[Ru(dmmbi)_3](PF_6)_2$ and proved to be important when exploring the reaction conditions needed to produce $[Ru(bpy)(dmmbi)_2](PF_6)_2$.

The last complex $[Ru(bpy)(dmmbi)_2](PF_6)_2$ was not synthesized successfully. Various reactions utilizing both $[Ru(dmmbi)_3](PF_6)_2$ and $H_2[Ru(bpy)Cl_4]$ as starting materials were performed, but all resulted in $[Ru(bpy)_2(dmmbi)](PF_6)_2$ as the major product. The reactions using $[Ru(dmmbi)_3](PF_6)_2$ indicated that 2,2'-bipyridine out competes dmmbi in ligand substitution, which suggested that $[Ru(bpy)_2(dmmbi)](PF_6)_2$ is the thermodynamic product. The reactions using $H_2[Ru(bpy)Cl_4]$ indicated that the starting material itself may need to be purified, as shown through ^1H NMR spectroscopy. Factors such as successful purification of the $H_2[Ru(bpy)Cl_4]$, an exchange of the counterion, and adjusting the amount of excess $H_2(dmmbi)(PF_6)_2$ and NaOAc would provide the foundation necessary for future syntheses, since the conditions would theoretically be similar to those for synthesizing $[Ru(bpy)_2(dmmbi)](PF_6)_2$.

Elemental analysis failed to provide data on the percentages of carbon, hydrogen, and nitrogen atoms contained within each ruthenium complex. Only $[Ru(bpy)_3](PF_6)_2$

demonstrated actual and expected percentages that agreed within 0.40% of each other. This is most likely due to a KPF_6 residue that could have precipitated along with the complexes because when we incorporated amounts of KPF_6 into the molar mass of each complex, the actual and newly generated expected values agreed within 0.40%.

^1H NMR verified that each complex had been synthesized based on the expected proton peaks, and COSY NMR clarified the structures further by providing data on which proton peaks were coupled together. ^1H NMR showed four peaks (twenty-four protons total after integrating) for $[Ru(bpy)_3](PF_6)_2$, eleven peaks (twenty-eight protons after integrating) for $[Ru(bpy)_2(dmmbi)](PF_6)_2$, and four peaks (thirty-six protons after integrating) for $[Ru(dmmbi)_3](PF_6)_2$. The ^1H and COSY NMR data for $[Ru(bpy)_3](PF_6)_2$ and $[Ru(dmmbi)_3](PF_6)_2$ were compared to the those of their respective free-floating ligands {2,2'-bipyridine and $H_2(dmmbi)(PF_6)_2$}. For $[Ru(bpy)_3](PF_6)_2$, it was found that the fixed position of the bpy ligands as opposed to the free-floating 2,2'-bipyridine had significant effects on the deshielding of the protons in the meta positions on the pyridine rings. For $[Ru(dmmbi)_3](PF_6)_2$, the most notable change was the loss of the carbene carbon proton signal, which was attributed to the deprotonation of the carbene carbons prior to coordinating to the metal center. The ^1H and COSY NMR data of $[Ru(bpy)_2(dmmbi)](PF_6)_2$ were then compared to the other two complexes. The peaks belonging to 2,2'-bipyridine were split into two sets of four because of the different amounts of deshielding experienced by the pyridine rings as a result of a change in symmetry. The number of peaks belonging to the dmmbi ligand did not change, yet the deshielding of the methylene proton peak in $[Ru(bpy)_2(dmmbi)](PF_6)_2$ was greater. This was likely due to the extent to which π-backbonding affects $[Ru(bpy)_2(dmmbi)](PF_6)_2$ as opposed to $[Ru(dmmbi)_3](PF_6)_2$.

^{13}C NMR provided the carbon peaks exhibited by each complex, which further verified that each complex was synthesized successfully. Five carbon peaks were found for $[Ru(bpy)_3](PF_6)_2$, fourteen peaks were found for $[Ru(bpy)_2(dmmbi)](PF_6)_2$, and four peaks were found for $[Ru(dmmbi)_3](PF_6)_2$. The number of peaks for $[Ru(bpy)_3](PF_6)_2$ were consistent with the structure. However, fifteen peaks were expected for $[Ru(bpy)_2(dmmbi)](PF_6)_2$ and five peaks were expected for $[Ru(dmmbi)_3](PF_6)_2$. When compared to the ^{13}C NMR for $H_2(dmmbi)(PF_6)_2$, it was found that the peak representing the methylene carbon was absent in each complex. This was attributed to the greater molecular masses of the complexes as opposed to $H_2(dmmbi)(PF_6)_2$ alone, which would further be exacerbated by the presence of only one dmmbi ligand in $[Ru(bpy)_2(dmmbi)](PF_6)_2$. The methylene carbon would also produce the weakest signal as there is only one methylene carbon in the dmmbi ligand as opposed to double the amount of the other carbons.

IR spectroscopy was used as a qualitative analysis to further confirm the structure of each complex. Given the complexity of the molecules, the data was difficult to decipher and primarily served to identify specific vibrational modes present within the complexes. All compounds (complexes and ligands) exhibited the expected CH single-bond stretching and CC/CN double-bond stretching in the functional group region (4000 – 1500 cm^{-1}). Aromatic CH bending was only observed for 2,2'-bipyridine and $[Ru(bpy)_3](PF_6)_2]$. The mixed ligand complex $[Ru(bpy)_2(dmmbi)](PF_6)_2$ was also expected to demonstrate this vibrational mode, but ultimately did not. This was attributed to the weaker intensity of the entire spectrum caused by the replacement of one bpy ligand by dmmbi and the greater molecular mass of $[Ru(bpy)_2(dmmbi)](PF_6)_2$ as opposed to $[Ru(bpy)_3](PF_6)_2]$. The uniform

ligand complexes $[Ru(bpy)_3](PF_6)_2$] and $[Ru(dmmbi)_3](PF_6)_2$ also shared an unidentified vibrational mode in the functional group region not present in the other compounds. Given that each complex contains only one type of ligand, it was attributed to a possible symmetric/asymmetric stretch that occurs when such uniformity around the metal center exists. One other unidentified vibrational mode worthy of noting is that exhibited in the fingerprint region (1500 – 600 cm^{-1}) by all molecules except 2,2'-bipyridine. It was concluded that this was caused by an interaction originating from the PF_6^- counterion itself since that was the main similarity between the four other compounds.

UV-Vis spectroscopy provided information on the types of electron transitions taking place within each complex (π–π*, MLCT, LMCT, *d*–*d** etc.). The magnitude of each band's molar absorptivity helped to identify the type of transition. The absorption spectra of the free-floating ligands 2,2'-bipyridine and $H_2(dmmbi)(PF_6)_2$ were compared to those of the complexes. $[Ru(bpy)_3](PF_6)_2$ exhibited almost identical π–π* bands to 2,2'-bipyridine in the near-UV region. $[Ru(dmmbi)_3](PF_6)_2$ also exhibited a similar π–π* band as $H_2(dmmbi)(PF_6)_2$ with the exception of having one additional π–π* band at 277 nm. This was attributed to the loss of degeneracy of the π orbitals on the dmmbi ligand caused by deprotonation of the carbene carbons and the coordination of the ligands to the metal center. $[Ru(bpy)_2(dmmbi)](PF_6)_2$ demonstrated a mixture of the π–π* bands from both 2,2'-bipyridine and $H_2(dmmbi)(PF_6)_2$. In the visible region, one MLCT band occurred for $[Ru(bpy)_3](PF_6)_2$, two MLCT bands occurred for $[Ru(bpy)_2(dmmbi)](PF_6)_2$, and one LMCT band occurred for $[Ru(dmmbi)_3](PF_6)_2$. The one MLCT band for $[Ru(bpy)_3](PF_6)_2$ was characteristic of the complex. The two MLCT bands exhibited by $[Ru(bpy)_2(dmmbi)](PF_6)_2$ were caused by a change in symmetry from pseudo–O_h {as in

$[Ru(bpy)_3](PF_6)_2\}$ to C_{2v}. This would cause a change in degeneracy of the *d* orbitals, resulting in two *d*–π* transitions taking place. The one band occurring for $[Ru(dmmbi)_3](PF_6)_2$ was assigned as a LMCT (π–*d*) band due to the higher energy of the carbene carbons bound to the ruthenium metal center. $[Ru(dmmbi)_3](PF_6)_2$ is not capable of exhibiting MLCT bands as the dmmbi ligands do not exhibit low lying π* orbitals as the 2,2'-bipyridine ligands do. Given the smaller magnitudes of *d*–*d** bands, if these transitions occurred at all they were likely masked by the other charge transfer bands.

Cyclic voltammetry (CV) provided insight into the electron transfer capabilities of each complex. For each complex, the ruthenium metal center underwent reduction in the positive potential range while the 2,2'-bipyridine ligands underwent reduction in the negative potential range. It was found that as the 2,2'-bipyridine ligands were replaced by dmmbi, the reduction potentials for the ruthenium metal center and the remaining bpy ligands decreased. This indicated that dmmbi makes it significantly harder for reduction to occur within the complex. This observation was attributed to the capacity for π-backbonding to occur between the dmmbi ligand and the ruthenium metal center. The electron density donated to the metal center from dmmbi through this phenomenon would in effect be redistributed via the metal throughout the rest of the complex. For this reason, the dmmbi ligand was classified as an electron donating group.

A combination of the data from NMR spectroscopy, IR spectroscopy, and CV helped confirm the success of each synthesis through the structural insights provided by the data. Elemental analysis was less clear. It determined that the expected %C, %H, and %N values agreed with the actual values obtained for $[Ru(bpy)_3](PF_6)_2$. Once additional

KPF_6 masses were accounted for, the actual and expected percentages for $[Ru(bpy)_2(dmmbi)](PF_6)_2$ and $[Ru(dmmbi)_3](PF_6)_2$ agreed as well. ^1H NMR clarified the types of protons present, COSY NMR determined which proton signals were coupled together, and ^{13}C NMR demonstrated the types of carbons present within each structure. IR spectroscopy gave a qualitative analysis of the types of vibrational modes present and the similarities between each compound. CV, while not specifically intended for structural analysis, confirmed the presence of the ruthenium metal center and the number of 2,2'-bpyridine ligands in each complex. Each NMR analysis also provided important data on the electron density distribution in each complex via the changes in chemical shifts. UV-Vis spectroscopy provided data on the types of electron transitions taking place. Finally, CV provided important data on the electron transfers taking place within each complex. Taken all together, these data were internally consistent confirming the proposed structures of these complexes.

Future work would entail obtaining the last mixed ligand complex $[Ru(bpy)(dmmbi)_2](PF_6)_2$. As stated previously, one possible approach would be purification of the $H_2[Ru(bpy)Cl_4]$ complex. Based on the groundwork established by this thesis, reaction methods utilizing $[Ru(dmmbi)_3](PF_6)_2$ or $H_2[Ru(bpy)Cl_4]$ could then be explored further. Once synthesized, the $[Ru(bpy)(dmmbi)_2](PF_6)_2$ could then be characterized similarly to the other complexes synthesized. After successfully synthesizing the ruthenium complexes with the dmmbi ligand, ways to synthesize the osmium derivatives of these ruthenium complexes could be investigated.

Finally, the remaining characterizations not performed in this thesis could be completed. This would include Emission (EM) spectroscopy and Mass Spectrometry (MS).

EM spectroscopy would provide data on the luminescent properties of the complexes. MS would further prove that each synthesis was successful and provide structural insights based on the mass of each complex.

REFERENCES

(1) Ruthkosky, M.; Kelly, C. A.; Castellano, F. N.; Meyer, G. J. Electron and Energy Transfer from Cu^{I} MLCT Excited States. *Coordination Chemistry Reviews* **1998**, *171*, 309–322.

(2) Sun, Y.; Hudson, Z. M.; Rao, Y.; Wang, S. Tuning and Switching MLCT Phosphorescence of $[Ru(Bpy)_3]^{2+}$ Complexes with Triarylboranes and Anions. *Inorganic Chemistry* **2011**, *50* (8), 3373–3378. https://doi.org/10.1021/ic1021966.

(3) IEA (International Energy Agency). Key World Energy Statistics 2020. *Int. Energy Agency* **2020**, *33* (August), 4649.

(4) Overview of Greenhouse Gases. *United States Environmental Protection Agency*. 2021.

(5) The Sources and Solutions: Fossil Fuels. *United States Environmental Protection Agency*. 2022.

(6) What Is Ozone? *United States Environmental Protection Agency*. 2021.

(7) Cohen, A. J.; Brauer, M.; Burnett, R.; Anderson, H. R.; Frostad, J.; Estep, K.; Balakrishnan, K.; Brunekreef, B.; Dandona, L.; Dandona, R.; Feigin, V.; Freedman, G.; Hubbell, B.; Jobling, A.; Kan, H.; Knibbs, L.; Liu, Y.; Martin, R.; Morawska, L.; Pope, C. A.; Shin, H.; Straif, K.; Shaddick, G.; Thomas, M.; van Dingenen, R.; van Donkelaar, A.; Vos, T.; Murray, C. J. L.; Forouzanfar, M. H. Estimates and 25-Year Trends of the Global Burden of Disease Attributable to Ambient Air Pollution: An Analysis of Data from the Global Burden of Diseases Study 2015. *The Lancet* **2017**, *389* (10082), 1907–1918. https://doi.org/10.1016/S0140-6736(17)30505-6.

(8) BP Energy. Statistical Review of World Energy Globally Consistent Data on World Energy Markets. and Authoritative Publications in the Field of Energy. *BP Energy outlook 2021* **2021**, *70*, 8–20.

(9) Shockley, W.; Queisser, H. J. Detailed Balance Limit of Efficiency of P-n Junction Solar Cells. *Journal of Applied Physics* **1961**, *32* (3), 510–519. https://doi.org/10.1063/1.1736034.

(10) How a Solar Cell Works. *American Chemical Society*. 2022.

(11) NREL. Best Research-Cell Efficiency Chart. 2020.

(12) Nazeeruddin, M. K.; Baranoff, E.; Grätzel, M. Dye-Sensitized Solar Cells: A Brief Overview. *Solar Energy* **2011**, *85* (6), 1172–1178. https://doi.org/10.1016/j.solener.2011.01.018.

(13) Ji, Z.; Natu, G.; Wu, Y. Cyclometalated Ruthenium Sensitizers Bearing a Triphenylamino Group for P-Type NiO Dye-Sensitized Solar Cells. *ACS Applied Materials and Interfaces* **2013**, *5* (17), 8641–8648. https://doi.org/10.1021/am402263q.

(14) Koivisto, B. D.; Robson, K. C. D.; Berlinguette, C. P. Systematic Manipulation of the Light-Harvesting Properties for Tridentate Cyclometalated Ruthenium(Il) Complexes. *Inorganic Chemistry* **2009**, *48* (20), 9644–9652. https://doi.org/10.1021/ic9007137.

(15) Kober, E. M.; Meyer, T. J. Concerning the Absorption Spectra of the Ions $M(Bpy)_3^{2+}$ (M = Fe, Ru,Os; Bpy =2,2'-Bipyridine). *Inorganic Chemistry* **1981**, *21*, 3967–3977.

(16) Weller, M.; Rourke, J.; Overton, T.; Armstrong, F. d-Metal Complexes: Electronic Structure and Properties. In *Inorganic Chemistry*, 7th ed.; Oxford University Press: New York, 2018; pp 593–596.
(17) Weller, M.; Rourke, J.; Overton, T.; Armstrong, F. Coordination Chemistry, Reactions of Complexes. In *Inorganic Chemistry*, 7th ed.; Oxford University Press: New York, 2018; p 629.
(18) Turro, C.; Bossmann, S. H.; Turro, N. J.; Bossmann, S. H.; Jenkins, Y.; Barton, J. K. Proton Transfer Quenching of the MLCT Excited State of $Ru(Phen)_2(dppz)_2^+$ in Homogeneous Solution and Bound to DNA. *J Am Chem Soc* **1995**, *117* (35), 9026–9032. https://doi.org/10.1021/ja00140a020.
(19) Li, Y.; Liu, B.; Lu, X. R.; Li, M. F.; Ji, L. N.; Mao, Z. W. Cyclometalated Iridium(III) N-Heterocyclic Carbene Complexes as Potential Mitochondrial Anticancer and Photodynamic Agents. *Dalton Transactions* **2017**, *46* (34), 11363–11371. https://doi.org/10.1039/c7dt01903c.
(20) Frémont, P.; Marion, N.; Nolan, S. P. Carbenes: Synthesis, Properties, and Organometallic Chemistry. *Coordination Chemistry Reviews*. April 2009, pp 862–892. https://doi.org/10.1016/j.ccr.2008.05.018.
(21) Gründemann, S.; Kovacevic, A.; Albrecht, M.; Faller, J. W.; Crabtree, R. H. Abnormal Ligand Binding and Reversible Ring Hydrogenation in the Reaction of Imidazolium Salts with $IrH_5(PPh_3)_2$. *J Am Chem Soc* **2002**, *124* (35), 10473–10481. https://doi.org/10.1021/ja026735g.
(22) Bourissou, D.; Guerret, O.; Gabbaï, F. P.; Bertrand, G. Stable Carbenes. *Chemical Reviews* **2000**, *100* (1), 39–91. https://doi.org/10.1021/cr940472u.
(23) Son, S. U.; Park, K. H.; Lee, Y. S.; Kim, B. Y.; Choi, C. H.; Lan, M. S.; Jang, Y. H.; Jang, D. J.; Chung, Y. K. Synthesis of Ru(II) Complexes of N-Heterocyclic Carbenes and Their Promising Photoluminescence Properties in Water. *Inorganic Chemistry* **2004**, *43* (22), 6896–6898. https://doi.org/10.1021/ic049514f.
(24) Mahabir, R. Synthesis and Characterization of a New Class of Mixed Ligand Ruthenium Complexes Containing 2,2'-Bipyridine and 3,3'-Dimethyl-1,1'-Methylenebisimidazolium Carbene Ligands, St. John's Univeristy, 2011.
(25) Aznarez, F.; Sanz Miguel, P. J.; Tan, T. T. Y.; Hahn, F. E. Preparation of Rhodium(III) Di-NHC Chelate Complexes Featuring Two Different NHC Donors via a Mild NaOAc-Assisted C-H Activation. *Organometallics* **2016**, *35* (3), 410–419. https://doi.org/10.1021/acs.organomet.5b00993.
(26) Baird, C.; Cann, M. Chapter 3: The Chemistry of Ground-Level Air Pollution. In *Environmental Chemistry*, 5th ed.; W. H. Freeman and Company, 2012; p 80–81.
(27) Weller, M.; Rourke, J.; Overton, T.; Armstrong, F. d-Metal Organometallic Chemistry. In *Inorganic Chemistry*, 7th ed.; Oxford University Press: New York, 2018; p 652.
(28) Fortman, G. C.; Nolan, S. P. N-Heterocyclic (NHC) Ligands and Palladium in Homogeneous Cross-Coupling catalysis: a perfect union. *Chemical Society Reviews* **2011**, 40, 5151-5169. https://doi.org/10.1039/c1cs15088j.
(29) Private communication within the research group.
(30) Stanley, P. M.; Haimerl, J.; Thomas, C.; Urstoeger, A.; Schuster, M.; Shustova, N. B.; Casini, A.; Rieger, B.; Warnan, J.; Fischer, R. A. Host-Guest Interactions in a Metal-Organic Framework Isoreticular Series for Molecular Photocatalytic CO_2

Reduction. *Angew. Chem. Int. Ed.* **2021**, *60*, 17854–17860. doi.org/10.1002/anie.202102729
(31) Krause, R. A. Synthesis of Mixed Complexes of Ruthenium(II) with 2,2'-Dipyridyl. *Inorganica Chimica Acta*. **1977**, *22*, 209–213.
(32) Elgrishi, N.; Rountree, K. J.; McCarthy, B. D.; Rountree, E. S.; Eisenhart, T. T.; Dempsey, J. L. A Practical Begineer's Guide to Cyclic Voltammetry. *J. Chem. Educ*. **2018**, *95*, 197–206. DOI: 10.1021/acs.jchemed.7b00361
(33) Cowan, J. A. Chapter 2: Experimental Methods. In *Inorganic Biochemistry An Introduction*, 2nd ed.; Wiley-VCH, 1997; p 71.
(34) Huheey, J. E.; Keiter, E. A.; Keiter, R. L. Coordination Chemistry: Bonding, Spectra, and Magnetism. In *Inorganic Chemistry Principles of Structure and Reactivity*, 4th ed.; HarperCollinsCollegePublishers, 1993; p 440.
(35) Que, L. Electronic Absorption Spectroscopy. In *Physical Methods in Biochemistry*, 1st ed.; University Science Books, 2000; p 17.
(36) Grätzel, M. Photovoltaic performance and long-term stability of dye-sensitized meoscopic solar cells. *C. R. Chimie* **2006**, 9, 578–583.

Vita

Name	*Matthew Schneider*
Baccalaureate Degree	*Bachelor of Science*, *New York Institute of Technology, Old Westbury, NY* *Major: Chemistry*
Date Graduated	*May, 2020*